FEDERAL UNIVERSITY OF RIO GRANDE DO SUL
SCHOOL OF ENGINEERING
ELECTRICAL ENGINEERING POST GRADUATE PROGRAM

BRUNO FENSTERSEIFER DIAS

STUDY OF A RELUCTANCE MAGNETIC GEARBOX FOR ENERGY STORAGE SYSTEM APPLICATION

Porto Alegre
2020

BRUNO FENSTERSEIFER DIAS

STUDY OF A RELUCTANCE MAGNETIC GEARBOX FOR ENERGY STORAGE SYSTEM APPLICATION

Master's dissertation presented to the Electrical Engineering Graduate Program of the Universidade Federal do Rio Grande do Sul, as part of the requirements to obtain the Master's degree in Electrical Engineering.

Area: Energy - Electromagnetic devices

ADVISOR: Prof. Dr. Ály Ferreira Flores Filho

Porto Alegre

2020

BRUNO FENSTERSEIFER DIAS

STUDY OF A RELUCTANCE MAGNETIC GEARBOX FOR ENERGY STORAGE APPLICATION

This dissertation was deemed adequate for the obtaining of the Master's degree in Electrical Engineering title and approved in its final form by the advisor and the examining board.

Advisor: _____

Prof. Dr. Ály Ferreira Flores Filho, UFRGS

PhD by University of Wales College of Cardiff – Cardiff, Wales, UK

Examination board:

Prof. Dr. Carlos Guilherme da Costa Neves, UFPEL

Doctor by the Universidade Federal de Santa Catarina – Florianópolis, Brazil

Prof. Dr. Paulo Roberto Eckert, UFRGS - PPGEE

Doctor by the Universidade Federal do Rio Grande do Sul– Porto Alegre, Brazil

Prof. Dr. Valner João Brusamarello, UFRGS - PPGEE

Doctor by the Universidade Federal de Santa Catarina – Florianópolis, Brazil

PPGEE coordinator: _____

Prof. Dr. Sérgio Haffner

Porto Alegre, September 2020.

DEDICATION

I dedicate this work to my parents, in special to my father, without whom this work would not be possible, family and friends.

ACKNOWLEDGMENT

To the Electrical Engineering Graduate Program, for the opportunity to work in my field of research.

To my advisor, who has guided and helped me during the entire work.

To my colleagues from the PPGEE for their support.

To the students from LMEAE for all their assistance.

To CAPES, for the scholarship grant.

ABSTRACT

This work proposes the use of a magnetic gearbox to be applied on an energy storage system based on flywheel to allow the use of a conventional electric machine external to the vacuum chamber as the primary machine, maintaining the possibility of using a rotating mass with high speeds. Parametric simulations were performed using finite element software to determine the behaviour of the various variables of the magnetic gear in terms of its performance and design constraints. Finally, a prototype was built to validate the simulations and the considerations made.

Keywords: Magnetic gearboxes. Energy storage systems. Finite element analyses.

RESUMO

Este trabalho propõe o uso de uma engrenagem magnética para aplicação em um sistema de armazenamento de energia baseado em volante de inércia permitindo o uso de uma máquina elétrica convencional externa à câmara de vácuo como máquina primária, mantendo a possibilidade de utilizar altas velocidades da massa girante. Simulações paramétricas foram realizadas utilizando um *software* para simulação por elementos finitos para determinar o comportamento das diversas variáveis da engrenagem magnética quanto ao seu desempenho e restrições de projeto. Por fim um protótipo foi construído para validar as simulações e as considerações feitas.

Palavras-chave: Engrenagens magnéticas. Sistemas de armazenamento de energia. Análise por elementos finitos.

LIST OF ILUSTRATIONS

LIST OF TABLES

LIST OF ABREVIATIONS

AMG Axial Magnetic Gearbox

CMG Coaxial Magnetic Gearbox

CyMG Cycloidal Magnetic Gearbox

EDM Electrical Discharge Machining

LMEAE Laboratório de Máquinas Elétricas, Acionamentos e Energia

MPG Magnetic Planetary Gearbox

PPGEE Programa de Pós-Graduação em Engenharia Elétrica

RMG Reluctance Magnetic Gearbox

VC Vacuum Chamber

VCW Vacuum Chamber Wall

LIST OF SYMBOLS

α_{in} Polar arch angle

δ_h Deviation angle of the low speed rotor to the modulation ring

δ_l Deviation angle of the low speed rotor to the modulation ring

θ Reference axis at the centre of the modulation ring

θ_h Mechanical angle of high speed rotor

θ_l mechanical angle of low speed rotor

θ_r Inner rotor relative angle

ω_c Angular speed of ring carrier

ω_h Angular speed of the high speed rotor

ω_l Angular speed of the low speed rotor

ω_r Angular speed of the ring gear

ω_s Angular speed of the modulation ring

ω_{su} Angular speed of the sun gear

F_l magnets magnetomotive force

F_{lm} amplitude of the magnets magnetomotive force

G_{in} inner air gap

G_{out} Outer air gap

G_r Gear ratio

H_{fe} Back iron thickness

H_{mag} Magnets thickness

H_s Modulation ring thickness

K_c Eddy currents loss coefficient

K_e Additional loss coefficient

K_h Hysteresis loss coefficient

P_a Number of poles of the inner rotor

P_c Number of poles of the ring carrier

P_{eq} Equivalent permeance of inner rotor and modulation ring

P_h Permeance of the high-speed rotor

P_{ha} Average component of the permeance of the high-speed rotor

P_{hm} Amplitude of the permeance of the high-speed rotor

P_o Number of poles of the outer rotor

P_r Number of poles of the ring carrier

P_s Permeance of the modulation ring

P_{sa} Average component of the modulation ring permeance

P_{sm} Amplitude of the modulation ring permeance

P_{su} Number of poles of the sun gear

R_{in} Inner rotor inner radius

R_{out} Inner rotor radius

Skew Skewing angle

T Time

T_h Torque output of the high-speed rotor

T_l Torque output of the low-speed rotor

Z_h Inner rotor number of poles

Z_l Outer rotor number of poles

Z_s Number of modulation ring pieces

SUMMARY

1 INTRODUCTION

This chapter consists of a contextualization section, a section with this works goals and justifications and a section describing the chapters that follow.

1.1 CONTEXTUALIZATION

As the demand for energy rises and the use of renewable energies becomes more common, most of which have an inconstant energy production, energy storage systems have become more important to regulate the energy flows in energy grids.

Energy storage systems based on kinetic energy, where one of the most common topology is the flywheel, can store energy in a rotating mass with high velocity and inertia. Given that the energy stored increases with the square of the velocity, it is usual to use very high velocities rather than very high inertias. By applying forces and torques to the rotating mass, energy can be transferred to and from the rotating mass. In order to reduce the losses from friction with the air and others, this kind of topology uses vacuum chambers and magnetic levitation to increase performance.

The forces applied to the rotating mass of a Flywheel Energy Storage System (FESS) are produced by rotary electric machines usually. A separated magnetic actuator is responsible for levitating the rotating mass and maintaining it stable. In order to achieve this stable levitation there are a few options available. A fully active system can be used to levitate and maintain the stability. This approach has the disadvantage of requiring all the forces to be generated with current, which implies in higher losses. Since the gravitational forces can be considered constant, and are responsible for the larger part of the forces required to levitate and maintain the stability of the rotating mass, a passive system can be used to provide the forces to achieve the magnetic levitation. To compensate any oscillation a smaller active

system is added to assure the stability and safety of the levitation. This combination of a passive and an active system results in higher efficiencies than the one in a fully active system. This work is part of a project to develop an FESS that uses a High Temperature Superconductor (HTS) to provide the levitation forces that will be assisted by an active system to achieve a stable condition.

The use of an electric machine inside a vacuum chamber incurs in a few challenges, such as thermal dissipation issues due to the vacuum environment and the need to adjust the vacuum chamber to accommodate the electric machine. As the FESS topology usually employs very high velocities, the electric machine must be designed to be able to operate in the full spam of velocities, from start up to full speed. Both this issues can be solved by using a Magnetic Gearbox (MG) to transfer energy from the outside of the vacuum chamber and provide a speed gain from the electric machine to the rotating mass. Some MGs uses a modulation ring, a set of ferromagnetic pieces allocated between rotors, which can be inserted into a wall to achieve coupling between rotors on each side of the wall. The modulation ring also allows for rotors with different number of poles to be coupled, resulting in a speed conversion should one rotor be spun and the other be allowed to rotate. Combining the possibility to transfer energy through a wall and the speed conversion of a MG, a conventional electric machine can be used outside the vacuum chamber to transfer energy from and to the rotating mass. This work proposes the use of a MG as a way to solve the issues of the electric machine inside the vacuum chamber and the need for high speeds in the project previously described. If Fig. 1 is shown the proposed topology of the project, where in this work the use of the MG will be studied and explained.

Figure 1 - Project concept

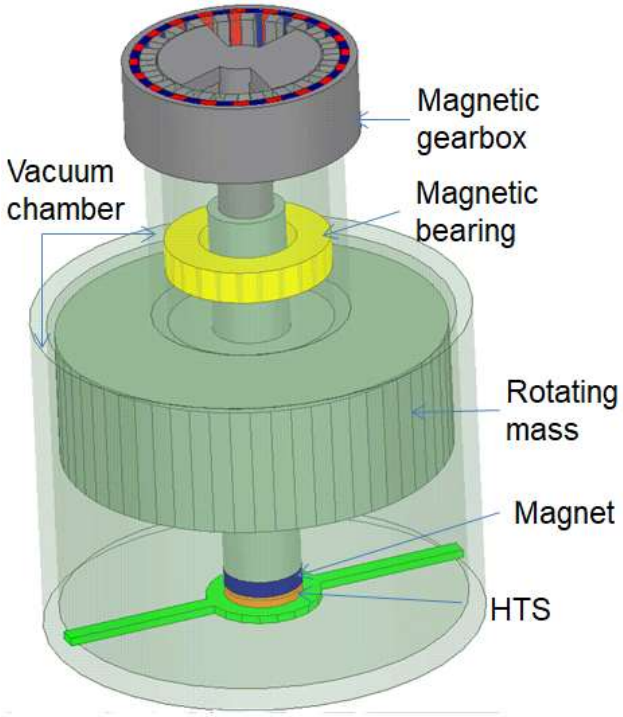

Source: The author

In Fig. 1 it can be seen a green cylinder attached on one end to a magnet and on the other end to the inner rotor of the MG. The magnet attached to the rotating mass is repelled by the HTS, resulting in a levitation force to be generated. The inner rotor of the MG, attached to the other end of the rotating mass is magnetically coupled with the outer rotor. Since the outer rotor is connected to the primary machine, a conventional electric machine, energy can be transferred from and to the rotating mass inside the vacuum chamber. The result is a FESS that has a conventional electric machine outside the vacuum chamber and uses a HTS to provide the bulk of forces required to levitate the rotating mass.

1.2 GOALS AND JUSTIFICATION

The goals of this work are:

- To study a way to transfer energy in between the external primary machine outside the vacuum chamber and the rotating mass inside the latter and without contact between them.
- Keep losses as low as possible when not transferring energy to and from the rotating mass.
- Provide a speed gain from the primary machine to the rotating mass, so conventional low-speed electrical machines can be used.
- To consider all the aspects involving energy storage systems with a magnetically levitated rotating mass to the design of the topology.

1.3 CHAPTERS DISTRIBUTION

The chapters that follow are divided into a chapter of the state of the art and literature review, a chapter for the proposed topology and its considerations, a chapter about the magnetic design and simulations carried out, a chapter about the mechanical design, and a chapter with the conclusions and recommendations.

2 MAGNETIC GEARBOXES

Magnetic Gearboxes (MG) have been the focus of studies and publications since 1940, with the development over the years described in [1]. The first coaxial planetary magnetic gearbox was first proposed in 2001 [2]. Since the 2000s, the incorporation of MG in motors has been proposed to reduce the overall size of the drive system [3]. The number of publications about MGs has increased as higher energy product magnets become more available and cheaper. One of the applications that have been generating several articles about MG is their use on wind generators [4-6].

One of the most important features of MG is the protection from overload. If an excessive torque is applied, the MG will lose synchronism and start slipping poles, instead of breaking as it occurs with mechanical gearboxes. Once the excessive torque is removed, the MG will automatically recover the synchronism. MGs also require less maintenance as they do not require lubrication and operate without contact between its parts. They also generate less noise [7-13].

The magnetic flux modulation principle can be explained as shown in [14]. In order to explain the magnetic flux modulation, an outer rotor with a given number of poles, all radially magnetized with alternating polarities, can be considered as the primary source of magnetic field. A set of modulation pieces made of ferromagnetic material, concentric with the outer rotor, can be used to modulate the magnetic flux. An inner rotor with a different number of poles, also with radial magnetization and alternating polarities and concentric with the outer rotor, can be used to be coupled to modulated magnetic flux. Considering these three main parts, the magnetic flux modulation can be explained as follows.

Fig. 2, 3 and 4 shows the flux modulation where the inner rotor sees only a north pole produced by the outer rotor, the flux modulation where the inner rotor sees a transition from

north pole to south pole and the flux modulation where the inner rotor sees only a south pole produced by the outer rotor.

Figure 2 - Flux modulation north

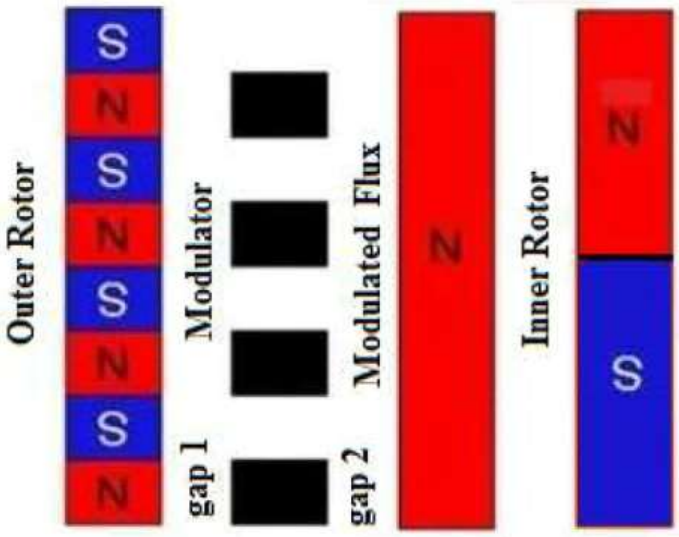

Source: [14]

In Fig. 2, it can be seen that the modulation ring pieces are aligned with the north poles of the outer rotor, and, consequently, the modulated magnetic flux seen by the inner rotor is a north pole.

Figure 3 - Flux modulation transition

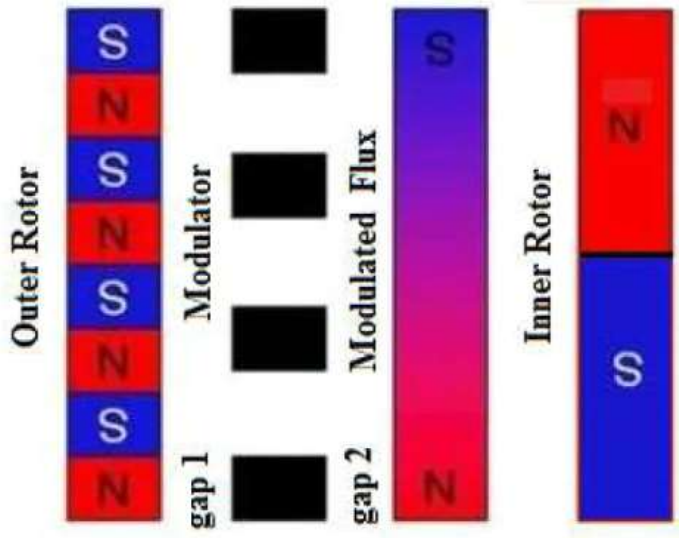

Source: [14]

In the case of Fig. 3, the modulation ring pieces are not perfectly aligned with either pole. Therefore, the resulting modulated magnetic flux is a mixture of both north poles and south poles.

Figure 4 - Flux modulation south

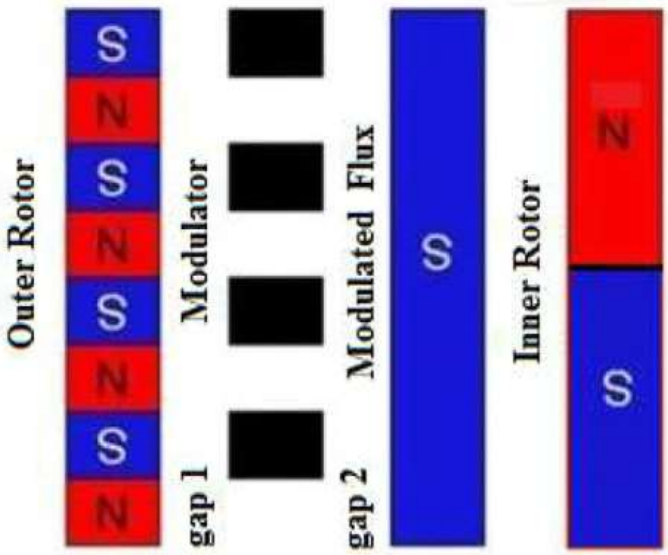

Source: [14]

Finally, in Fig. 4 the modulation ring pieces align with the south poles and the resulting modulated magnetic flux results in a south pole. This transition between poles generates a modulated magnetic flux with different magnetic pole transitions than the one produced by the outer rotor and allows for rotors with different number of poles to couple.

At any given time, since the magnets are never removed nor demagnetized, the outer rotor produces an alternating magnetic flux along its inner circumference. Even though all poles are always present, the distance and elevated magnetic reluctance prevents the majority of the magnetic flux to reach the inner rotor. As the magnetic reluctance of the modulator pieces is much smaller when compared to that of the material that surrounds the device, air or vacuum for example, the magnetic flux that goes through the modulation ring pieces can reach the inner rotor. Because of this, at any given time the modulation ring filters which parts of the

magnetic flux distribution of the outer rotor reach the inner rotor. By this effect, the inner rotor interacts not with the original flux distribution of the outer rotor alternating poles, but with the resulting magnetic flux that comes from the outer rotor but was filtered, or modulated, by the modulation ring pieces. As a result, even if the outer rotor has a different number of poles than the inner rotor, both rotors can still be coupled and produce torque. The inner rotor will be coupled to the modulated flux of the outer rotor and not the original magnetic flux produced by the magnets of the outer rotor. Considering that the inner rotor also has magnets, the same considerations can be made for the magnetic path from the inner rotor to the outer rotor. The outer rotor also couples to the modulated magnetic flux of the inner rotor, and not by the original magnetic flux produced by the magnets of the inner rotor.

Considering two concentric rotors, with evenly distributed magnets, with radial magnetization and alternating polarity, but with different number of poles between rotors, as an example. If both rotors are rotated by the same angle, the rotor with more poles will alternate more poles at a given reference axis than the rotor with fewer poles. For a variation of several poles from the rotor with more poles, it might not even change the pole facing the reference axis of the rotor with fewer poles. Fig. 5 shows an example with two concentric rotors, the outer rotor with 10 poles and the inner rotor with four poles and Fig. 6 shows the same rotors rotated by 90º clockwise.

Figure 5 - Concentric rotors with 10 and 4 poles

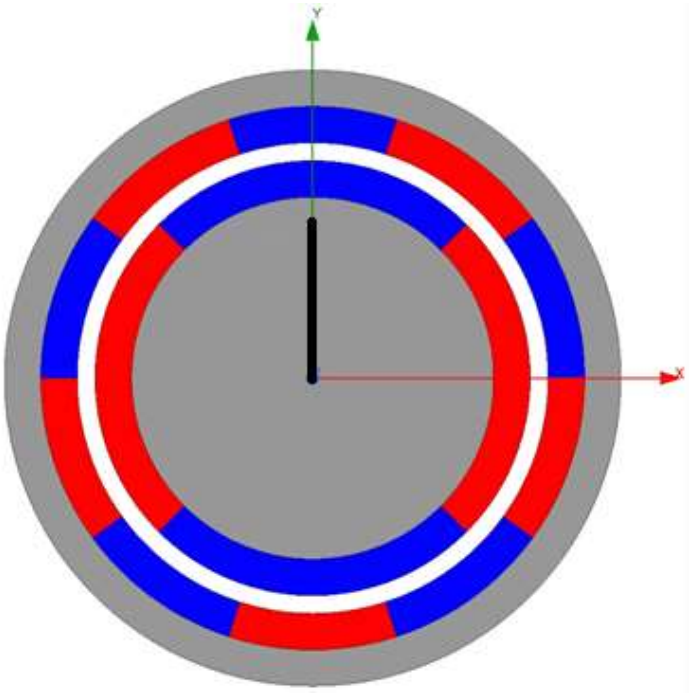

Source: The author

Figure 6 - Rotors rotated by 90º counter clockwise

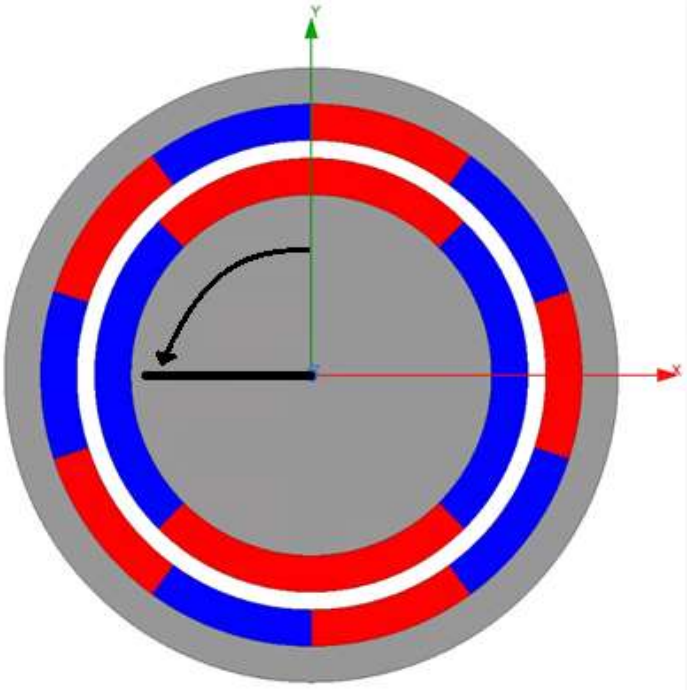

Source: The author

As seen in Fig. 5, originally both rotors have a north pole (blue magnets) centred at the y-axis. In Fig 6, where both rotors were rotated by 90º, the inner rotor, with four poles, changed from a north pole centred at the y-axis to the next south pole centred to the reference axis. At the same time, the outer rotor, with 10 poles, switched from a centred north pole at the y-axis to the next south pole, the next north pole and ended with the y-axis between the second north pole and the second south pole. If both rotors are coupled (which can be achieved with a modulation ring between them), for any rotation of the rotor with more poles, the other rotor with fewer poles will have to rotate by a larger angle to have an equivalent magnetic flux alternation.

Combining the magnetic flux modulation to couple concentric rotors with different number of poles and the relationship of number of poles and equivalent rotation to produce the same magnetic flux variation is possible to obtain two rotors magnetically coupled. A rotation of one rotor produces a rotation of the other rotor that can be larger or smaller, depending only on the number of poles of both rotors, in the same way as with mechanical gears and number of spurs.

The modulation ring pieces compose, in terms of magnetic reluctance, a square wave with central frequency equal to the number of pieces that compose the modulation ring if the reluctance of the region around them is to be considered infinite. The magnetic flux from the magnets of the outer rotor is filtered by the reluctance square wave resulting in the modulated magnetic flux seen by the inner rotor. If a modulation ring with 7 ferromagnetic pieces is placed between the rotors of the previous example with 4 and 10 poles, the result of the combination of the square wave and the 10 poles of the outer rotor will produce a harmonic spectrum with a frequency equal to the main frequency of the inner rotor with four poles. At the same time, the interaction of the magnetic flux of the 4-pole rotor and the 7 pieces

modulation ring will result in a modulated flux seen by the outer rotor with a frequency equal to the main frequency of the 10 pole outer rotor. This combination leads to Eq. 1 for the number of modulation ring pieces for a given combination of poles of the outer and inner rotors.

$$2 \cdot Z_s = Z_l + Z_h \tag{1}$$

In Eq. 1 Z_s is the number of pieces of the modulation ring, Z_l is the number of poles of the low speed rotor (higher number of poles) and Z_h is the number of poles of the high speed rotor (lower number of poles).

By multiplying in Eq. 1, each term by its corresponding speed, results in Eq. 2, which gives the speed relationship between rotors and modulation ring.

$$2 \cdot Z_s\omega_s = Z_l\omega_l + Z_h\omega_h \tag{2}$$

In Eq. 2, ω_s is the angular speed of the modulating ring, ω_l is the angular speed of the low speed rotor and ω_h is the angular speed of the high-speed rotor. If, for example, the modulation ring is kept stationary, Eq. 2 is converted to Eq. 3 that gives the speed relationship (gear ratio) between rotors.

$$G_r = \frac{\omega_h}{\omega_l} = -\frac{Z_l}{Z_h} \tag{3}$$

For the example with two rotors with 10 and 4 poles and a modulation ring with 7 pieces, the gear ratio G_r is -2.5, where the minus sign means that the rotors will have opposite running directions.

Among the most common MG are the Axial flux Magnetic Gearboxes (AMG), the Magnetic Planetary Gearboxes (MPG), the Coaxial Magnetic Gearboxes (CMG) and the Cycloidal Magnetic Gearboxes (CyMG).

AMG basic concept consists of two discs facing each other with magnets distributed over its circumference as alternating poles and ferromagnetic pieces between both discs as the modulation ring. Fig. 7 shows an example of an AMG.

Figure 7 - Axial magnetic gearbox

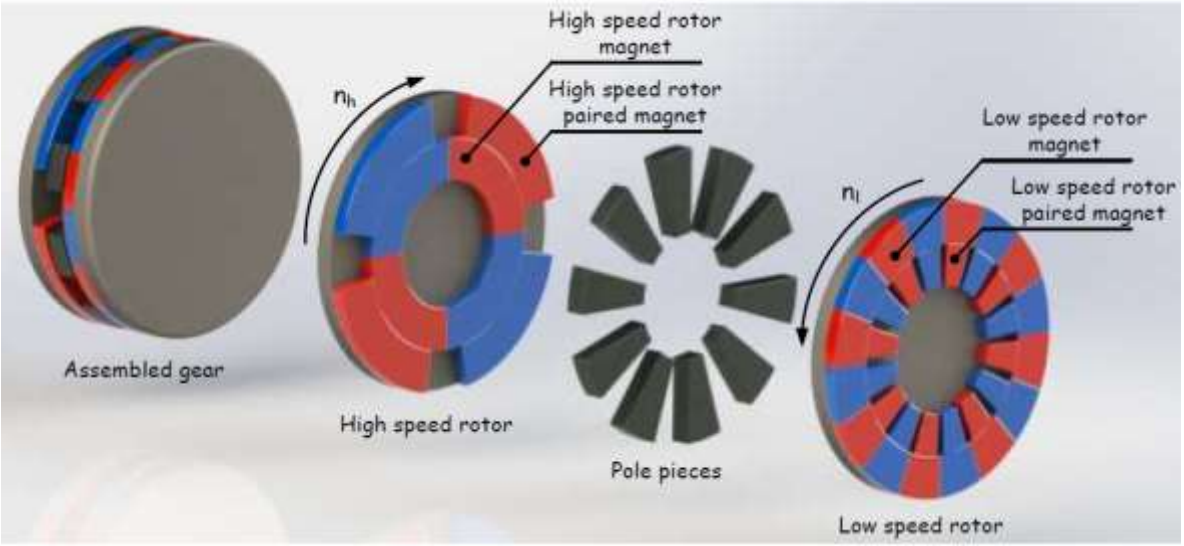

Source: [15]

AMG, such as the one shown in Fig. 7, which was first proposed by Mezani [15], has a simpler construction as compared to CMG, but has been the focus of fewer papers when compared to CMG. In terms of gear ratio, the number of poles and the choice for a static modulation ring or a static disc allow different configurations. For a static modulation ring Eq. 4 and Eq. 5 respectively, [16] gives the gear ratio and the number of modulation ring pieces.

$$G_r = \frac{Z_l}{Z_h} \tag{4}$$

$$Z_l = 2 \cdot Z_s + Z_h \tag{5}$$

In Eq. 4 and 5, the gear ratio G_r and the number of modulation ring pieces Z_s are given by the number of poles of the low speed rotor Z_l and the number of poles of the high-speed

rotor Z_h. The AMG, in terms of size, has some limitations as the torque generated can be improved by increasing the radius but by increasing the axial length, even with magnets, does not provide the same benefits as with other MGs.

The MPG, such as the one shown in Fig. 8, has three transmission modes that were described in [17], where the first one has the planet gear carrier as the output and the magnetic sun and the ring gear as the driving gears, resulting in the angular velocity relationship of Eq. 6.

Figure 8 - Magnetic planetary gearbox

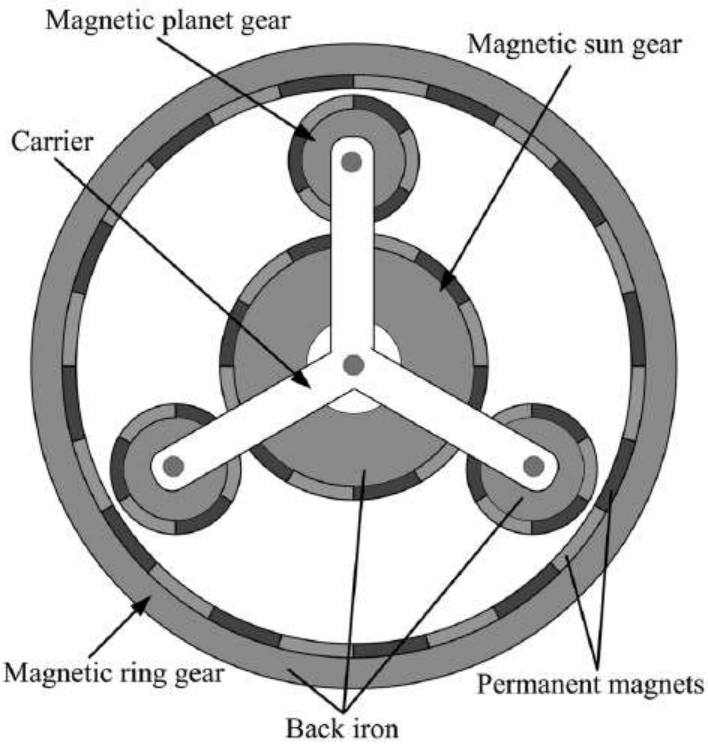

Source: [17]

$$\omega_c = \frac{P_{su}}{P_{\mathrm{su}} + P_r}\omega_{su} + \frac{P_r}{P_{su} + P_r}\omega_r \tag{6}$$

In Eq. 6, ω_c, ω_{su}, ω_r are the angular velocity of the planet gear carrier, the magnetic sun gear and the ring gear respectively, and P_{su} and P_r are the number of poles of the magnetic sun gear and the number of poles of the ring gear respectively.

The second transmission mode uses the magnetic sun gear is the output and the gear carrier and ring gear are the inputs. For the second transmission mode, Eq. 7 gives the angular velocity relationship.

$$\omega_{su} = \frac{P_{su} + P_r}{P_{su}}\omega_c - \frac{P_r}{P_{su}}\omega_r \tag{7}$$

For the last transmission mode, the magnetic ring gear is used as output and the magnetic sun gear and the gear carrier are the input. The last transmission mode has the angular velocity relationship determined by Eq. 8.

$$\omega_r = \frac{P_{su} + P_r}{P_r}\omega_c - \frac{P_{su}}{P_r}\omega_{su} \tag{8}$$

The CyMG uses two rotors with different number of poles and a non-uniform rotor air gap to produce a speed gain, as described in [3]. A CyMG that uses the magnetic flux focusing approach to increase torque output is shown in Fig. 9.

Figure 9 - Cycloidal magnetic gearbox

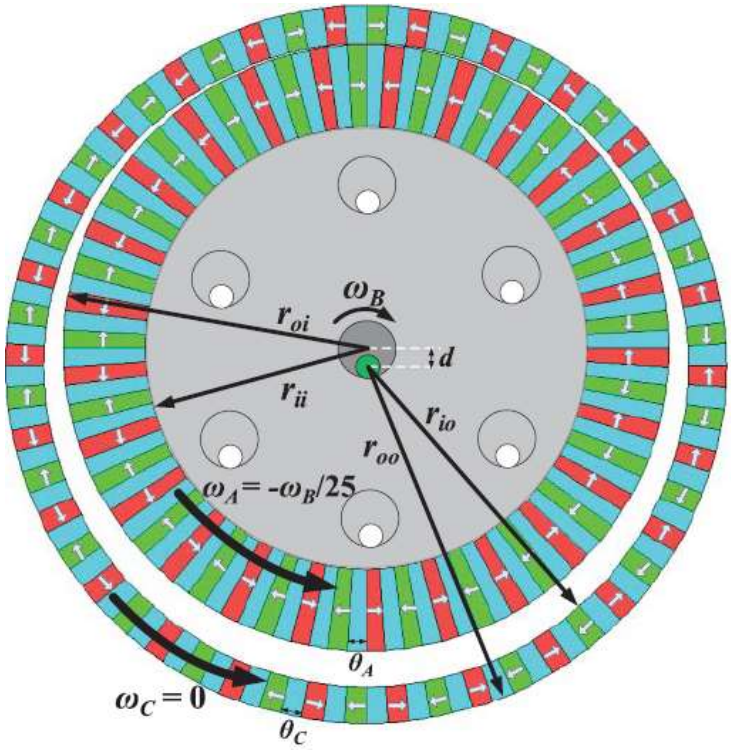

Source: [3]

The inner rotor shown in Fig 8 has a rotational motion and an orbital motion. The gear ratio for the CyMG can be obtained using Eq. 9.

$$G_r = \frac{P_a}{P_a - P_0} \tag{9}$$

In Eq. 9, P_a is the number of poles of the inner rotor and P_o is the number of poles of the outer rotor.

The CMG uses two rotors separated by a ring of ferromagnetic pieces, as shown in Fig. 10.

Figure 10 - Coaxial magnetic gearbox

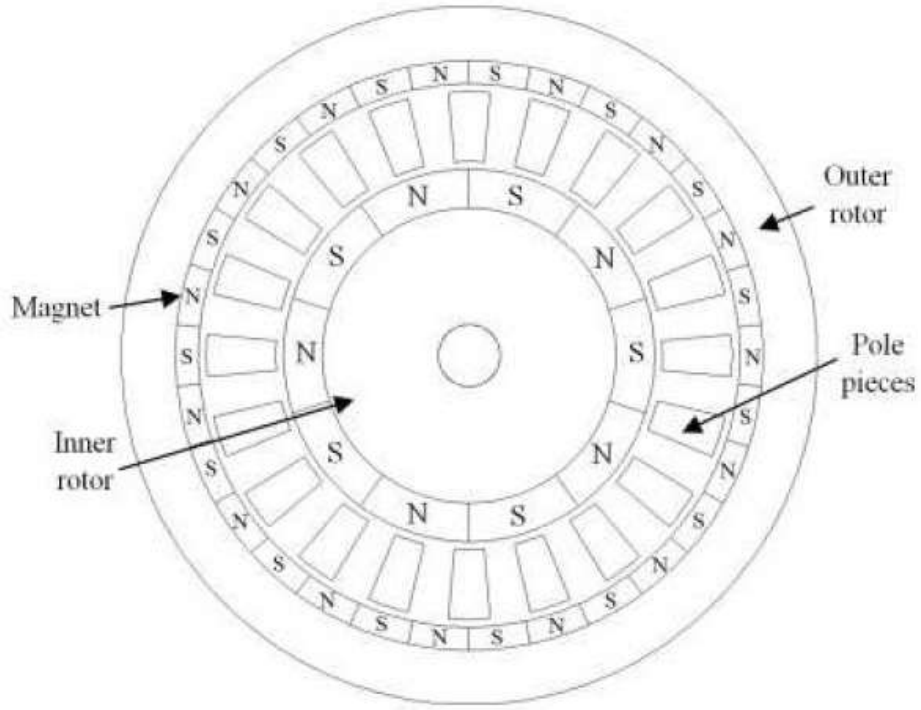

Source: [14]

The speed gain of CMGs is given by the number of poles in the both rotors and the number of segments in the modulation ring. In [18] several combinations of pole pairs and number of segments in the modulation ring were simulated and several considerations, regarding torque ripple and torque output, are presented. Eq. (10) gives the speed gain G_r in

terms of number of poles of the both rotors for a stationary modulation ring and Eq. (11) gives the number of modulation ring pieces required to establish the synchronism [14].

$$G_r = \frac{Z_l}{Z_h} = \frac{\omega_h}{\omega_l} = \frac{T_l}{T_h} \tag{10}$$

$$Z_l = 2 \cdot Z_s \pm Z_h \tag{11}$$

In Eq. 10 and 11, Z_l is the number of poles, ω_l is the angular velocity and T_l is the output torque of the outer rotor (low speed rotor). Also in Eq. 10 and 11, Z_h is the number of poles, ω_h is the angular velocity and T_h is the output torque of the inner rotor (high speed rotor). In Eq. 11, Z_s is the number of pieces of the modulation ring. The expression in Eq. 11 contains a ± sign because depending on the choice: either the rotors will have the same direction of rotation (case of – sign), or will have an opposite one (case of + sign).

If the modulation ring is used as a rotating part and the outer rotor is stationary, the equation for the speed gain and number of modulation pieces changes to Eq. 12 and 13 [14].

$$G = \frac{Z_s}{Z_h} = \frac{\omega_h}{\omega_s} \tag{12}$$

$$2 \cdot Z_s = Z_h + Z_l \tag{13}$$

For the case of a stationary outer rotor (ω_l = 0), as stated by Eq. 12 and Eq. 13, the number of poles in the outer rotor is a consequence of the chosen speed gain, determined by the number of modulation pieces and the number of poles in the inner rotor.

The use of MGs in the naval industry was proposed in [18-19] as a way to reduce the size of the propulsion system when compared to a conventional system with the drive system connected to the propeller. It also makes use of the modulation ring as a wall to isolate the propeller from the drive system.

In the same way as with induction machines, where the rotor is skewed to reduce the harmonics, the segmentation in two parts and skewing of the rotors of MG was proposed in [20] as a way to mitigate the torque ripple.

Most recently, in 2016 a reluctance version of MGs was proposed in [21] as an alternative to achieve higher speeds. The Reluctance Magnetic Gearbox (RMG) is a radial magnetic gearbox with the inner rotor made of electrical steel and no magnets. Fig 11 shows the original RMG proposed.

Figure 11 - Original reluctance magnetic gearbox

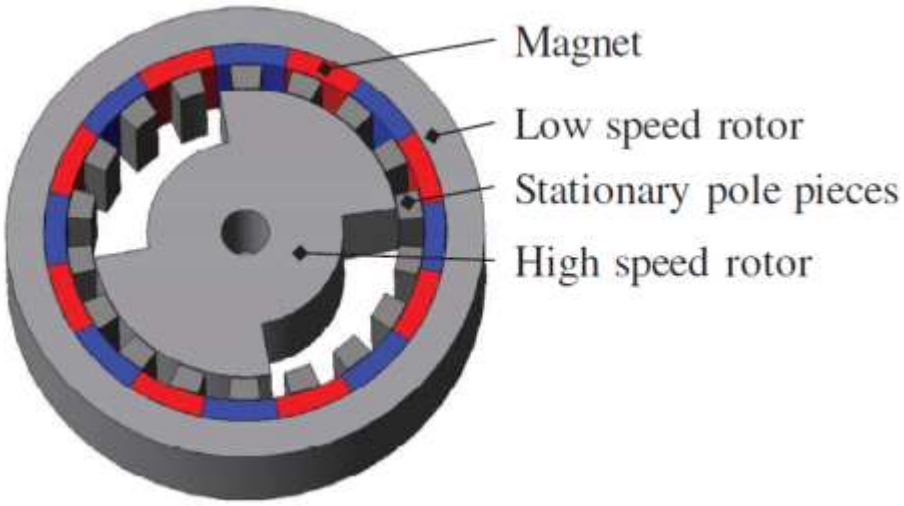

Source: [21]

The RMG has a rotor with magnets and a rotor made of electrical steel. The absence of magnets makes the inner rotor more robust and allows for higher speed since the mechanical issue of holding the magnets is removed. Fig 12 shows the mechanical strength limit for proposed.

Figure 12 - Original reluctance magnetic gearbox

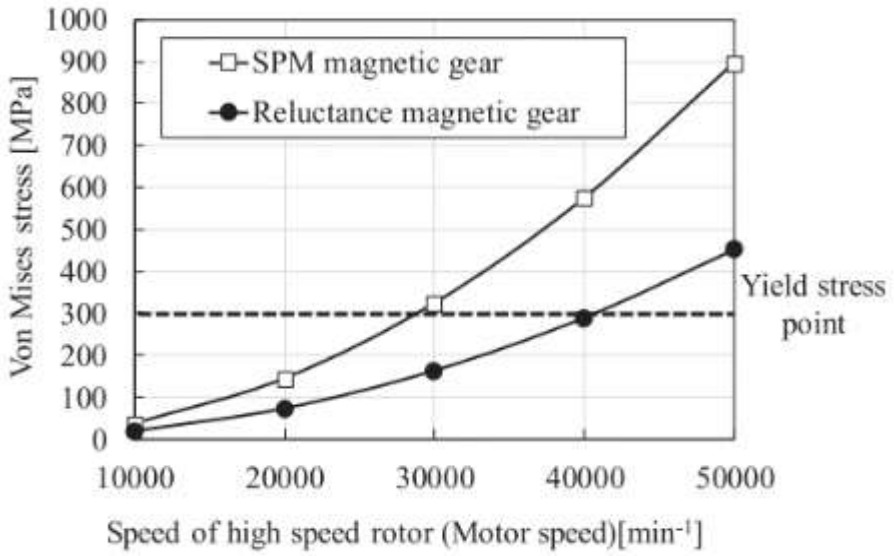

Source: [22]

As seen in Fig. 12, for very high speeds, the use of magnets becomes an issue as holding them in place becomes difficult. The stress point for the RMG, can achieve higher speeds for the same stress value of 300Mpa than a rotor with magnets on the surface. The absence of the magnets makes the RMG cheaper and easier to produce, but it also reduces the overall torque output. Eq. 14 gives the gear ratio of for this type of MG and Eq. 15 gives the number of pole pieces.

$$G = \pm\frac{Z_s}{Z_h} = \pm\frac{\omega_h}{\omega_s} \tag{14}$$

$$Z_s = \mp Z_h + Z_l \tag{15}$$

In Eq. 14 and Eq. 15, the ± sign denotes two possibilities, one where the rotors turn in different directions and one where both rotors turn in the same direction.

The principle of operation of an RMG, as expressed in [22], is stated by the following equations, where the *l* subscript denotes the low speed rotor (outer rotor) and the *h* subscript denotes the high-speed rotor (inner rotor).

Since only the outer rotor has magnets, Eq. 15 gives the magnetomotive force of the outer rotor.

$$F_l = F_{lm}\, cos\{Z_l\theta_l - Z_l\omega_l t\} = F_{lm}\, cos\{Z_l\theta - Z_l\omega_l t - Z_l\delta_l\} \quad (15)$$

In Eq. 15, F_l is the magnetomotive force of the permanent magnets in the outer rotor and F_{lm} is the amplitude of the magnetomotive force of magnets in the outer rotor. As for the arguments seen in Eq. 15, Z_l is the number of poles of the outer rotor, ω_l is the angular speed of the outer rotor, θ_l is the mechanical angle of the outer rotor. In this work, θ is the reference axis at the centre of a modulation ring piece, δ_l is the deviation angle between the centre of pole pieces and the outer rotor and t is time. Fig 13 shows the described variables and the magnetic flux from the magnets in a linear view.

Figure 13 - Linear view of the RMG

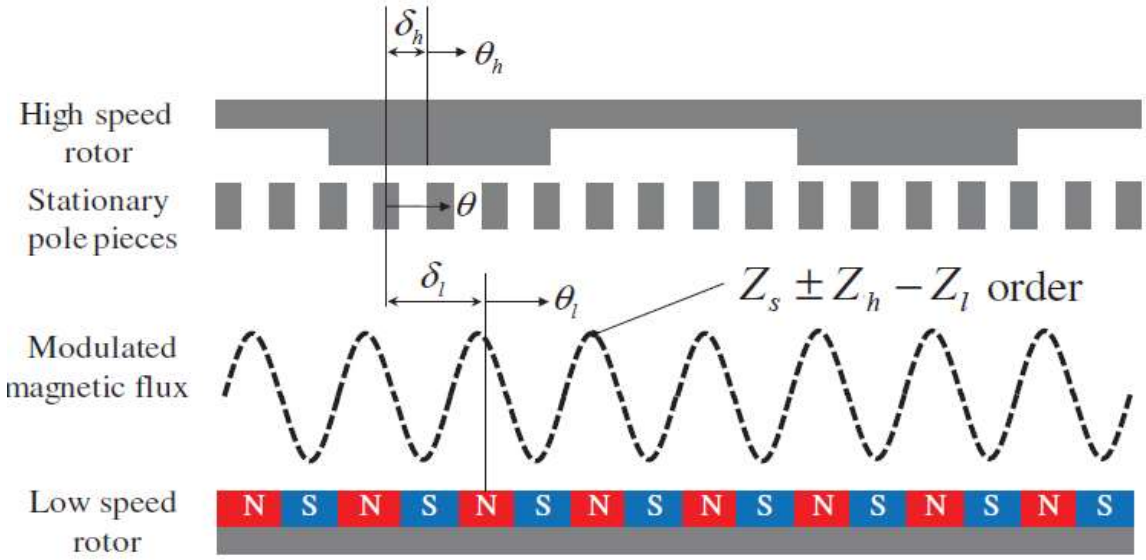

Source: [22]

The relative angles are shown in Fig. 14.

Figure 14 - Relative angles

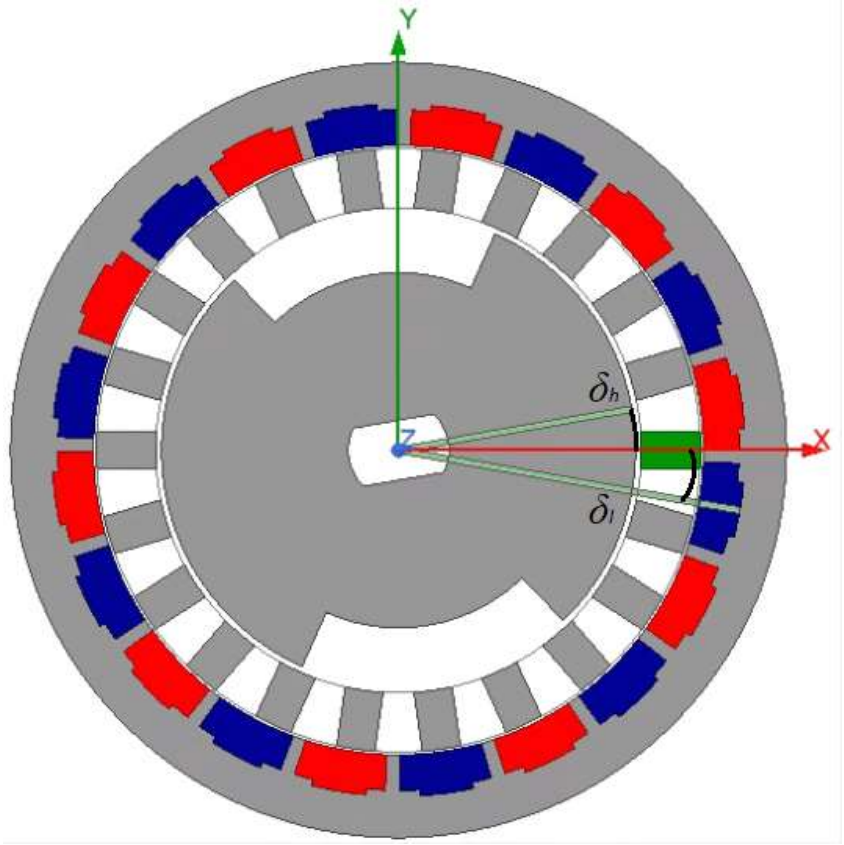

Source: The author

In Fig. 14, the green modulation ring piece is the reference piece and the relative angles are given by the centre of the inner rotor and the centre of the reference piece for the low speed rotor and the centre of the magnet and the reference piece for the low speed rotor.

Eq. 16 expresses the permeance of the modulation ring pieces.

$$P_s = P_{sa} + P_{sm}cos\{Z_s\theta\} \tag{16}$$

In Eq. 16 P_s is the permeance, P_{sa} is the average component of the permeance, P_{sm} is the amplitude of the permeance of the modulation ring pieces and Z_s is the number of pieces of the modulation ring and θ is the reference angle at the centre of a modulation ring piece.

Eq. 17 expresses the permeance of the inner rotor.

$$P_h = P_{ha} + P_{hm}cos\{Z_h\theta_h - Z_h\omega_h t - Z_h\delta_h\} \tag{17}$$

In Eq. 17, in terms of permeance values, P_h is the permeance, P_{ha} is the average component of the permeance and P_{hm} is the amplitude of the permeance of the high-speed rotor. Z_h is the number of poles of the high-speed rotor. For the velocity and angles, θ_h is the mechanical angle of the high-speed rotor, ω_h is the angular speed of the high-speed rotor and δ_h is the deviation angle between the centre of pole pieces and the high-speed rotor.

Using Equations 15, 16 and 17, the magnetic flux in the air gap can be obtained using Eq. 18 and Eq. 19.

$$\varphi_{\theta,t} = F_l P_{eq} \tag{18}$$

$$\begin{aligned}\varphi_{\theta,t} = {} & F_{lm}P_{ha}P_{sa}\,cos(Z_l\theta - Z_l\omega_l t - Z_l\delta_l) \\ & + \frac{1}{2}F_{lm}P_{ha}P_{sm}\cdot\begin{Bmatrix} cos[(Z_s+Z_l)\theta - Z_l\omega_l t - Z_l\delta_l] \\ + cos[(Z_s-Z_l)\theta - Z_l\omega_l t - Z_l\delta_l]\end{Bmatrix} \\ & + \frac{1}{2}F_{lm}P_{sa}P_{hm}\cdot\begin{Bmatrix} cos[(Z_h+Z_l)\theta - (Z_h\omega_h + Z_l\omega_l)t - (Z_h\delta_h + Z_l\delta_l)] \\ + cos[(Z_h-Z_l)\theta - (Z_h\omega_h - Z_l\omega_l)t - (Z_h\delta_h - Z_l\delta_l)]\end{Bmatrix} \\ & + \frac{1}{4}F_{lm}P_{sa}P_{hm}\cdot\begin{Bmatrix} cos[(Z_s+Z_h+Z_l)\theta - (Z_h\omega_h + Z_l\omega_l)t - (Z_h\delta_h + Z_l\delta_l)] \\ + cos[(Z_s+Z_h-Z_l)\theta - (Z_h\omega_h - Z_l\omega_l)t - (Z_h\delta_h - Z_l\delta_l)] \\ + cos[(Z_s-Z_h+Z_l)\theta - (-Z_h\omega_h + Z_l\omega_l)t - (-Z_h\delta_h + Z_l\delta_l)] \\ + cos[(Z_s-Z_h-Z_l)\theta - (-Z_h\omega_h - Z_l\omega_l)t - (-Z_h\delta_h - Z_l\delta_l)]\end{Bmatrix}\end{aligned} \tag{19}$$

The term P_{eq} in Eq. 17 is the equivalent permeance of the inner rotor combined with the permeance of the modulation ring. In Eq. 18 the seventh and ninth terms contributes to the coupling of the rotors. Assuming the use of values for the number of poles and modulation ring pieces according to Eq. 10 and 11, the torque output for the inner rotor is given by Eq. 20 and Eq. 21 gives the torque for the outer rotor.

$$T_h = \frac{1}{8}F_{lm}^2 P_{s0}P_{hm}Z_h\,sin[(Z_l\omega_l \mp Z_h\omega_h)t - Z_l\delta_l \pm Z_h\delta_h] \tag{20}$$

$$T_l = \frac{1}{8}F_{lm}^2 P_{s0}P_{hm}Z_l\,sin[(Z_l\omega_l \mp Z_h\omega_h)t - Z_l\delta_l \pm Z_h\delta_h] \tag{21}$$

Considering a RMG with a 20-poles low speed rotor rotating at 3600 rpm, a stationary modulation ring with 22 pieces and a high-speed rotor with 2 poles rotating at -36000 rpm,

Eq. 19 can be rewritten as Eq. 22, where both rotors are synchronized and have a relative angle.

$$\varphi_{\theta,t} = F_{lm}P_{ha}P_{sa}\,cos(20\theta - 72000t - 20\delta_l) \tag{22}$$

$$+\frac{1}{2}F_{lm}P_{ha}P_{sm}\cdot\begin{Bmatrix} cos[42\theta - 72000t - 20\delta_l] \\ +cos[2\theta - 72000t - 20\delta_l] \end{Bmatrix}$$

$$+\frac{1}{2}F_{lm}P_{sa}P_{hm}\cdot\begin{Bmatrix} cos[22\theta - 2\delta_h - 20\delta_l)] \\ +cos[-18\theta + 144000t - 2\delta_h + 20\delta_l] \end{Bmatrix}$$

$$+\frac{1}{4}F_{lm}P_{sa}P_{hm}\cdot\begin{Bmatrix} cos[44\theta - 2\delta_h - 20\delta_l)] \\ +cos[4\theta + 144000t - 2\delta_h + 20\delta_l] \\ +cos[40\theta - 144000t + 2\delta_h - 20\delta_l] \\ +cos[+2\delta_h + 20\delta_l] \end{Bmatrix}$$

In Eq. 22 it can be seen that the only term that depends only on the relative angles is the ninth term, which is the one who contributes to produce torque. Considering the same RMG, Eq. 20 and Eq. 21 can be rewritten into Eq. 23 and Eq. 24.

$$T_h = \frac{1}{4}F_{lm}^2P_{s0}P_{hm}\,sin[-20\delta_l \pm 2\delta_h] \tag{23}$$

$$T_l = \frac{5}{2}F_{lm}^2P_{s0}P_{hm}\,sin[-20\delta_l \pm 2\delta_h] \tag{24}$$

In Eq. 23 and Eq. 24, given that the permeance and the magnetomotive force are constant values, the average torque of each rotor depends only on the relative angles.

3 PROPOSED TOPOLOGY

The goal of this work is to design a prototype capable of transmitting energy into a rotating mass inside a Vacuum Chamber (VC) that is magnetically levitated as part of a flywheel system. The prototype should be able to provide a speed gain of 10 from the primary machine to the rotating mass with 36,000 rpm on the high-speed side. Losses should be mitigated specially when the prototype is not charging nor discharging. Considerations should be taken regarding the magnetically levitated rotating mass, in terms of minimum air gap.

The proposed topology consists of a Reluctance Magnetic Gearbox (RMG) with the modulation ring as part of the Vacuum Chamber Wall (VCW) and a skewed inner rotor as a way to move the primary machine of a Flywheel Energy Storage System (FESS) out of the VC. The proposed topology is shown in Fig. 15, and an alternative topology is presented in Fig. 16.

Figure 15 - Proposed topology of RMG integrated into an FESS

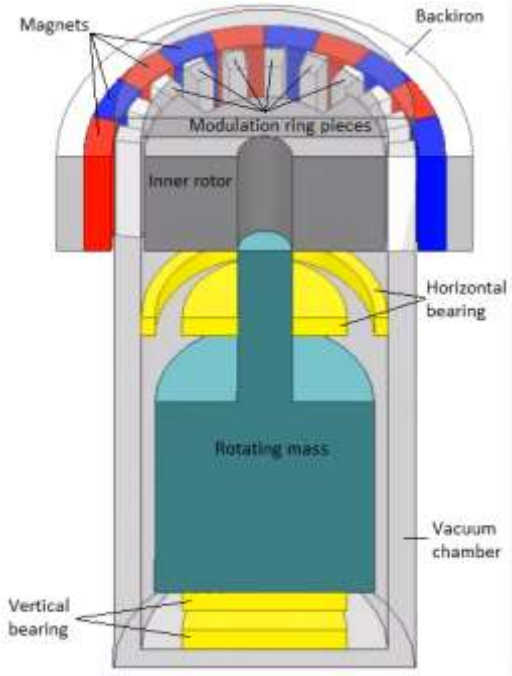

Source: The author

Figure 16 - Alternative topology of RMG integrated into an FESS

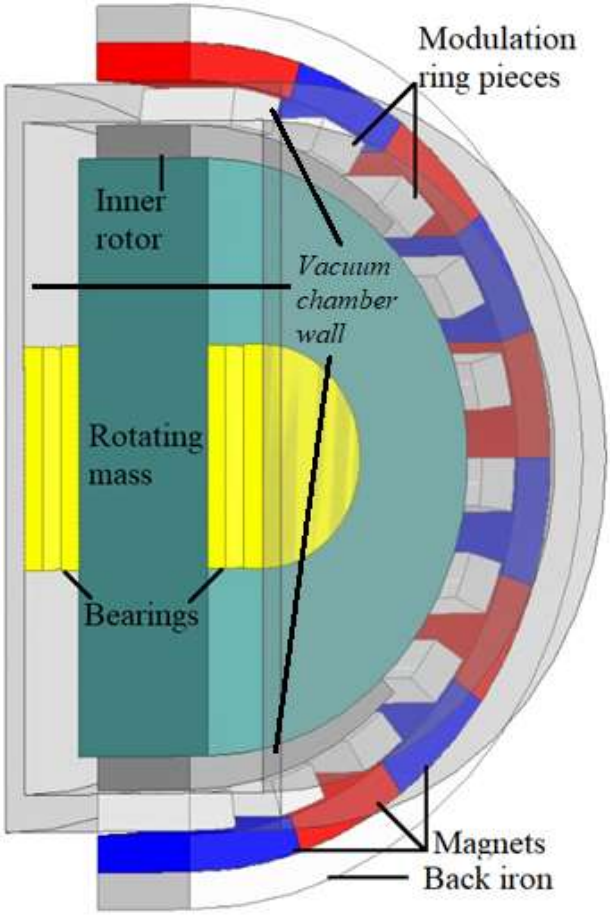

Source: The author

By making the modulation ring a part of the VCW, it is possible to transfer energy from a primary machine attached to the outer rotor to the rotation mass inside the VC attached to the inner rotor. Considering that the inner rotor has no magnets, with the removal of the outer rotor there would be no magnetic forces acting upon the inner rotor, and by consequence the rotation mass. This would allow for a no magnetic losses state from the MG once the outer rotor is decoupled, which is a very important feature for an energy storage system. The use of an RMG also makes it easier to skew the inner rotor, and by skewing the inner rotor, it is possible to reduce the torque ripple transferred to the rotating mass.

The alternative topology, seen in Fig. 16, incorporates the inner rotor to the rotating mass instead of just connecting to it. This approach places the inner rotor on the

circumference of the rotating mass, maximizing the radius of the inner rotor and the absence of a connection shaft makes the full length of the VC to be available for the rotating mass. The downside is the structural integrity as the rotating mass must also support the inner rotor at its edges and the torque applied to it. Given that very high speeds are usually achieved by this kind of device, the rotating mass material must be strong enough to sustain all this combined forces. The lack of a connection shaft also requires the horizontal magnetic bearing to be moved to the other top of the rotating mass, which makes the stability of the horizontal plane harder to implement.

3.1 FLYWHEEL ENERGY STORAGE SYSTEMS

Flywheel energy storage systems (FESS) are devices that store energy mechanical energy in a similar way as batteries store energy in a chemical way. Typically, a rotor with high inertia is accelerated at very high speeds to store energy in its movement. This acceleration is usually done with an electrical machine. Once accelerated, the rotating mass will store its mechanical energy until it is necessary. Since the energy transfer in this system depends on increasing and decreasing the velocity of the rotating mass, the machine responsible for accelerating the rotating mass should be able to work both as a motor and as a generator. The mechanical energy stored depends on the inertia and the square of the velocity, being more usual to use higher velocities than higher inertias. As the movement of the rotating mass results in friction losses and ventilation losses, this kind of device usually has a magnetically levitated rotating mass in a vacuum chamber. Given that this work proposes the use of a MG between the primary machine and the rotating mass, it must consider that the rotating mass will be levitated by the levitation and stability system, the speed gain from the primary machine and the rotating mass and the losses, especially when the device is not charging nor discharging.

3.2 USE OF A RELUCTANCE MAGNETIC GEARBOX

It is possible to use MGs with axial flux and radial flux to use the modulation ring as part of the VCW. Planetary Magnetic Gearboxes can have more than one gear ratio, depending on which rotors are connected. CyMG is shown in the literature [3] to achieve high gear ratios and torque densities at the same time. The use of different topologies of MGs, as seen in Chapter 2, is assessed under the characteristics of a flywheel as follows.

3.2.1 Magnetic planetary gearbox

Magnetic Planetary Gearboxes (MPG) can have more than one gear ratio at the same time [17], depending on which rotors are connected. Even though having more than one gear ratio available would be an interesting feature, coupling and decoupling a magnetically levitated rotor at high speed to different connection points would be difficult to accomplish. With the primary machine outside the VC, it is easier to control the speed of the inner rotor by controlling the speed of the outer rotor rather than changing the gear ratio. The lack of a modulation ring would also be a problem since a way to transfer energy inside the vacuum chamber wall would have to be implemented. In addition, considering that the assembly of a MPG would be more difficult than other MGs, this option was not chosen.

3.2.2 Cycloidal Magnetic Gearbox

A Cycloidal Magnetic Gearboxes (CyMG) has an eccentric inner rotor, with a variable air gap. Even though the literature shows that this kind of MG can produce high torque densities [3], a variable air gap would produce attraction forces that would change as the inner rotor rotates. Since all forces acting upon the inner rotor would have to be cancelled by the levitation system, a variable air gap would be difficult to incorporate. In the same way as for

PMG, CyMG have no modulation ring, implying in a difficulty to transfer energy to the inner part of the VC. For those reasons, the CyMG was not chosen for this application.

3.2.3 Axial Flux Magnetic Gearbox

Among MGs, there are two main types: axial flux and radial flux MGs. The use of an Axial Flux Magnetic Gearbox (AMG) would make the incorporation of the modulation ring to the VCW easier, since the wall to be modified would be a plain one, with the ferromagnetic pieces being inserted in simple holes. Another feature of using AMGs is that the VC could have a larger diameter then the diameter of the rotor inside the VC. Should the axis be vertically levitated, the attraction force between the rotor inside the VC and the modulation ring would help sustain the levitation. The problem with the attraction force is that it is not constant, so the levitation system would have to take it into account, and with the air gap being critical to the performance of the topology, every variation would have to be compensated. Aside from that, if the rotor inside the VC were horizontally levitated, the attraction force would provide no benefits, and would still have to be nullified. As mentioned in the previous chapter, AMG generally have a smaller torque density. Considering that the magnets inside the VC would maintain its interaction with the modulation ring even when the device is not charging nor discharging, a reluctance version of the AMG would have to be proposed. Considering all of these aspects, a CMG was chosen for the proposed topology.

3.2.4 Coaxial Magnetic Gearbox

The Coaxial Magnetic Gearbox (CMG) consists of an outer rotor, a modulation ring and an inner rotor, all concentric, offer many advantages and is one of the types of MGs with the most papers about it. According to [19] the torque density of CMG is higher than that of AMG. Since the flux is radially distributed in an even air gap, the attraction forces on the

inner rotor are mostly evenly distributed along its circumference. Because of this distribution, most of the forces are cancelled by the symmetric distribution. With all parts and the flux being concentric, should an axial displacement occur, a force would appear to oppose it, trying to realign the parts. This effect is good for non-intentional displacements, but it is an issue for the decoupling of the device.

By having magnets on both the inner and outer rotor, the removal of the outer rotor would leave the inner rotor magnetically coupled to the modulation ring by the magnets in the inner rotor. In this configuration, the only way to decouple the rotating mass would be by moving the inner rotor away from the modulation ring. Since the modulation ring is a part of the VCW, moving it would not be a suitable option. As the inner rotor is attached to the rotating mass, it is possible to move the inner rotor but the entire levitation system would have to be designed to allow it, and the mass and inertia of the rotating mass would still be a problem.

3.2.5 Reluctance Magnetic Gearbox

The Reluctance Magnetic Gearbox (RMG) is a type of CMG with no magnets in the inner rotor. Instead of coupling the magnetic fluxes of the magnets of both rotors, the RMG uses the flux of the magnets in the outer rotor modulated by the modulation ring to couple the inner rotor using reluctance torque. Being a type of CMG it has the advantages of this type of MG. An extra advantage is the possibility of a no magnetic loss state should the magnets of the outer rotor be removed, when there would be no magnetic sources. This kind of MG has a lower torque density compared to a conventional CMG. It is also more suitable for high-speed application for having a more robust inner rotor.

3.3 MODULATION RING AS PART OF THE VACUUM CHAMBER WALL

The use of Magnetic Gearboxes (MGs) as a way to transfer energy to controlled environments has been proposed in papers such as in [23] for clean rooms or explosive, corrosive and contaminating environments and in naval applications to separate the drive system from the propeller [18-19]. If energy is to be transferred with a physical connection, the isolation would become difficult and the friction between the VCW and the shaft that would connect both sides of the wall would be enormous, especially considering high speeds. The high speed, the vacuum environment around the rotor inside the VC and the magnetically levitation aspect makes the use of active systems in the inner rotor difficult. For that reason, the use of a MG with the modulation ring as part of the VCW for the kinetic energy transferring system presents itself as a good option. Fig. 17 shows the proposed insertion.

Figure 17 - Modulation ring pieces inserted into the vacuum chamber wall

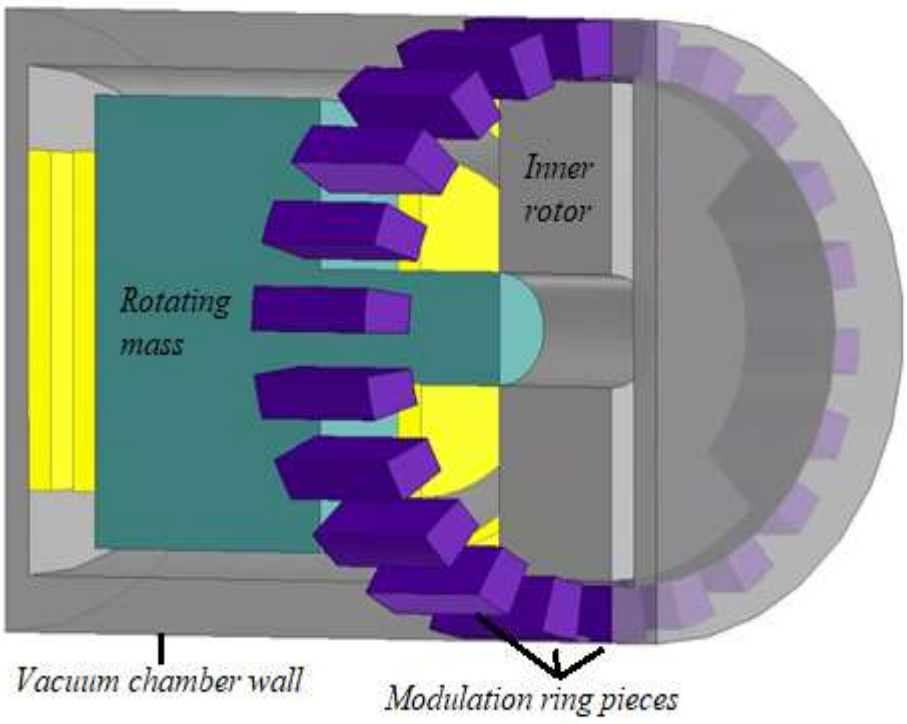

Source: The author

From the MG point of view, this insertion does not produce any changes in terms of the topology. The ferromagnetic parts and the structure holding them are extended to connect to the VCW and closed to seal the VC. For the VC, as long as the segments that now compose the VCW are sealed and have mechanical resistance to withstand the forces produced by the difference in pressure from both sides, nothing has changed in terms of the mechanical structure.

4 MAGNETIC DESIGN

This chapter explains how the magnetic design of the prototype was conducted; the simulations that were made to verify the behaviour of the prototype towards changes in its geometry and the magnetic considerations. The mechanical restrictions and their implications will be presented and shown in the next chapter, with some being mentioned in this chapter.

4.1 SIMULATION PROCEDURES

For the simulations presented in this chapter and in the next chapter, the procedures undertaken to obtain the values are shown in this section.

The drawing of the RMG was done from the inside towards the outside. The first part was the inner rotor, as shown in Fig. 18.

Figure 18 - Inner rotor drawing

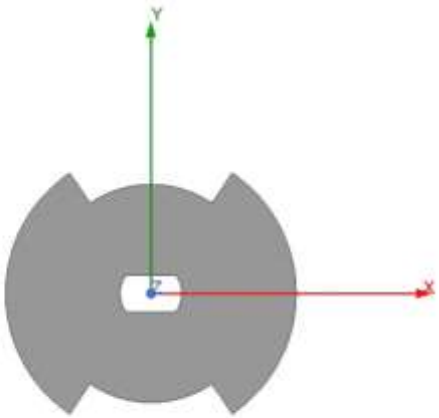

Source: The author

The inner rotor was drawn with a segment from the centre up to the R_{out} value. This segment was swept by the polar arc angle were both values were set as a variable parameter.

The R_{in} was made with a cylinder for the value of 30 mm and combined with the swept segment. A hole was made inside the inner rotor with a 17 mm circle and a 10 mm square.

Next came the drawing of the modulation ring pieces. Initially a single modulation ring piece was drawn using a segment that started in the X-axis, at a position given by the value of R_{out} plus the value of the G_{in} ending at a position given by R_{out} plus G_{in} plus H_s. All variables set as a parameter that could be changed. For the default values G_{in} was 1 mm and H_s was 10 mm. This segment was swept around the Z axis by an angle set by 360º divided by twice the number of modulation ring pieces times a ratio variable to change the width of the modulation pieces. After that, the modulation ring piece was centred at the X-axis. Fig. 19 shows the created modulation ring piece.

Figure 19 - Modulation ring drawing

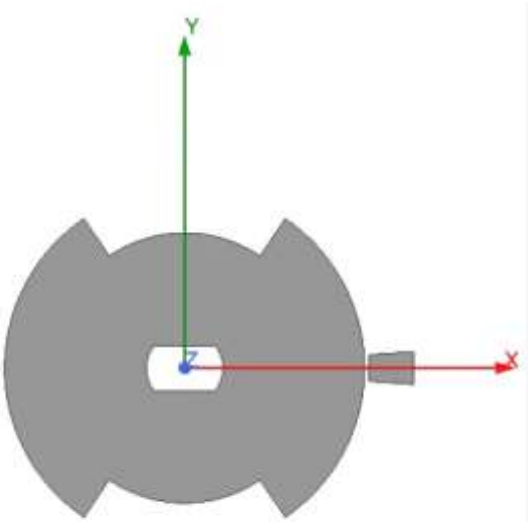

Source: The author

This modulation ring piece was duplicated around the Z-axis to form the modulation ring. In between the pieces as placed the aluminium structure to fill the spaces between each modulation ring piece.

To form the outer rotor the first step was to make the magnets, shown in Fig. 20.

Figure 20 - Magnets drawing

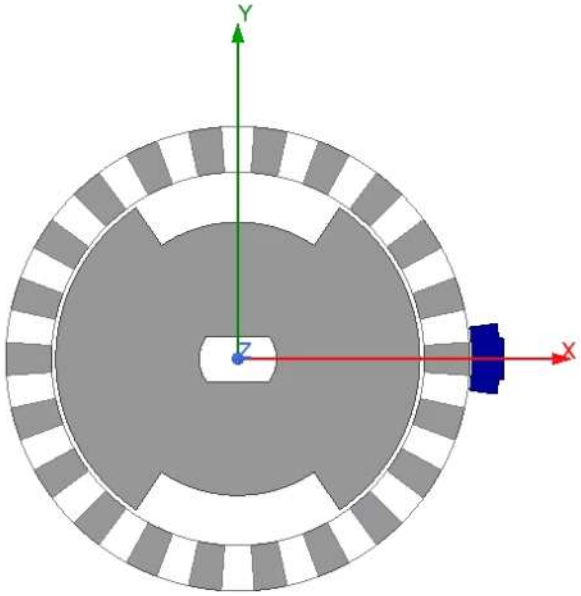

Source: The author

The magnets were made initially in the same way as the modulation ring, using a segment that started at a position given by R_{out} plus G_{in} plus H_s plus G_{out} and ended at a position given by the same position plus H_{mag}. By sweeping this segment around the Z-axis by and angle equivalent to 360º divided by the number of poles of the outer rotor the first magnets is obtained. This initial magnet is combined with a swept segment 1-mm long and with half the arc of the magnets to make the dovetail.

The last part in the drawing of the RMG is to make the back iron. It can be done by making a segment in the X-axis that starts at the position given by the R_{out}, plus the G_{in}, plus the H_s, plus the G_{out}, plus the H_{mag} and ends at the same position plus H_{fe}. Sweeping this segment by 360º the back iron is formed. Fig. 21 shows the final RMG drawn.

Figure 21 - Back iron drawing

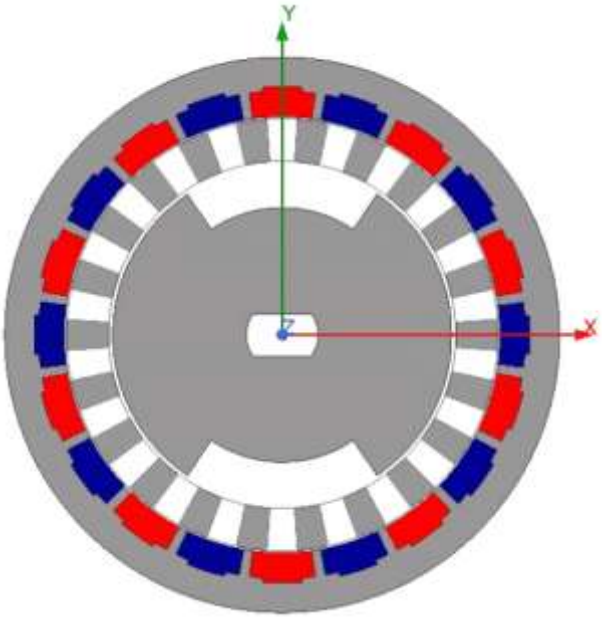

Source: The author

The last part is to add the back iron teeth, which can be done by making the same segment used in the making of the magnets and sweeping it around the Z-axis by the angle of the back iron teeth angle. The tooth is than rotated 9º to be placed between two magnets. Duplicating the tooth around the Z-axis by an angle of 18º each and combining it with the back iron the final back iron is done. To fix the magnets a copy of the back iron can be used and subtracted of the magnets.

The boundary region used was set to be 2 mm away from the back iron, since the is almost no magnetic flux going out of the back iron. The boundary parameter used was the balloon, since it offers the fastest resolutions and does not distort the magnetic flux through it.

Each simulations conducted was transient with a time span varying from zero up to 5 ms with steps of 1 μs unless stated otherwise in the respective section.

A moving band was set in a cylinder with whose radius is given by R_{out} plus half the G_{in}, that envelops the inner rotor and part of the inner air gap. A second moving band was used made with a cylinder with a radius 1 mm longer than that of the back iron and a hole

with a radius equivalent to the sum of the R_{out}, plus the G_{in}, plus the H_s and half the G_{out}. This second band envelops the magnets, the back iron and half the outer air gap. Fig. 22 shows the two bands.

Figure 22 - Moving bands

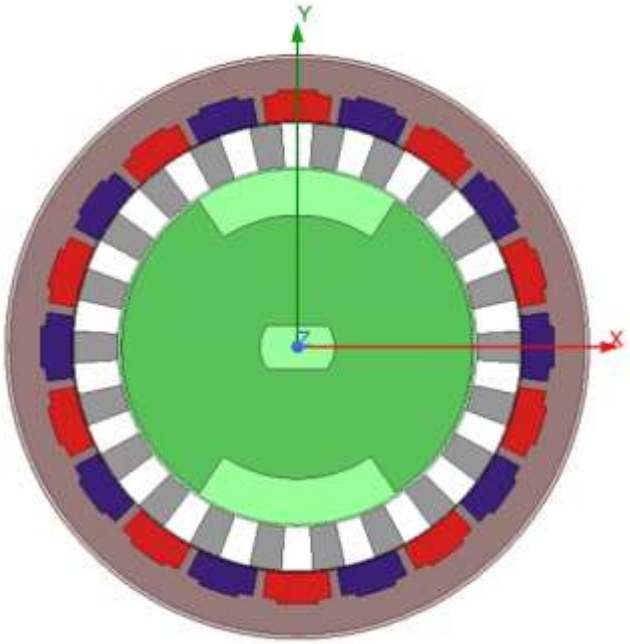

Source: The author

The magnetization of the magnets was set as radially were the north pole was set as positive towards the radius and the south pole as negative towards the radius. The speed of the inner moving band was set as negative to adjust to the negative gear ratio.

4.2 PROPOSED TOPOLOGY OVERVIEW

As explained in the last chapter, the proposed topology is a Reluctance Magnetic Gearbox (RMG) with segmented inner rotor used as a way to move the primary machine of a Flywheel Energy Storage System (FESS) out of the vacuum chamber. An RMG has an inner rotor with a certain number of poles and no magnets, in the same way as a conventional reluctance machine. An outer rotor with another number of poles contains magnets with radial

magnetization and alternating polarity that provide the magnetic flux to the prototype. Between the rotors is a group of ferromagnetic pieces evenly distributed that are used to modulate the flux from the outer rotor to the inner rotor. As presented in Eq. 14 and 15, the number of poles in both rotors determines the speed gain and the number of modulation pieces, with two possibilities, i.e. a number for both rotors rotating in the same direction and a number for opposite rotating directions.

After simulating the machine for variations of its geometry, the base values were obtained based on the results. The choice for each value will be addressed in the following sections. The base values and materials used for the simulations made and the ones used for the assembled prototype are given in Table 1.

Table 1 Base values for simulations and prototype dimensions

Variable	Value
Inner rotor inner radius, R_{in}	30 mm
Inner rotor radius, R_{out}	40 mm
Polar arch angle, α_{in}	112º
Relative angle, θ_r	48º
Inner air gap length, G_{in}	1 mm
Modulation ring thickness, H_s	10 mm
Outer air gap length, G_{out}	0.5 mm
Magnets thickness, H_{maq}	6 mm
Back iron thickness, H_{fe}	8 mm
Skewing angle, Skew	10º/0º
Axial length	50 mm
Inner rotor poles, Z_h	2
Outer rotor poles, Z_l	20
Modulation ring pieces, Z_s	22
Back iron teeth angle	2.5º
Dovetail length	1 mm
Magnets type	NdFeB N35
Residual magnetic flux density	1.23 T
Coercive magnetic field strength	-890 kA/m
Electrical steel sheets	E230
Back iron material	AISI 1020

The choice for each value will be better explained in the following sections. The variables are shown in Fig. 23.

Figure 23 - Main variables of the RMG

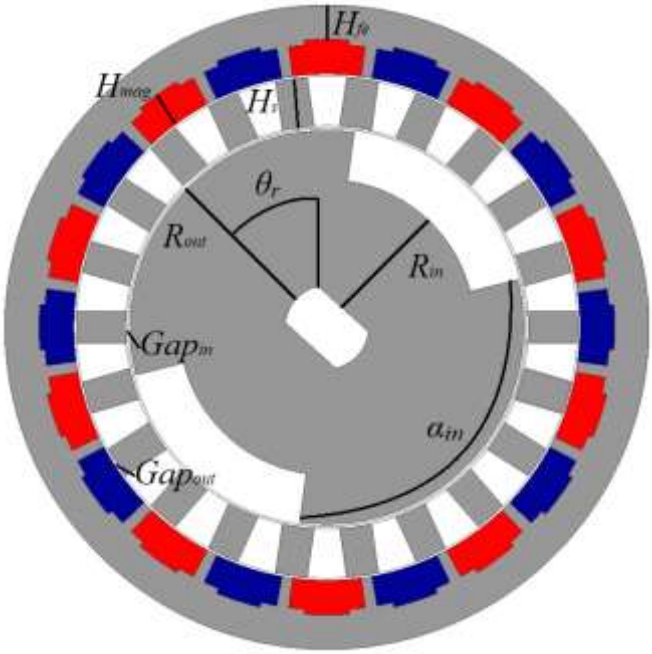

Source: The author

4.3 INNER AIR GAP

The air gap between the inner rotor and the modulation ring is also the air gap between the rotating mass of the FESS and the Vacuum Chamber Wall (VCW). As the rotating mass, and by consequence, the inner rotor will be levitated by means of electromagnetic forces, the air gap between the inner rotor and the modulation ring also sets the maximum oscillation the levitation system has to maintain or risk a collision. Considering that the inner rotor will be rotating at 36,000 rpm at maximum speed, a collision with the modulation ring and by consequence the VCW would be catastrophic. In terms of safety, the bigger the inner air gap, the better, as it reduces the restrictions on the levitation system and its stability.

In RMG the main magnetic flux path to the inner rotor comprises the magnets, towards the outer air gap between the outer rotor and the modulation ring, the ferromagnetic

pieces in the modulation ring, through the inner air gap, and then the inner rotor. The magnetic path from the inner rotor is through the inner air gap, to the modulation pieces, the outer air gap and back to the magnets. The magnetic circuit is also being short circuited by the back iron in on the other side. Fig. 24 shows the described magnetic path.

Figure 24 - Main magnetic path of RMG

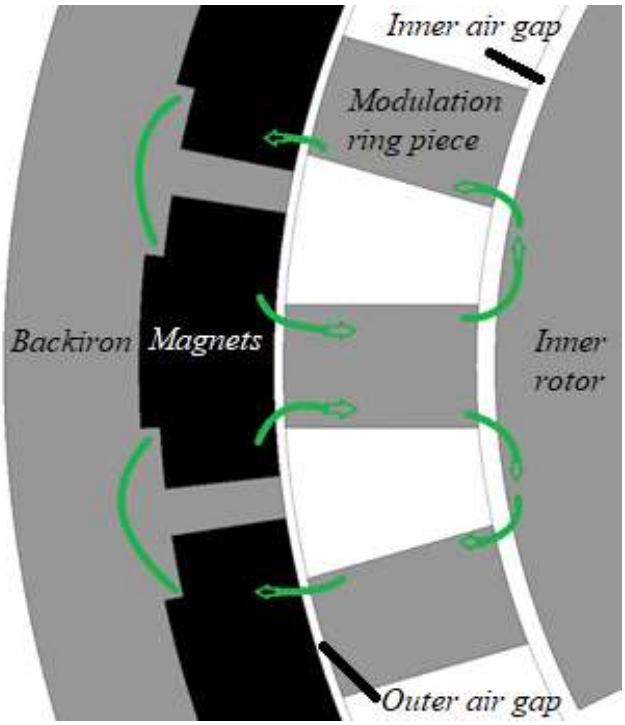

Source: The author

In Fig. 24, the green lines are the main flux paths of the RMG.

The magnetic reluctance of the air is much higher than that of the materials used in the modulation pieces, inner rotor and back iron, and so has a high impact on the total reluctance. Since the linkage magnetic flux must be stablished through the inner air gap twice the length of the latter along the path, it has an even bigger effect on the total reluctance. As it will be shown in the next sections, the torque output in the inner rotor is directly dependent on the magnetic flux density. From a basic equation of relationship between magnetic flux,

electromotive force and magnetic reluctance, shown and explained in [24], the higher the magnetic reluctance the lower the magnetic flux density and the lower the torque output.

From a safety and stability point of view, the bigger the inner air gap, the better for the levitation system. From a performance point of view, the smaller the air gap the better the output torque. To solve this compromise between safety and performance, the inner air gap length was set to the same 1-mm long as implemented in [25] for a magnetically levitated rotor as a parameter of an air gap that was implemented and allows for stable magnetic levitation.

Even though the inner air gap was set based on a value that would allow a safe magnetic levitation, the behaviour of the output torque in terms of the air gap length was simulated by means of a parametric model using Ansys Electronics Desktop® software. The parameters used were the base topology presented in Table 1, varying only the inner air gap. Fig. 25 shows the results of the parametric simulation of the inner air gap varying from 0.35 mm up to 1.5 mm with steps of 0.01mm for each simulation.

Figure 25 - Average torque output of inner rotor for various inner air gap length

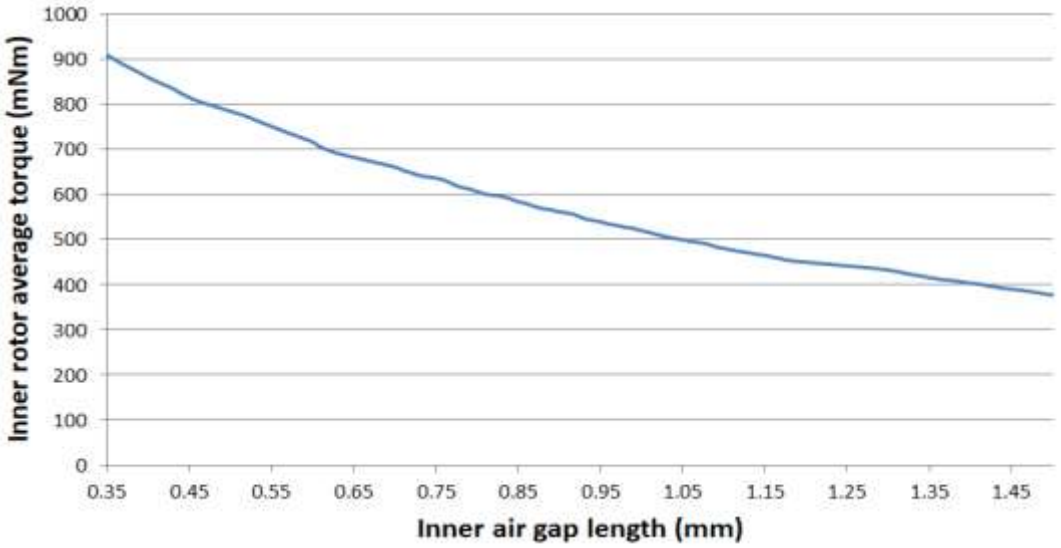

Source: The author

In Fig. 25, it is easy to see that the average torque output of the inner rotor diminishes as the inner air gap increases. Associating the equivalent permeance of the inner airgap to the permeance of the modulation ring in Eq. 19, an increase of the air gap length results in a diminished permeance of the modulation ring, and as a consequence a diminished main magnetic flux and a diminished torque output.

4.4 OUTER AIR GAP

The magnetic path the main linkage magnetic flux in an RMG comprehends twice the length of the inner air gap as well as the outer air gap. For that reason, the analyses made for the inner air gap is also valid for the outer air gap. The outer air gap separates the magnets and the modulation ring pieces while the inner air gap separates de modulating ring pieces and the inner rotor. When considering the magnetic aspects, the increase in the outer air gap reduces the coupling between the modulation ring and the inner rotor and the magnets in the outer rotor, while the increase in the inner air gap decreases the coupling between the inner rotor and the rest of the topology. Since the magnetic flux stablished through the magnets can only go through the outer air gap into the modulation ring pieces or get straight to the next magnet as leakage flux, which has a very high reluctance associated with because the path is mainly composed of air, the main effect is a reduction of the main flux. The increase of the inner air gap length has the same effects but it also increases the amount of magnetic flux that goes across the outer air gap, through the modulation ring pieces, but returns through another modulation ring piece instead of going through the inner rotor to generate torque. This extra parallel path makes the drop of the average torque output of the inner rotor larger for increases of the inner air gap length than the ones observed for increases of the outer air gap length. The main magnetic flux path and the main leakage flux paths are shown in Fig. 26.

Figure 26 - Magnetic paths of RMG

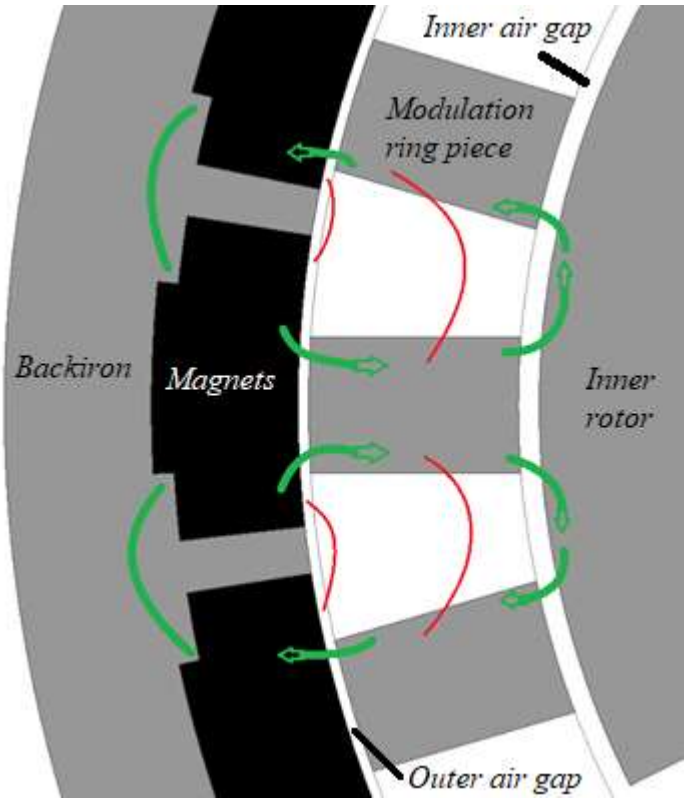

Source: The author

In Fig. 26, the green lines are the main flux lines and the red lines are the main leakage flux lines.

Considering a stationary VCW and a fixed primary machine attached to the outer rotor, both parts have mechanical support in a very similar way as to a conventional electric machine. For that reason, a shorter outer air gap can be used to increase performance as the safety issue is not so difficult to overcome. It is not uncommon to find electrical machines with air gaps as small as 0.35 mm. Given that, the modulation ring must fit between two high-speed rotors and to prevent any issues regarding vibrations and mechanical tolerances, the outer air gap was set to 0.5 mm. Since both air gaps must be crossed twice by the main flux and the same material constitutes both, the reluctance of the inner air gap shows dominance over the reluctance of the outer rotor for having twice the length. This also helps explain for

the drop in the average torque output to be higher for increases of the inner air gap when compared with the outer air gap.

To verify the behaviour of the torque output of the inner rotor for different outer air gaps, a parametric simulation using FEA software was conducted. Fig. 27 shows the results of the simulations for outer air gaps varying from 0.35 mm up to 1.5 mm with steps of 0.01 mm.

Figure 27 - Average torque output of inner rotor for various outer air gap length

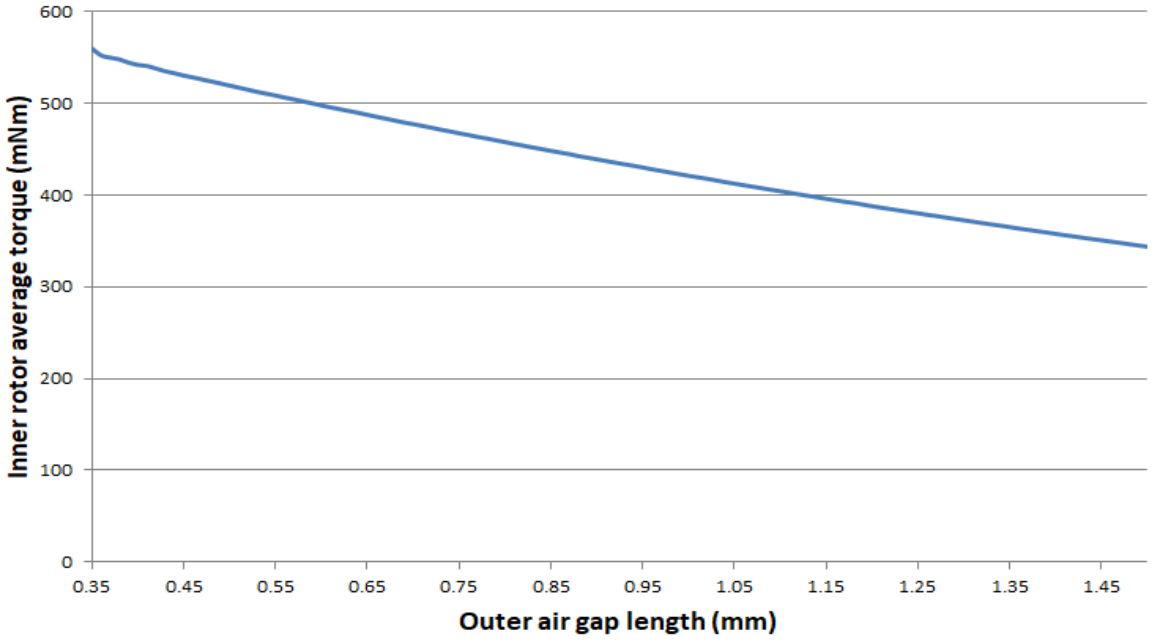

Source: The author

As expected, the results shown in Fig. 27 show a decrease in the average torque output as the outer air gap length increases. The average torque output for inner and outer air gaps, of 1 mm and 0.5 mm respectively, were simulated and the results are shown in Table 2.

Table 2 Inner rotor average torque output in mNm for different air gaps

Air gap length	G_{in} 0.5 mm	G_{in} 1 mm
G_{out} 0.5 mm	775 mNm	519 mNm
G_{out} 1 mm	627 mNm	421mNm

By comparing the case for an outer air gap of 0.5 mm and inner air gap of 1 mm and a combination of outer air gap of 1 mm and inner air gap of 0.5 mm, both cases have the same total air gap length. The combination with larger outer air gap resulted in a 20.8% larger

average torque output. This result shows good accordance with what was explained about the increase in flux leakage in the modulation ring when the inner air gap is increased. Since both the air gaps can be associated with the modulation ring permeance, an increase of either air gaps would result in a decrease of the modulation ring permeance and a smaller magnetic flux and torque output.

4.5 INNER ROTOR

The inner rotor is the connection between the rotating mass and the rest of the assembly. It is composed of laminated ferromagnetic material and its number of poles depends on the speed gain needed. A two-pole inner rotor has an inner cylinder attached to arcs that compose the poles, called polar arcs. The axial length was set for the project as being 50 mm. The inner rotor was segmented axially in five 10-mm parts. The main variables for the inner rotor are the inner rotor inner radius, R_{in}, the inner rotor radius, R_{out}, the polar arcs angle, α_{in} and the skewing angle, *Skew*. The inner rotor inner radius is the radius of the inner cylinder that is connected to the shaft that makes the connection between the inner rotor and the rotating mass. The inner rotor radius is the total radius of the inner rotor that corresponds to the radius from the centre of the inner rotor up to the edge of the poles. The polar arch angle, α_{in}, is the total angle formed by one pole. The skewing angle is the angular displacement angle between the segments. The proposed inner rotor is shown in Fig. 28.

Figure 28 - Inner rotor

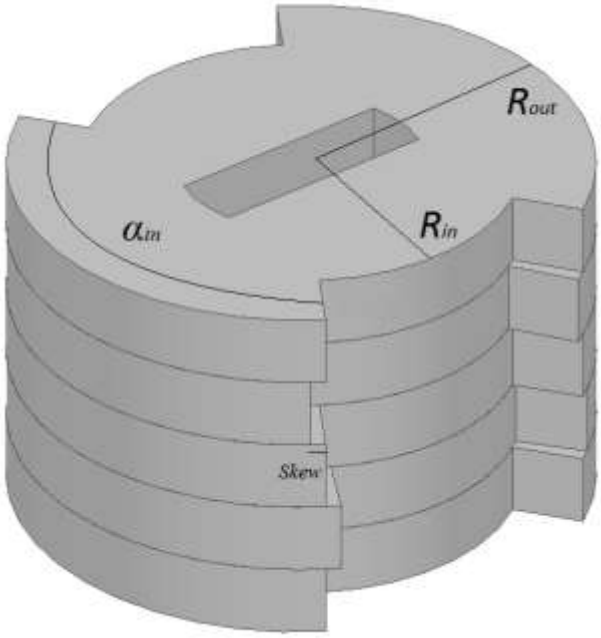

Source: The author

4.5.1 Inner rotor inner radius

The majority of the magnetic flux on the inner rotor is concentrated at the edges of the poles. For that reason, the R_{in} plays a smaller magnetic role as long as it is not too close to the value of the R_{out}. For values of R_{in} close to the values of the R_{out} part of the flux starts to interact with the interpolar region of the inner rotor, which reduces the reluctance force generated on the rotor. This effect is similar to a reluctance machine whose poles are too short and close to the centre of the rotor. The difference between the reluctance of the poles and the interpolar regions starts to diminish as R_{in} increases, reducing the torque produced. Fig. 29 shows the magnetic flux density of the topology for a given relative position between the inner rotor and outer rotor.

Figure 29 - Magnetic flux in the RMG

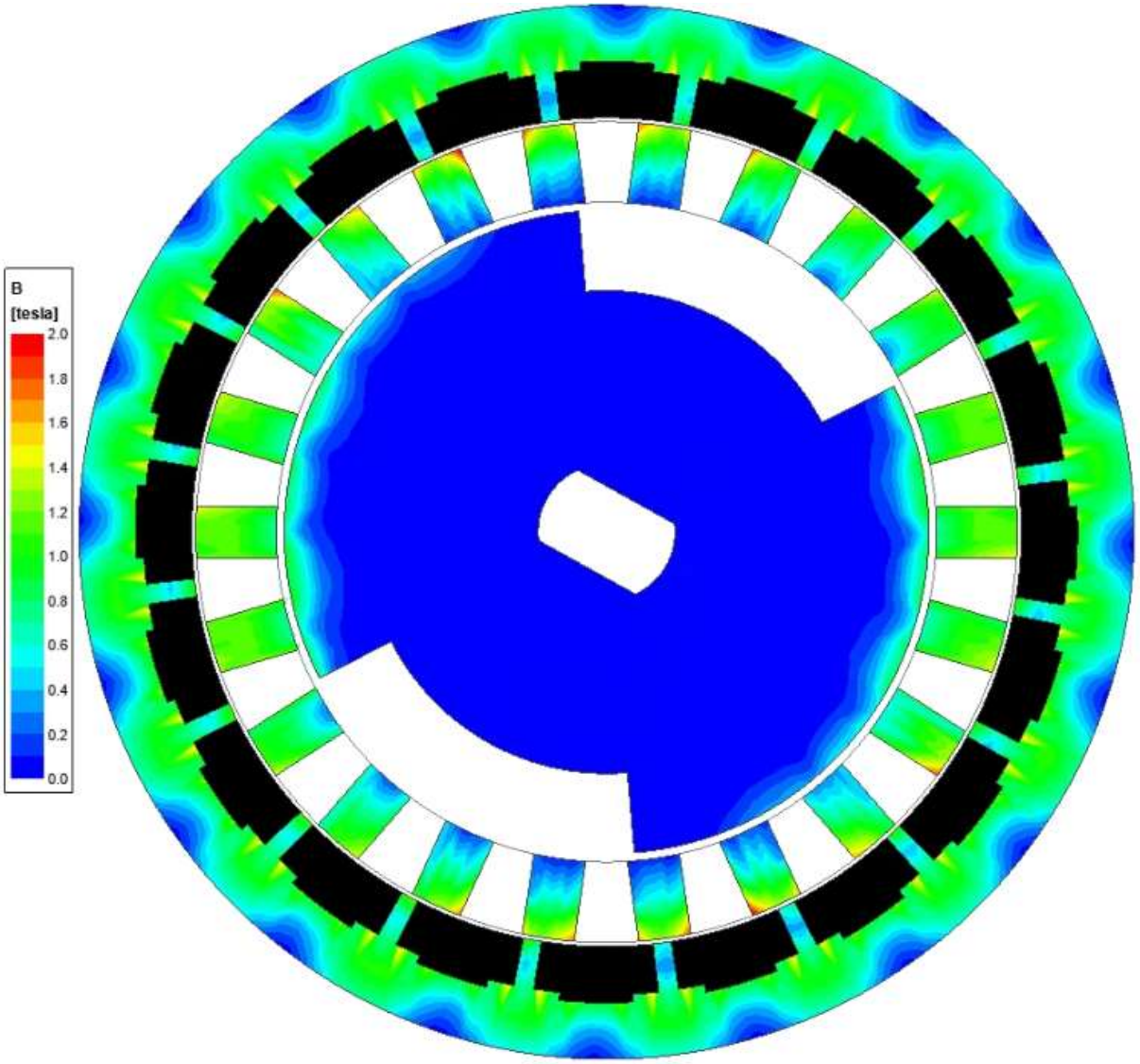

Source: The author

As presented in Fig. 29, the magnetic flux in the inner rotor is concentrated on the edges of the poles. In order to evaluate the values where R_{in} gets too close to the R_{out}, FEA parametric simulations were conducted for values of R_{in} varying from 15 mm up to 39 mm with steps of 0.1 mm. The result of the parametric simulations is shown in Fig. 30.

Figure 30 - Average torque output of inner rotor for various R_{in}

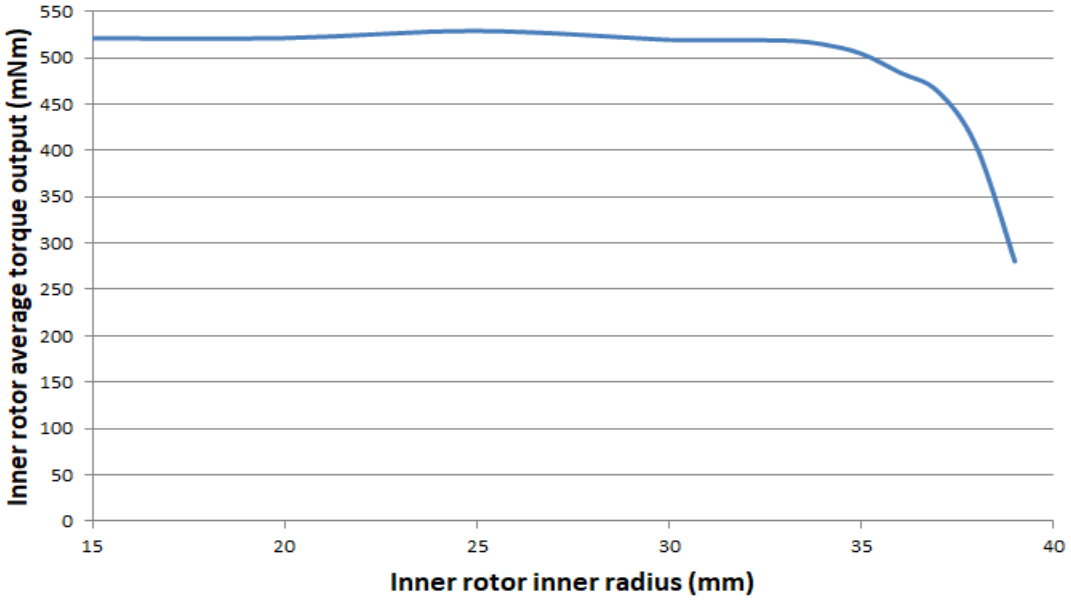

Source: The author

The average torque output for different values of R_{in}, as shown in Fig. 30, is stable from small values up until it gets close to the value of R_{out}, when a substantial drop can be seen. Given that R_{in} has little impact on the performance of the topology, the chosen value was set to 30 mm, a value that does not result in any impact on the torque output but also provides a more robust inner rotor. Associating the R_{in} to the permeance of the inner rotor, for values of R_{in} much smaller than the value of the R_{out}, the R_{in} has no effect, but, as the values become closer, the amplitude of the variable part of the permeance in Eq. 16 diminishes, which reduces the overall torque output in Eq. 19.

4.5.2 Inner rotor radius

As explained for R_{in}, the magnetic interaction of the inner rotor is concentrated on the edges of the poles. Since all the forces produced on the inner rotor are of magnetic origin and in its majority concentrated on the edges, the average torque output can be assumed to be the result of the combined magnetic forces applied on the pole edges, which are at a distance

from the centre. The R_{out} is the distance from the centre that the magnetic pressure is applied and for that reason, the torque output is directly dependent of it. By using parametric simulations of FEA for values of R_{out} varying from 35 mm up to 80 mm with steps of 0.1 mm the results of Fig. 31 were obtained.

Figure 31 - Average torque output of inner rotor for various R_{out}

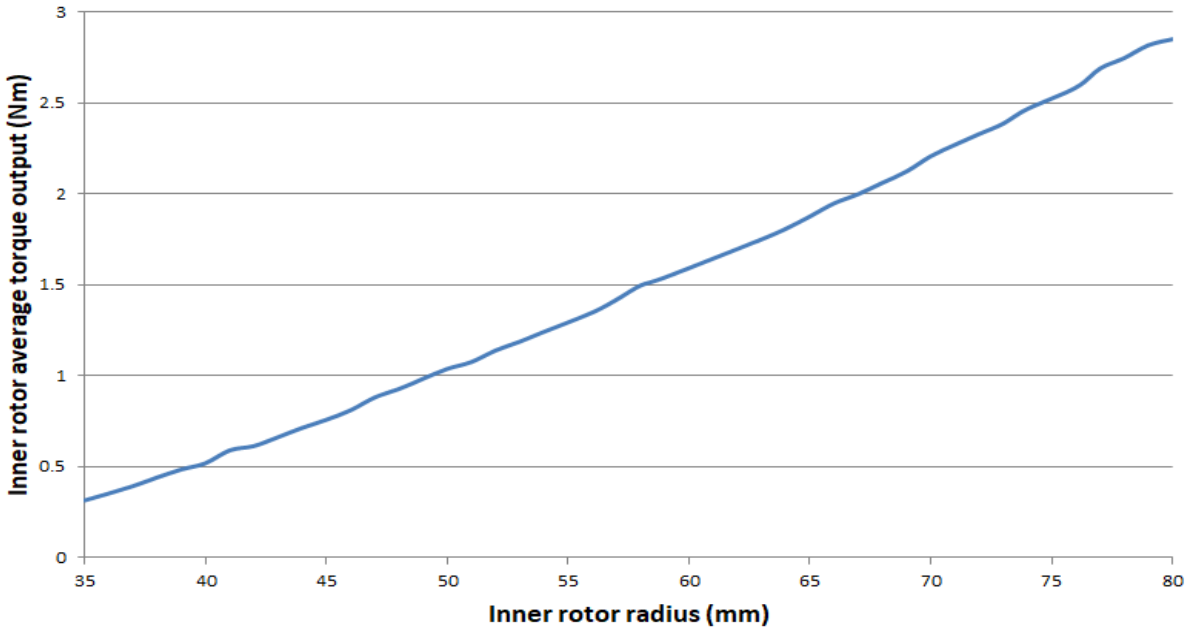

Source: The author

The results presented by Fig. 31 makes it easy to see that even for small increases of R_{out}, large increases in torque output can be achieved. The only problem with changing R_{out} comes from the fact that it is inside the VC and because of that, it can be a problem when considering the size of the vacuum chamber. This problem will be better discussed in the next chapter.

4.5.3 Inner rotor polar arch angle

For a two-pole inner rotor, using a 90º polar arch angle can be intuitive, but it is important to analyse the consequences of using different angles. For values of inner rotor

polar arch angles varying from 10º, yielding very thin poles, up to 170º, when there is almost no separation between poles, with steps of 0.1º, a parametric simulation, whose results are shown in Fig. 32, was conducted to evaluate the effects of different inner rotor polar arcs angles.

Figure 32 - Average torque output of inner rotor for various inner rotor polar arch angles

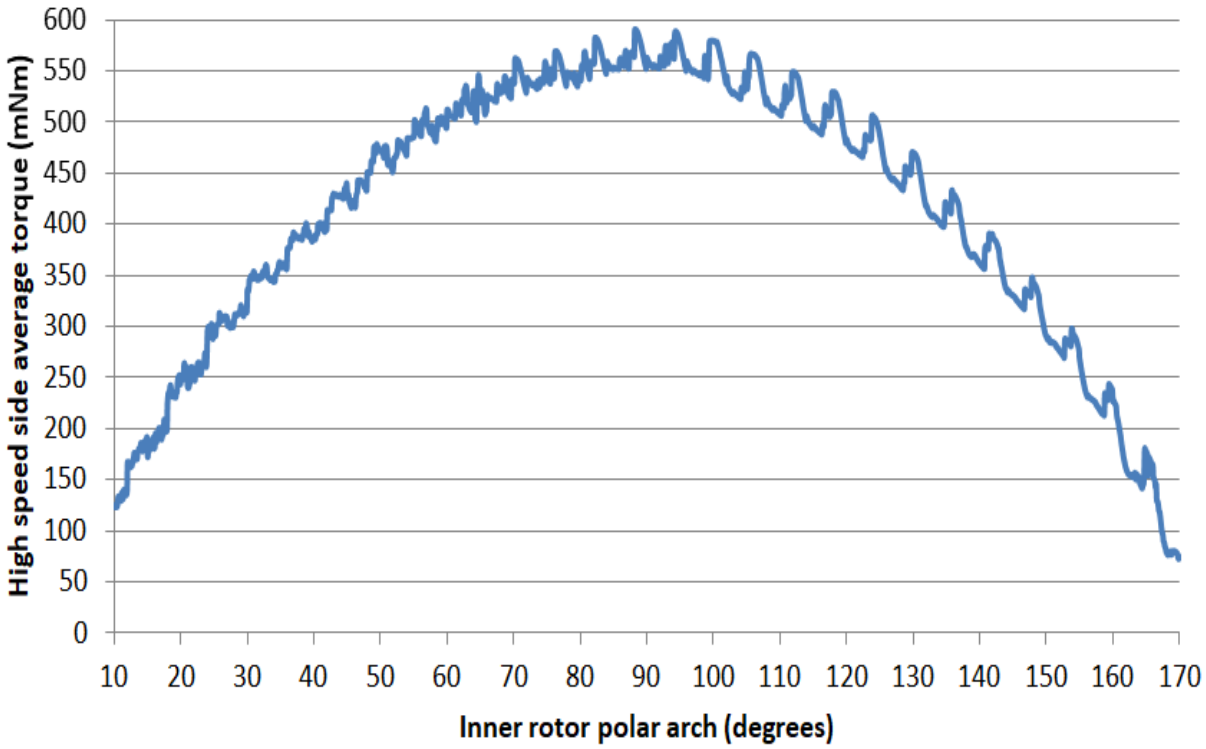

Source: The author

The results of the simulations presented in Fig. 32 reveal that even though the main effect is close to a sinusoidal function of the polar arch, there are also some variations that produce peaks on top of the sinusoidal function. As it was presented in [22], the torque output has some higher frequency components then that of the inner rotor and outer rotor nominal speed. This topic will be resumed in another section, where the relative angle between the inner rotor and the rest of the topology in conjunction with the polar arch angle is addressed.

4.5.4 Inner rotor relative angle

The operation principle of an RMG is that both the inner and the outer rotor are to be synchronized at different speeds, depending on the number of poles of each rotor and the number of modulation pieces. As shown by the literature [7-13], MGs lose synchronism when an excessive torque is applied, with rotor slipping until the excessive torque is reduced and the MG regains synchronism. Much like in a synchronous machine, the RMG can have a relative angle between the synchronized rotors, which results in torque being produced by the RMG in an attempt to nullify that angle. An analogy can be made with the load angle of a synchronous machine for the behaviour of the torque output regarding the relative angle. However, in a RMG each rotor synchronizes itself with a different speed. By keeping one of the rotors or the modulation ring as reference, the relative angle changes with time as both rotors rotate with different speeds and with the same or opposite directions.

In order to verify the effects of different relative angles, Fig. 33 shows the results of a parametric simulation using FEA, where the relative angle was varied from 0º up to 180º, with steps of 0.1º.

Figure 33 - Average torque output of inner rotor for various inner rotor relative angle

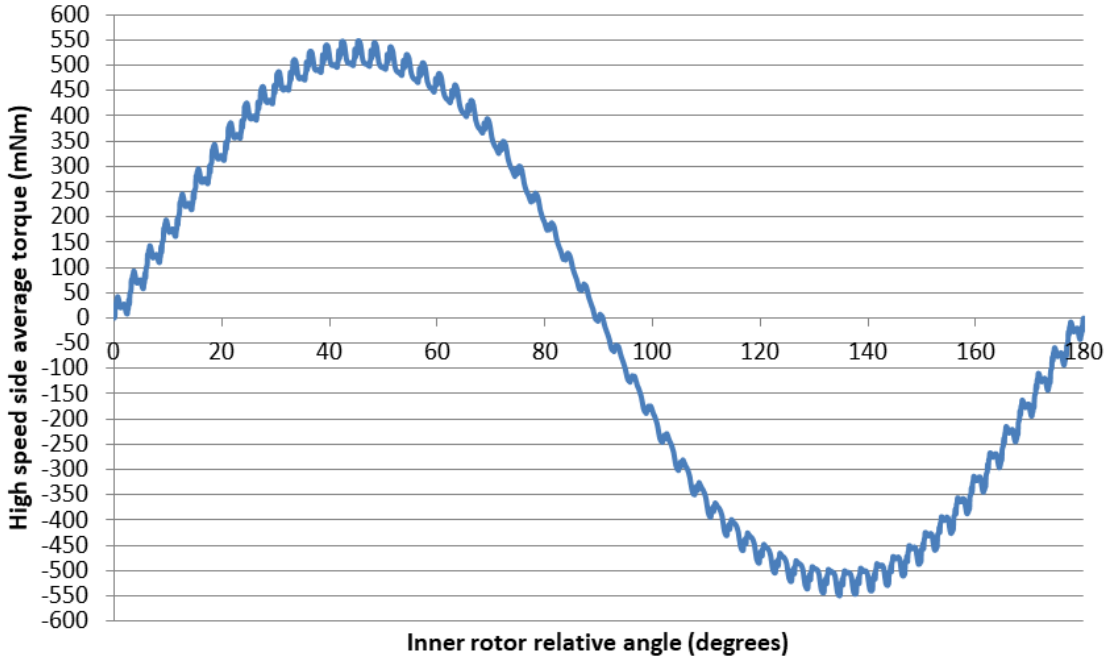

Source: The author

In Fig. 33, an 180 º symmetry can be seen, which was expected for a two-pole inner rotor. As seen for the inner rotor polar arch angle, the result of varying the relative angle can be expressed as a sinusoidal function with a higher order function producing peaks on top of that. The same explanation for the origin of the higher order function mentioned in the polar arch angle section can be used for the relative angle.

4.6 MODULATION RING PIECES

The working principle of an RMG is the flux modulation that couples both rotors at different speeds. Since the flux modulation occurs in the modulation ring, it is the connection between both rotors. The magnetic flux produced by the magnets stablishes through the outer air gap into the ferromagnetic modulation pieces. At this point, part of the flux follows the ferromagnetic material as main flux and part crosses the gap between the modulation pieces into the next modulation piece and then back to the outer air gap and to the next magnet. This part of the flux can be considered as leakage and does not contribute to the torque generation

on the inner rotor since it does not pass through the inner rotor. The main flux that follows through the ferromagnetic piece of the modulation ring crosses the inner air gap into the inner rotor and then back to the inner air gap between the next modulation piece and the inner rotor. The magnetic path of the main flux follows the ferromagnetic piece again through the outer air gap into the next magnet. Fig. 34 illustrates these magnetic flux paths.

Figure 34 - Magnetic flux path through the outer air gap

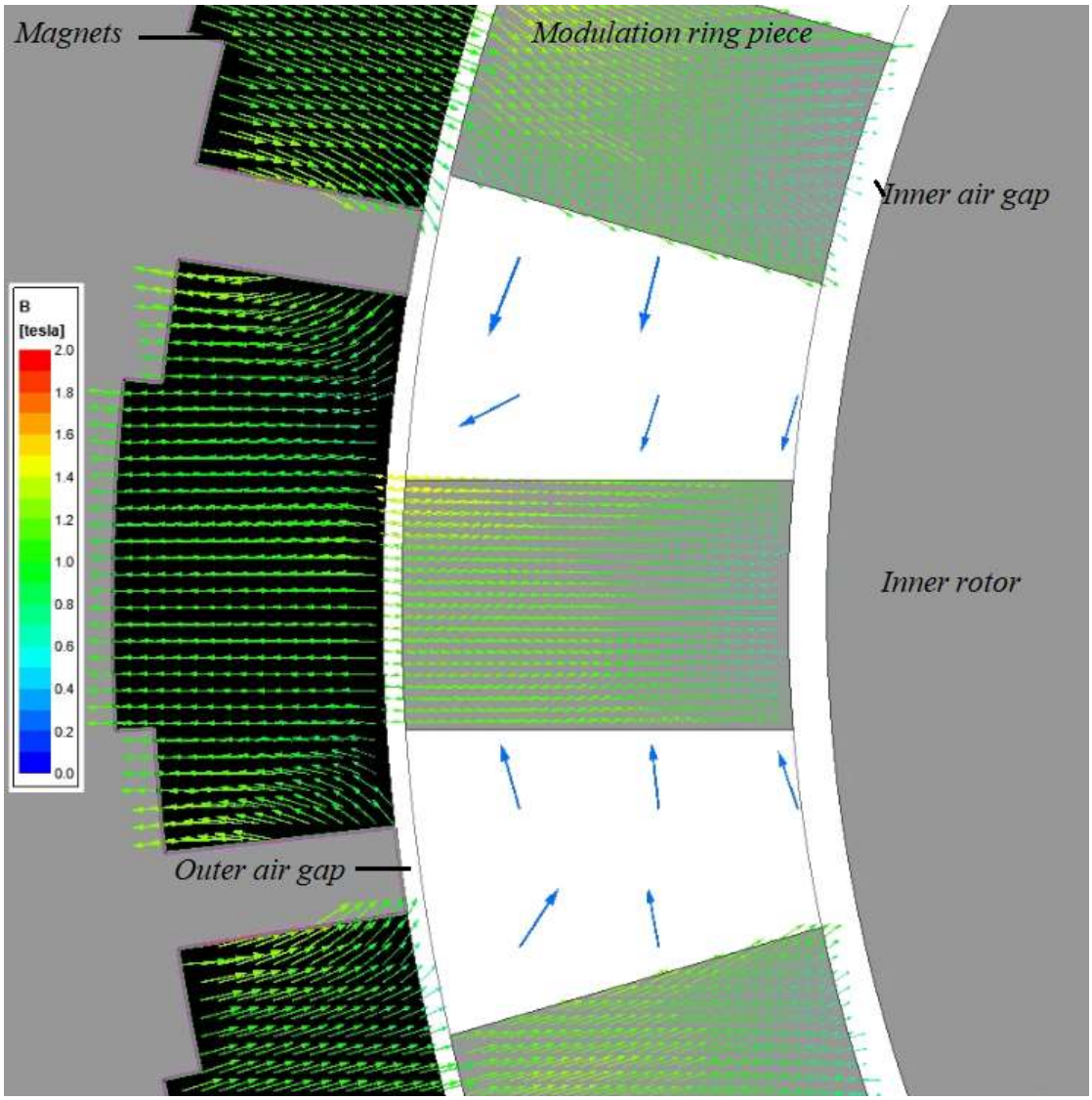

Source: The author

When the main flux is crossing the first outer air gap into the first modulation piece, it has two main paths. The first is to follow the described path with two inner air gaps, two

times the length of a modulation piece (through the first one and back through the second) a section of the inner rotor and the outer air gap. This is the path with the magnetic flux that produces torque. A third flux path is through the gap between two modulation pieces, a part of the first and the second modulation pieces and the outer air gap again. This third path produces the leakage flux and tries to slow down the outer rotor, producing magnetic losses. The difference of the total reluctance of both paths is what determines if the flux will be modulated (first path as main flux) or will just be producing losses as leakage flux. The magnetic flux through the modulation ring is shown in Fig. 35.

Figure 35 - Magnetic flux path through the modulation ring

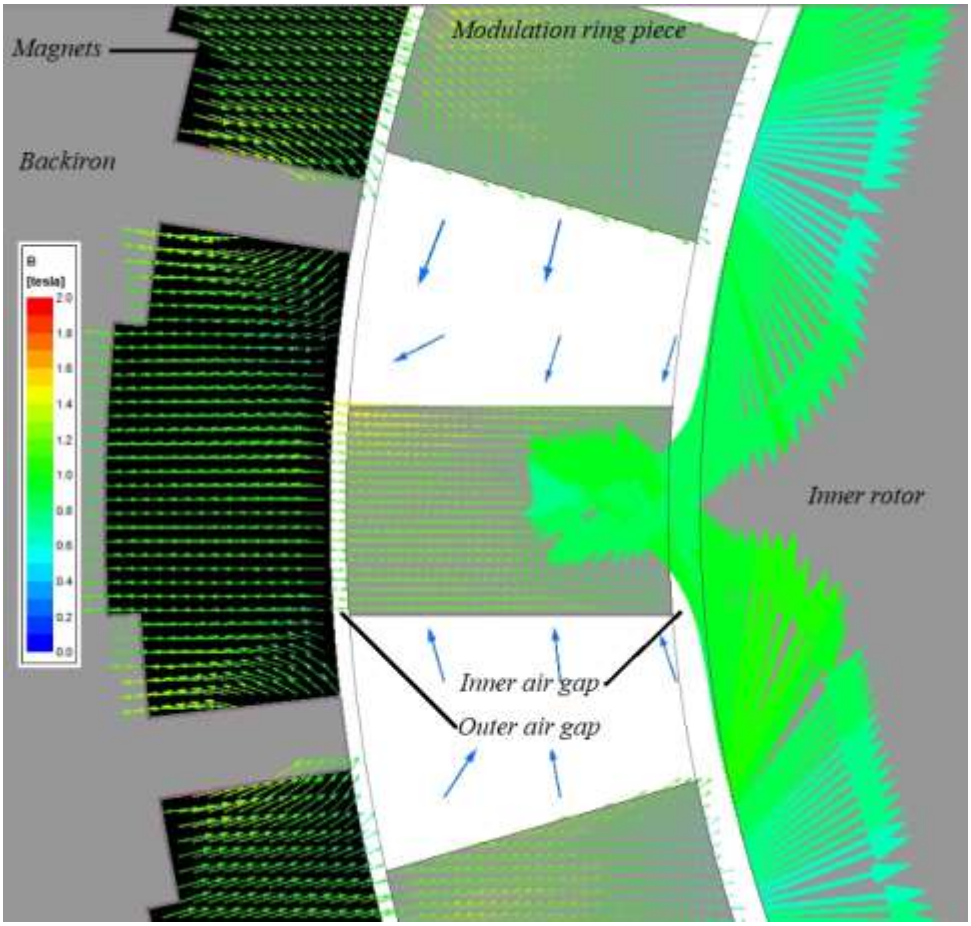

Source: The author

In both paths, the outer air gap appears and as such, it will not play a major role in the balance between the main flux and this type of leakage flux. It is important to remember that,

as explained for the outer air gap, it still reduces the coupling between the modulation ring and the magnets, and increasing it increases another type of leakage flux that goes straight from one magnet to another. As a result, the difference in both paths relies on two times the length of the inner air gap, two times the H_s and a section between modulation pieces of the inner rotor against the gap between the modulation pieces and a part of the thickness of the modulation pieces. By using a ferromagnetic material for the modulation pieces with a very high relative magnetic permeability it is possible to disregard the modulation pieces when determining the total reluctance for both paths as they have a much smaller reluctance then the air gaps. As a result, the difference between the main flux and the leakage flux between modulation pieces relies on two times the length of the inner air gap and the gap between modulation pieces. For that reason, RMG with a lower number of modulation pieces will have a larger gap between modulation pieces and, therefore, less of the described flux leakage. Even for a large air gap as the one adopted with 1 mm, the total value is still much smaller than that of the gap between modulation pieces. For large RMG the gap between modulation pieces is naturally large and this leakage flux gets smaller. For small RMG the difference starts to decrease and smaller air gaps should be used. As expressed previously, the difference between the relative magnetic permeability of ferromagnetic materials and that of the air can be used to disregard the reluctance of the modulation pieces, but as the modulation ring gets thicker, its reluctance starts to increase and it can no longer be disregarded. By means of parametric simulations using FEA software, the impact on the average torque output of increases of H_s was studied. Fig. 36 contains the results of the simulation, where the H_s was increased from 2 mm to 40 mm with steps of 0.1 mm.

Figure 36 - Average torque output for various H_s

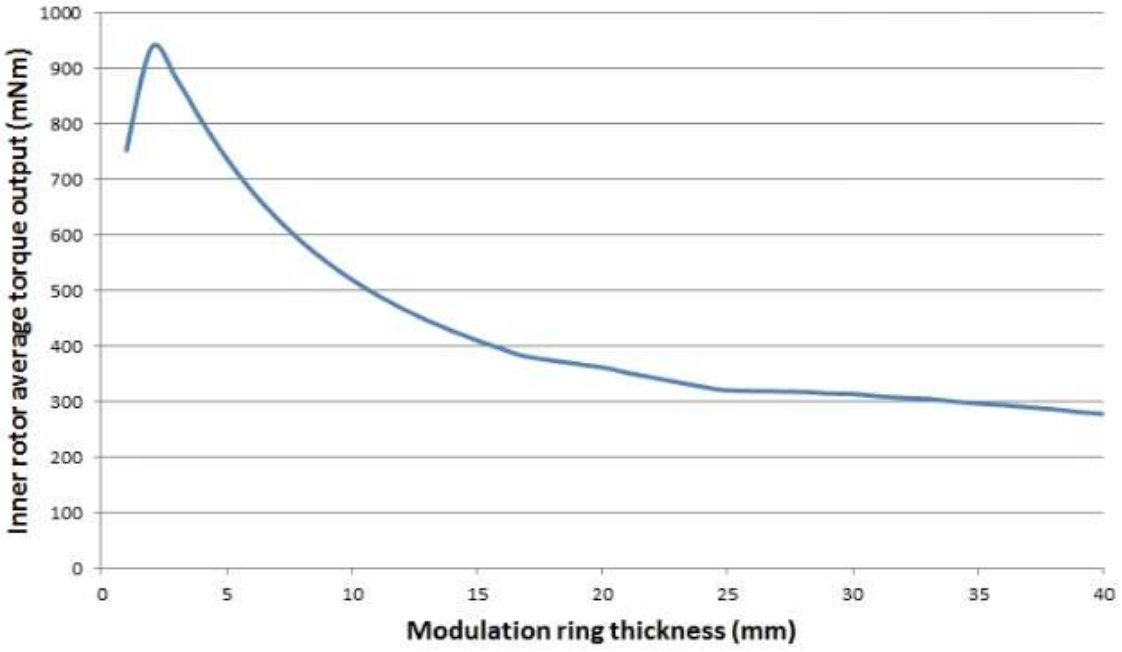

Source: The author

As it can be seen in Fig 36, as H_s increases the torque output decreases, with the modulation pieces reluctance increasing with its length and becoming more and more relevant until it becomes dominant for very large values of H_s. For very small H_s the torque output increases as it gets closer to an optimal value. This effect can be explained by comparing the inner air gap length combined with the outer air gap and the total air gap between the magnets and the inner rotor that is composed by the inner air gap, the outer air gap and H_s as air gap. Combining both air gaps, for the values adopted, it totals 1.5 mm of length. If the modulation ring has only 2 mm, for example, the total air gap between the magnets and the inner rotor would be a total of 3.5 mm. This would allow for a part of the flux to go straight to the inner rotor, not being modulated as a result.

The width of the modulation ring pieces not only can a major influence on the magnetic permeance, but also influences the modulation of the magnetic flux. The influence of the ratio between the width of the modulation ring pieces and the material that separates the

pieces was verified using parametric simulations. In Fig. 37 the torque output is shown for different ratios of modulation ring pieces and the separation between them. For a ratio of 0.5, the modulation ring has half the width of the region that separates two pieces for example. The simulations covered a spam of ratios from 0.1 up to 1.9 varying in steps of 0.01.

Figure 37 - Average torque output for various modulation ring pieces widths

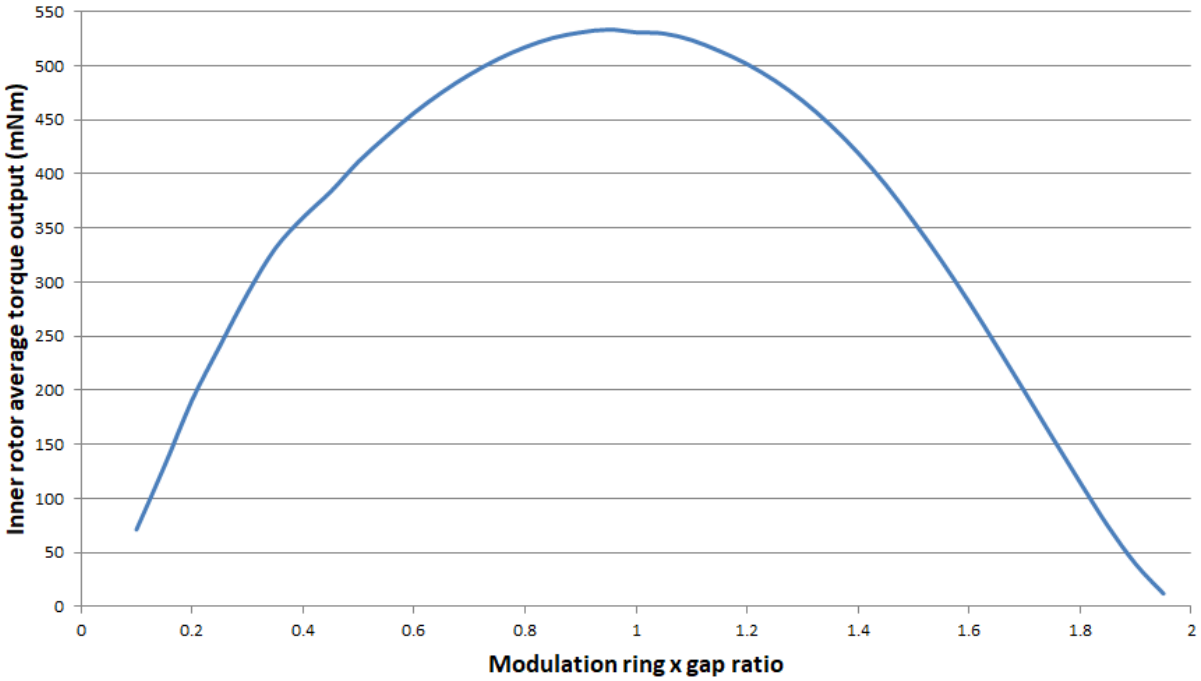

Source: The author

As seen in Fig. 37 for small widths of the modulation ring pieces the torque output diminishes, mainly due to the magnetic permeance of the modulation ring being reduced as the cross section of them being reduced. As the modulation ring gets wider, the torque output also diminishes due to the reduced magnetic reluctance of the separation region, leading to higher flux leakage that goes from one modulation ring to another, without passing through the inner rotor. Another reason for the decrease of the torque output is that with larger modulation ring pieces more harmonics are introduced to the modulated flux, which does not contributes to the torque production.

The combined effect of H_s and R_{out} will be discussed in the next chapter.

4.7 MAGNETS THICKNESS

The main difference of an RMG to a conventional CMG is the inner rotor being made entirely of ferromagnetic material instead of having magnets. Since only the outer rotor has magnets, the magnets in the outer rotor can be considered the only magnetic source. By using magnets with higher energy density, such as NdFeB and SmCo, it is possible to increase the magnetic flux and by consequence the torque output. Increasing H_{mag} allows them to work with values closer to the residual flux density. Being among the strongest magnets available, NdFeB was chosen, with the N35 grade being adopted for economic and market availability. By using the FEA software to run parametric simulations, the H_{mag}, and by consequence their point of operation was simulated for values varying from 2 mm up to 14 mm in steps of 0.1 mm. The value of 6 mm was set based on technical limitations and because this value, as shown in Fig. 38, is at a point were increases have diminished returns.

Figure 38 - Average torque output of inner rotor for various H_{mag}

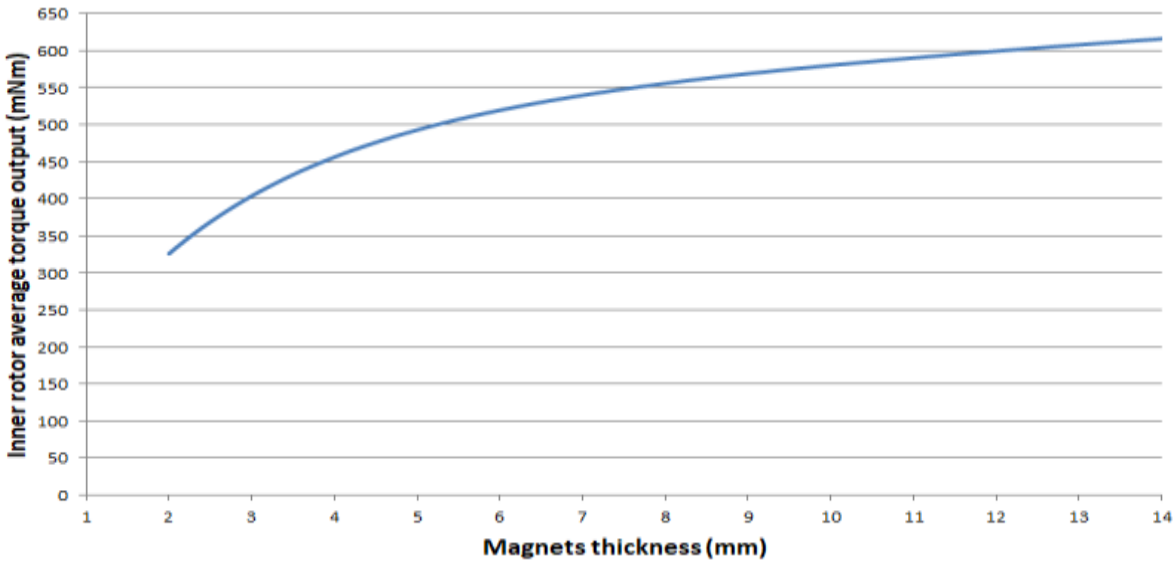

Source: The author

As expected, for very small H_{mag}, small increases provide torque output gains but as the thickness increases, it begins to provide smaller gains, since the magnets are limited by the value of the residual flux density.

4.8 BACK IRON THICKNESS

The magnetic interaction that produces useful torque happens in the inner part of the topology, between the magnets and the edge of the inner rotor. As such, the back iron has two main purposes: to provide mechanical structure to the outer rotor holding the magnets and magnetically short circuit the magnets on the outer side. In order to obtain the maximum flux in the inner part of the topology, the magnetic potential drop in the outer part must be as low as possible. This magnetic potential drop can be reduced by increasing the thickness of the back iron, which reduces the magnetic reluctance. When the magnetic potential drop in the back iron becomes too low, it no longer affects the main flux in the inner part, as its value is much lower than the one in the inner part. Once the value of the magnetic reluctance drops to the point it will not have impact on the main flux there is no magnetic gain to keep increasing its thickness. The parametric FEA simulations whose results are shown in Fig. 39 were made for back irons thicknesses varying from 2 mm up to 20 mm in 0.1-mm steps.

Figure 39 - Average torque output of inner rotor for various back iron thickness

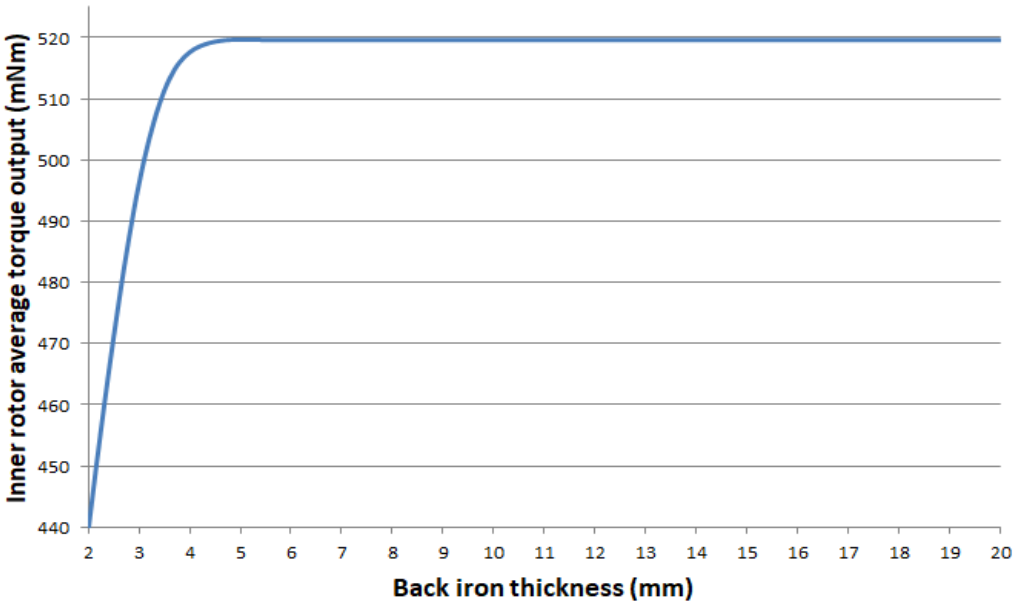

Source: The author

As it can be seen in Fig. 39, as the back iron thickness is increased, so does the torque output as the magnetic potential drop in the outer part reduces and the main flux increases. After the magnetic potential in the outer part reduces to the point it will not change the main magnetic flux, increasing the back iron thickness will produce no magnetic gain. It should be noted that for mechanical reasons the back iron thickness might require increases. The mechanical aspects of the back iron thickness will be better explained in the next chapter.

4.9 MAGNETS POINT OF OPERATION

The point of operation of the magnets determines the magnetic flux provided by the magnets to the magnetic circuit. Given that it is affected by the reluctance of both the back iron and the inner part of the RMG, the point of operation chances for different relative positions between the magnets and the modulation ring pieces. In Fig. 40 is shown the magnetic flux of one magnet while is changes from aligned with a modulation ring piece to aligned with the region between the modulation ring pieces.

Figure 40 - Torque output of inner rotor over time

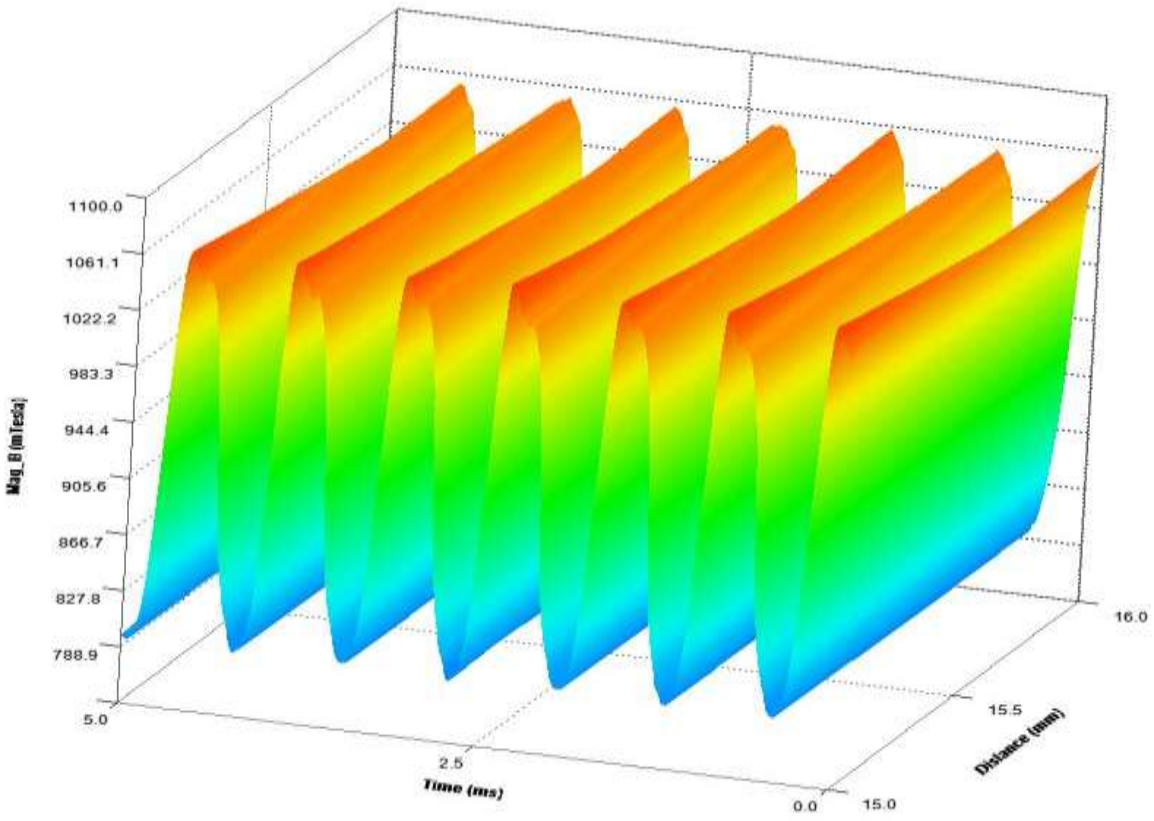

Source: The author

The magnetic flux variation of the magnets ranged from 0.79 T at its lowest and 1.06 T at its highest, resulting in a maximum drop of 30% from the residual magnetic flux of the magnets.

4.10 SKEWING

As explained in the MG chapter, depending on the speed gain chosen the torque ripple can reach higher or lower values. This torque ripple can be mitigated using the skewing effect. Considering a conventional rotor without skewing, the torque produced corresponds to an average value with a higher frequency function added, as shown in Fig. 41.

Figure 41 - Torque output of inner rotor over time

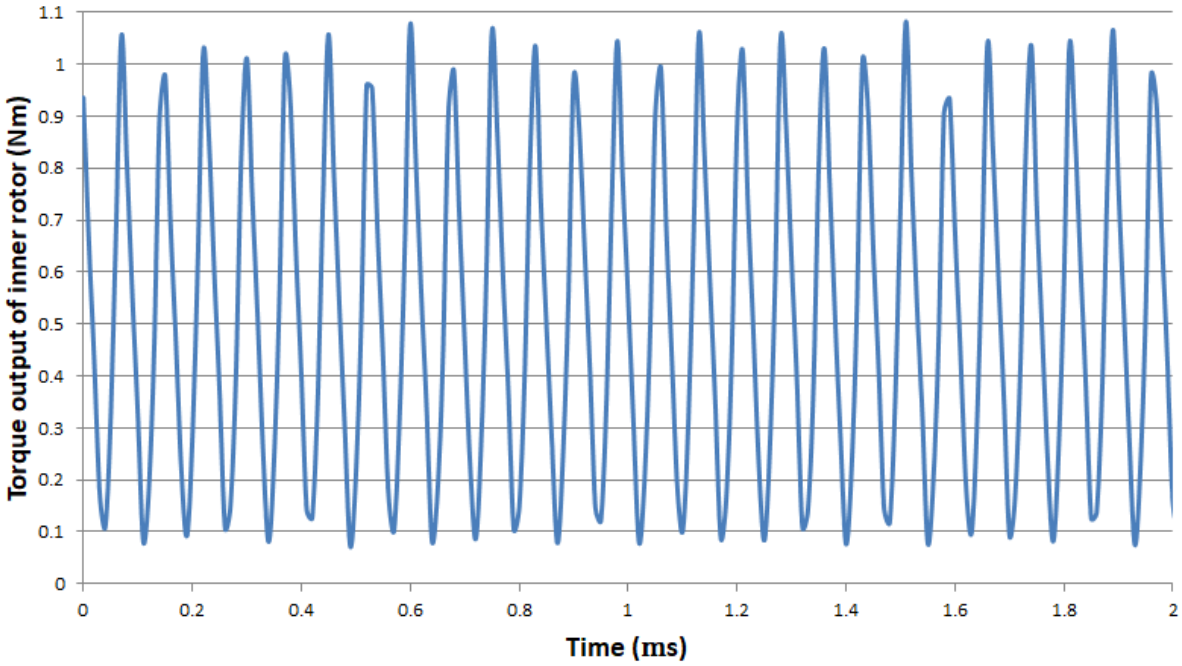

Source: The author

It is possible to consider the inner rotor as several small sheets connected, each with a torque output as shown in Fig. 41 but with values divided by the total of sheets, all in phase with each other. Even though reducing the frequency of the higher part of the torque output or its magnitude is very difficult, changing the phase of each single sheet can be achieve by simply displacing it angularly. Fig. 42 presents an example for a rotor divided into 3 parts, each with 120º of angular displacement of each other.

Figure 42 - Torque output of inner rotor slices with angular displacement over time

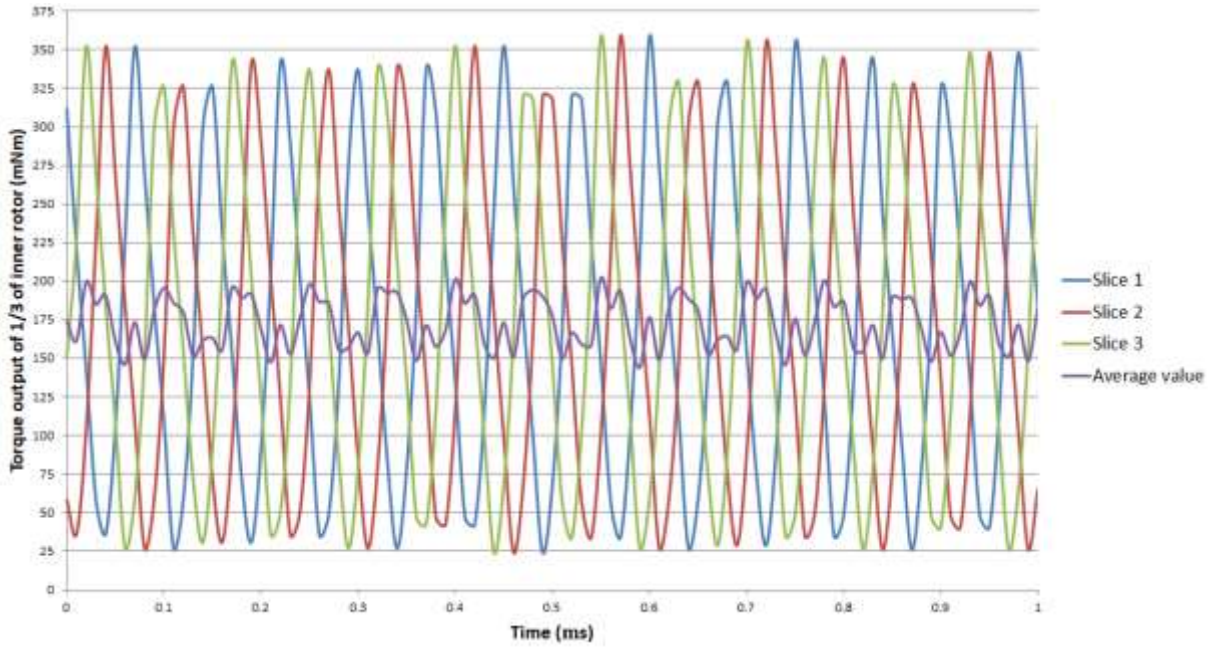

Source: The author

The results, shown in Fig. 42 are identical waves with different phases. The combined waves with different phases maintain the average value but the oscillation of one wave mitigates the oscillation of the other waves. However, if the slices were simply connected, the flux interaction between the slices would change the torque output of each one of them and the total result. Even with the displacement, it can be seen that the average value still has some oscillation, even though it is much smaller.

Using an inner rotor with five slices, where the second is angularly displaced by a given angle and the fourth is displaced by the same angle, but with opposite direction, it is possible to reduce the torque ripple. Fig. 43 contains the results of a parametric simulation skewing angles varying form 0 up to 5 degrees in steps of 1 degree.

Figure 43 - Torque output of inner rotor over time with skewing

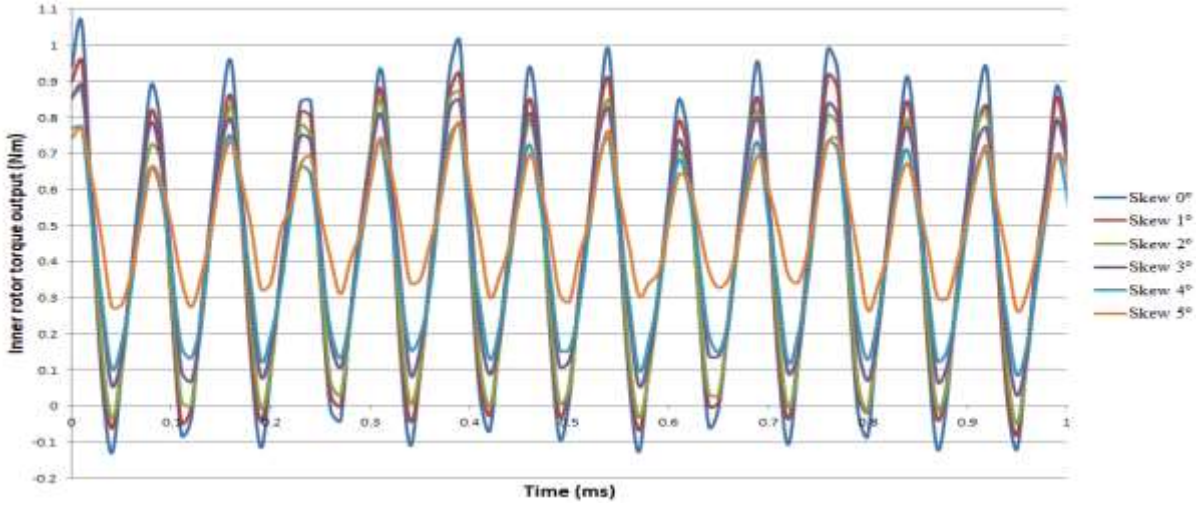

Source: The author

It is clear from the results of Fig. 43 that the torque ripple is mitigated as the skewing angle is increased, where the larger peaks are for the zero degree of skewing and the wave with the smaller oscillation for the 5 degrees, and the others converging in between.

In order to determine the effects of various angles for skewing, Fig. 44 shows the results of parametric simulations made for skewing angles varying from 0 degrees up to 10 degrees, with steps of 0.1 degrees.

Figure 44 - Ripple factor for different displacement angles

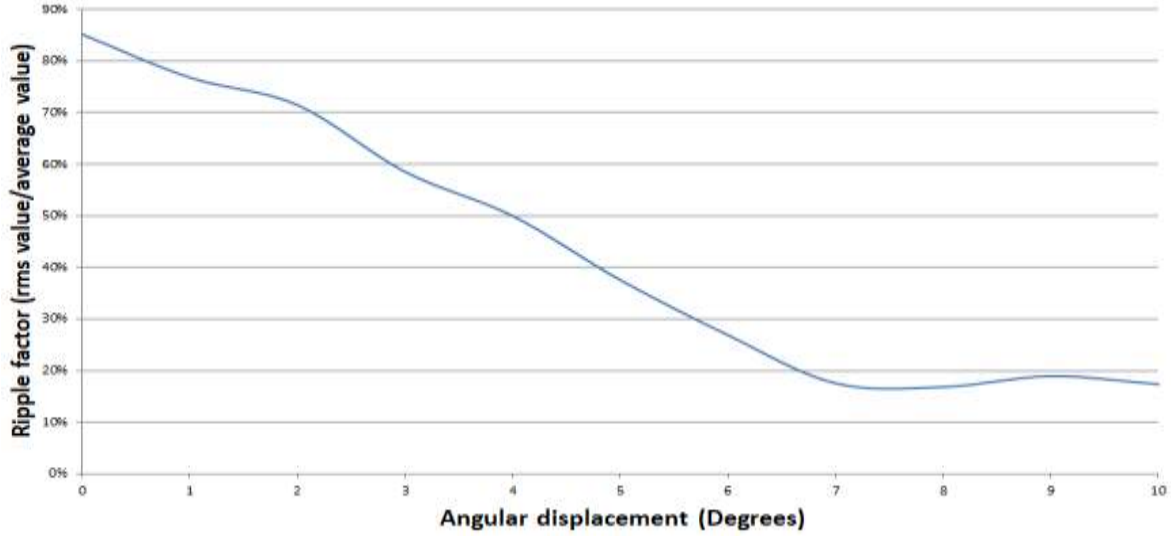

Source: The author

The ripple factor, given by the rms value divided by the average value, for the different angles in Fig. 44 decreases as the angle increases up to 7 degrees, when it stabilizes. The drop from about 80 to 20 of the ripple factor makes clear the advantage of using the skewing effect.

4.11 POLAR ARCH ANGLE AND RELATIVE ANGLE

The magnetic flux that comes from the magnets in the outer rotor and is modulated by the modulation ring interacts with the inner rotor to produce a synchronism with different speeds. The lack of magnets in the inner rotor results in a reluctance force being responsible for the torque generation. The difference between the ferromagnetic inner rotor magnetic reluctance and the magnetic reluctance of the environment surrounding the inner rotor determines the torque produced. The alignment of the inner rotor with the magnetic flux determines if the torque produced will be in one direction or another, or even if there will be torque being produced. This effect is represented by the relative angle as explained in the relative angle section. A wider polar arch will envelop a larger area of the magnetic flux that arrives through the modulation ring. At the same time, a narrower polar arch will have the opposite effect. For both cases, the combination of the magnetic flux from each modulation piece and the inner rotor composes the total torque produced. As the polar arch of the inner rotor gets wider, if the magnetic flux being enveloped interacts with the inner rotor in a way it produces torque in the opposite direction from rest of the combined torque being produced, the result will be a diminishing torque generation. The same is valid for inner rotor getting narrower and enveloping less magnetic flux that produces torque in the same direction as the rest of the combined magnetic interaction. The opposite is also valid for cases where a wider inner rotor envelops more magnetic flux producing torque in the same direction or a narrower inner rotor enveloping less magnetic flux producing torque in the opposite direction.

Combining the alignment produced by the relative angle and the enveloping of magnetic flux for different polar arcs allows for different combinations of the same torque generation by varying both variables. The results shown in Fig. 45 were obtained from parametric simulations to analyse this combined effect.

Figure 45 - Torque output for different polar arch angles and relative angles

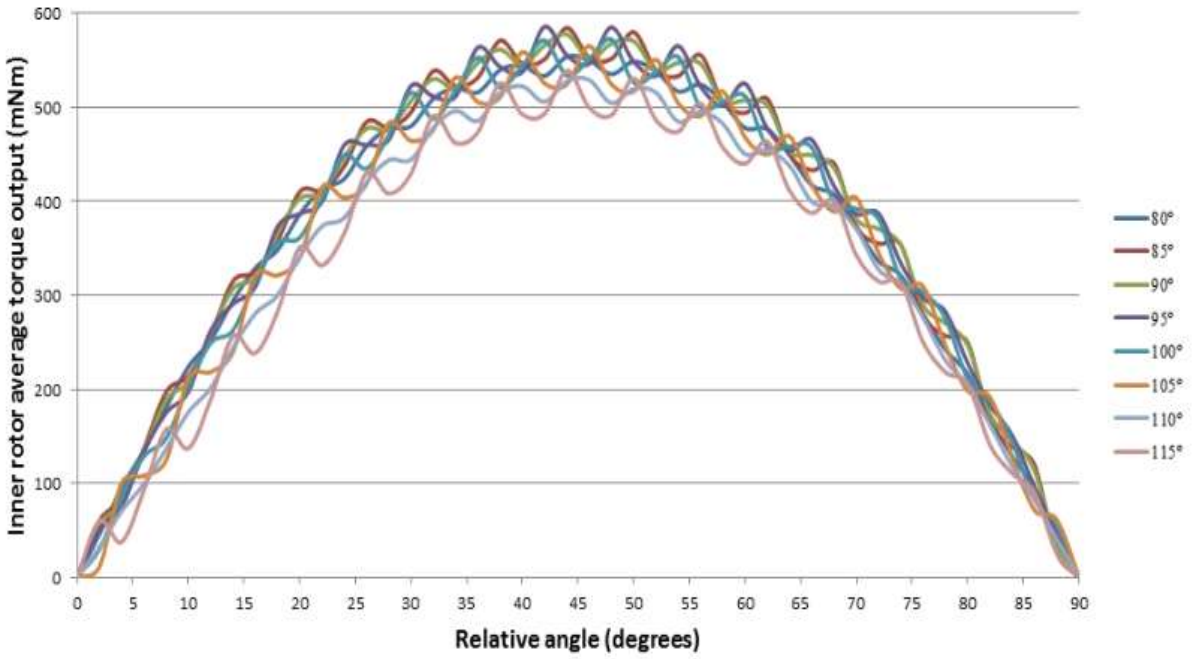

Source: The author

The results for relative angles varying from 0º up to 90º in steps of 0.1º and for polar arch angles varying from 80º up to 115º as shown in Fig. 45 confirm that the angle for maximum average torque changes for each polar arch angle, and for that reason both variables must be chosen together.

4.12 AXIAL LENGTH

The RMG has a 2D symmetry without the skewing effect. The 2D approximation is valid when not considering the end effects. Depending on the ratio between the axial length and the total radius, the end effect can become expressive and the 2D approximation is no

longer valid. Using FEA software to perform parametric simulations, the torque density in terms of different axial lengths varying from 25 mm up to 100 mm, with steps of 1 mm, was used to verify the impact of the end effects and the results are shown in Fig. 46.

Figure 46 - Average torque output for different axial lengths

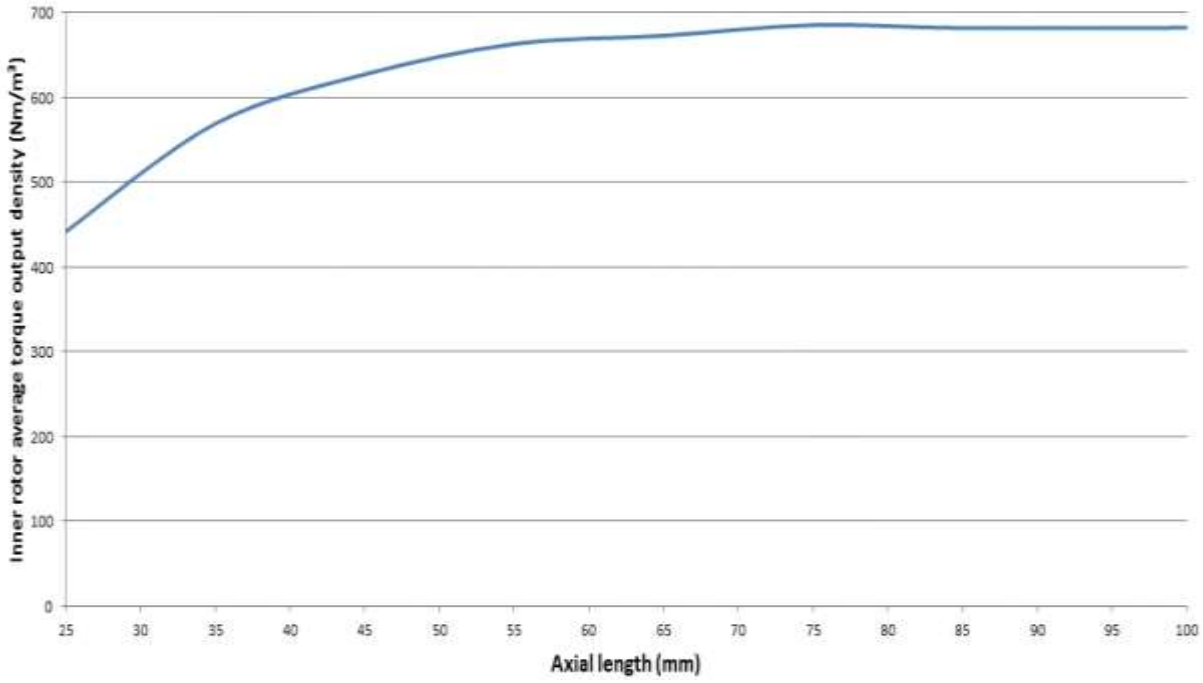

Source: The author

The total radius of the simulated RMG is 65.5 mm. It can be seen in Fig 46 that for values of axial length close to or larger than the total radius has a much similar torque density. For values of axial length of about half or smaller the torque density diminishes as the central part were the end effects has little influence becomes smaller when compared to the edges were the torque generation is smaller because of the end effect.

4.13 OPERATING SPEED

The proposed RMG was designed to operate at 36,000 rpm on the high-speed side. However, as cited in the previous chapter, the RMG can operate at different speeds as long as both rotors are synchronized and the load torque does not exceed the maximum torque. A

parametric simulation was conducted for both rotors synchronized at different speeds to verify the torque output, were the results are shown in Fig. 47.

Figure 47 - Average torque output for different synchronized speeds

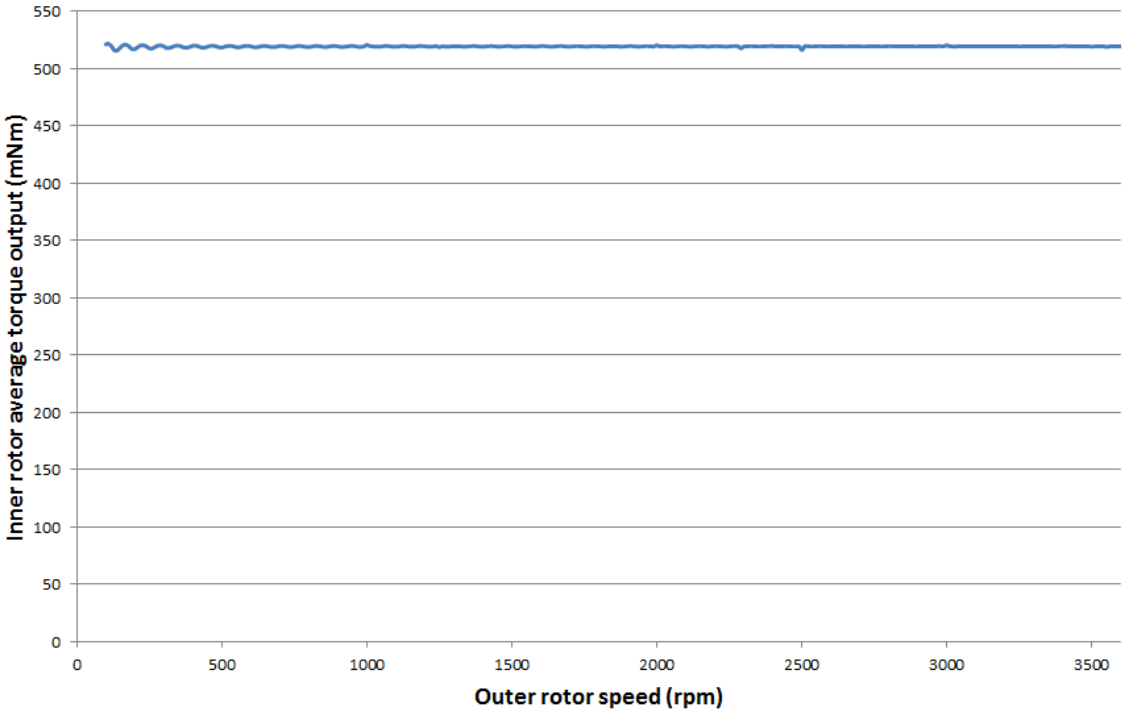

Source: The author

The simulations used for the results of Fig. 47 were conducted for a longer period in order to avoid under sampling for the lower speeds. The results show that for different speeds, as long as both rotors are synchronized, the torque output is the same.

4.14 NUMBER OF POLES

The gear ratio for this study was set to 10. To achieve this value it is possible to use more than one combination of poles for the inner and outer rotor. A combination of two poles for the inner rotor, 20 poles for the outer rotor and 22 modulation pieces has the minimum number of poles and, for a given radius, the widest magnets. Other possible combinations are four poles for the inner rotor, 40 poles for the outer rotor and 44 modulation pieces and a

combination of an inner rotor with 6 poles, an outer rotor with 60 poles and a modulation ring with 66 pieces. In order to compare the performance of each combination, the parametric simulation for the relative angle, already presented in this chapter for the combination with the inner rotor with 2 poles, was conducted for the 4 poles and 6 poles combinations, shown respectively by Fig. 48 and Fig. 49. For these simulations, the outer rotor teeth angle was reduced to 0.1º.

Figure 48 - Average torque output for different relative angles with an inner rotor with four poles

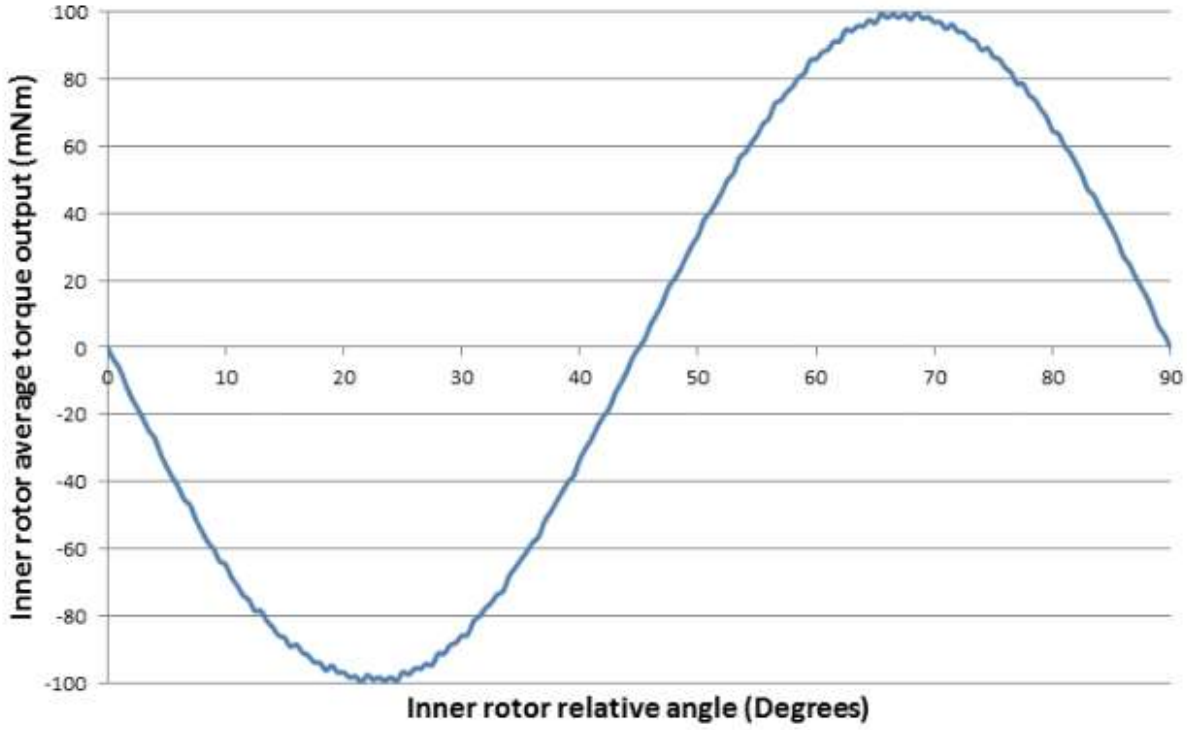

Source: The author

As seen in Fig. 48, the symmetry occur every 90º, as expected for a 4-pole machine. By comparing this combination with the original 2-pole combination, the highest average torque output is more than 5 times smaller for the 4-pole combination. Even with the spikes, seen for the two poles configuration, almost gone, the torque output is much smaller and for that reason, it was not chosen.

Figure 49 - Average torque output for different relative angles with an inner rotor with six poles

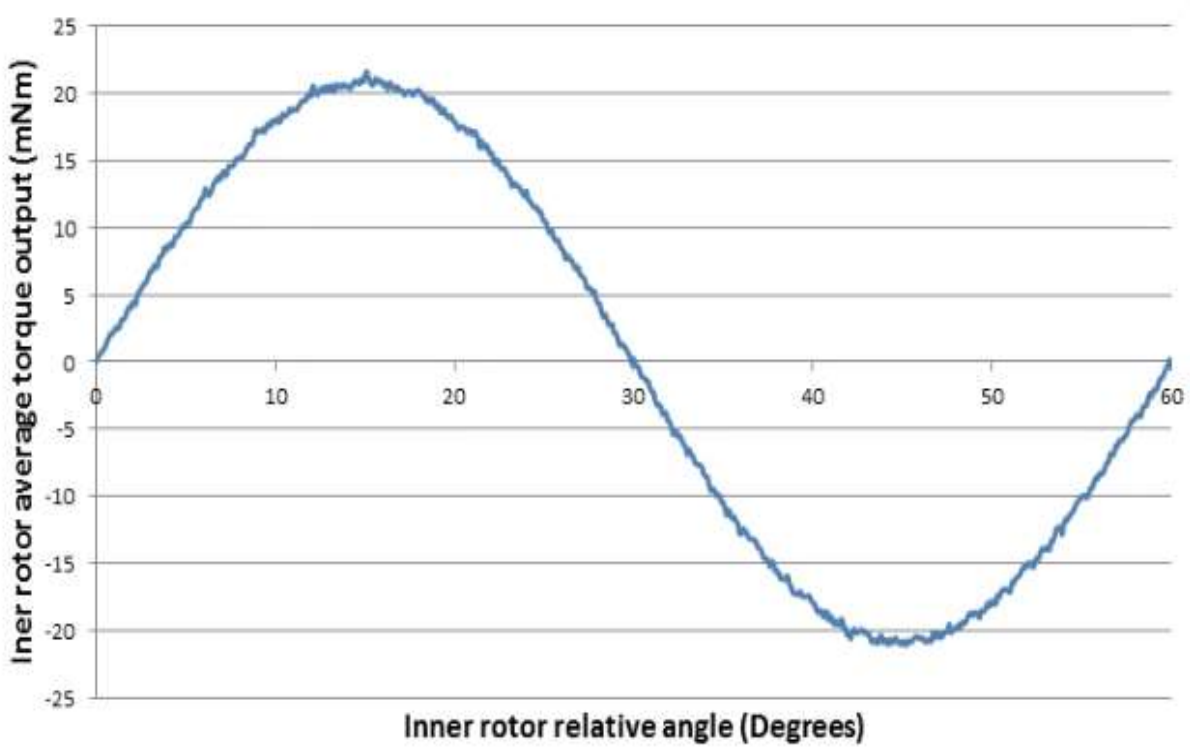

Source: The author

For six poles in the inner rotor, the symmetry was for every 60º, as expressed in Fig. 49. With an average torque output more than 4 times smaller than the 4-pole configuration and almost 25 times smaller than the 2-pole configuration, it can be seen that for higher pole counts the torque output diminishes severely.

This diminishing torque as the pole count gets higher can be explained by the reduction of the arch of each pole of the outer rotor. As previously explained, the space between the magnets concentrates the majority of the leakage flux that goes from one magnet strait to the next magnet. The 4-pole configuration has twice as many magnets as the 2-pole configuration. For a given radius, that means the 4-pole configuration has magnets with only half the polar arch of the 2-pole configuration. The region between the magnets is the same for any number of magnets so the central area, the one responsible by the majority of the magnetic flux that goes through the main magnetic path is diminished by the increase of the

number of poles. By maintaining the same area with high flux leakage and diminishing only the area that contributes the most to the torque production, the torque diminishes by more than half for twice the pole count.

4.15 MAGNETIC LOSSES

The magnetic losses of the proposed topology can be separated in two situations, when the rotating mass is decoupled and when it is charging or discharging. For an energy storage system, the losses when the device is just storing energy are critical as even a very small loss over large periods can result in a lot of energy lost. Since all the energy stored in the rotating mass must be transferred by the RMG and to recover this energy it must also go through the RMG, the efficiency of the energy storage system also depends on the efficiency of the RMG.

When the rotating mass is decoupled (when the outer rotor is removed), the rotating mass is connected to the inner rotor but the inner rotor has no magnetic field from the RMG acting upon it. Without the magnets from the outer rotor, there is no interaction between the inner rotor and the outside of the VC (disregarding the levitation system). As a result, there are no losses from the RMG when the device is decoupled. The primary machine, connected to the removed outer rotor can be shut down, also not having losses in steady state.

The losses when the rotating mass is coupled with the primary machine (through the RMG) were considered using FEM parametric simulations for the inner rotor, modulation ring and back iron to determine the average values for different relative angles (load angles) and for different speeds.

Different relative angles result in different average torque outputs, as shown in the previous sections, and, in combination with the total losses, provide an estimate of the resulting efficiency. Using the same parameters as in section 4.5.4, and the loss typical values

provided by the manufacturer, which resulted in the Steinmetz coefficients generated by the software, listed in Table III, the losses results are shown in Fig. 50.

Figure 50 - Iron losses for different relative angles

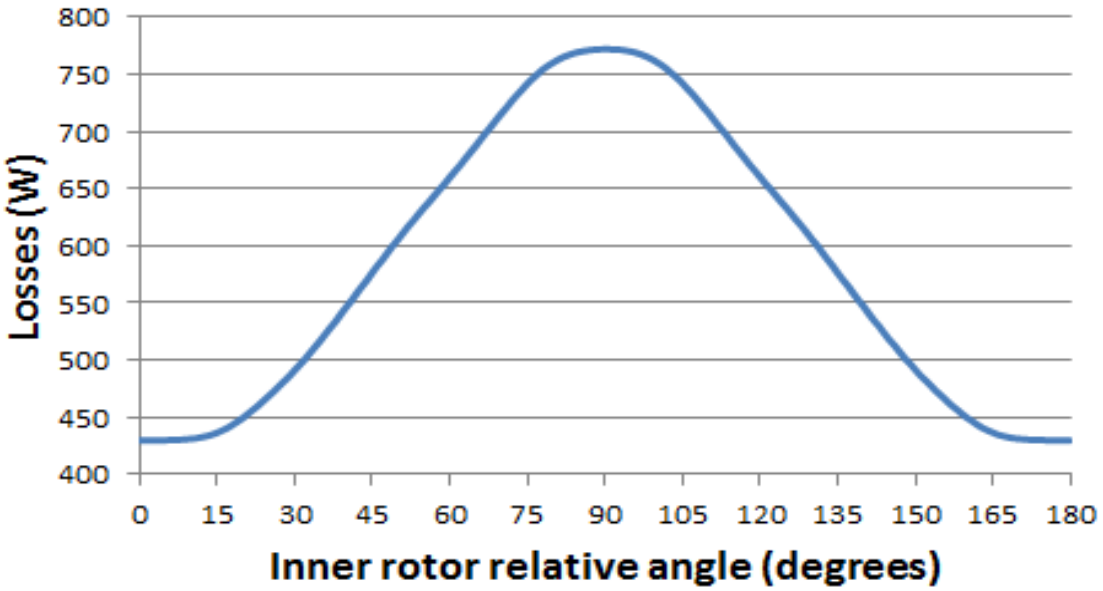

Source: The author

Table 3 Loss coefficients for E230 electrical steel

Coefficient	Symbol	Value (W/m³)
Hysteresis coefficient	K_h	151.6
Eddy current coefficient	K_c	0.8923
Additional losses	K_e	10.67

As seen in Fig. 50, the losses vary for different inner rotor relative angles. This happens because of the alignment of the inner rotor with the modulated magnetic flux. When the rotor is centred with the modulated magnetic flux all the magnetic flux flows through the inner rotor, rending the largest volume of the inner rotor under magnetic flux variation. When the inner rotor is fully misaligned with the modulated magnetic flux it results in the smallest volume of the inner rotor under magnetic flux variation, resulting in fewer losses.

Even though the losses are minimal when the rotor misaligned with the modulated magnetic flux, it is also a condition where the torque output is minimal. Comparing the loss

results and the average torque output results for different relative angles it is possible determine the conditions with the highest efficiency, shown in Fig. 51.

Figure 51 - Losses for different relative angles

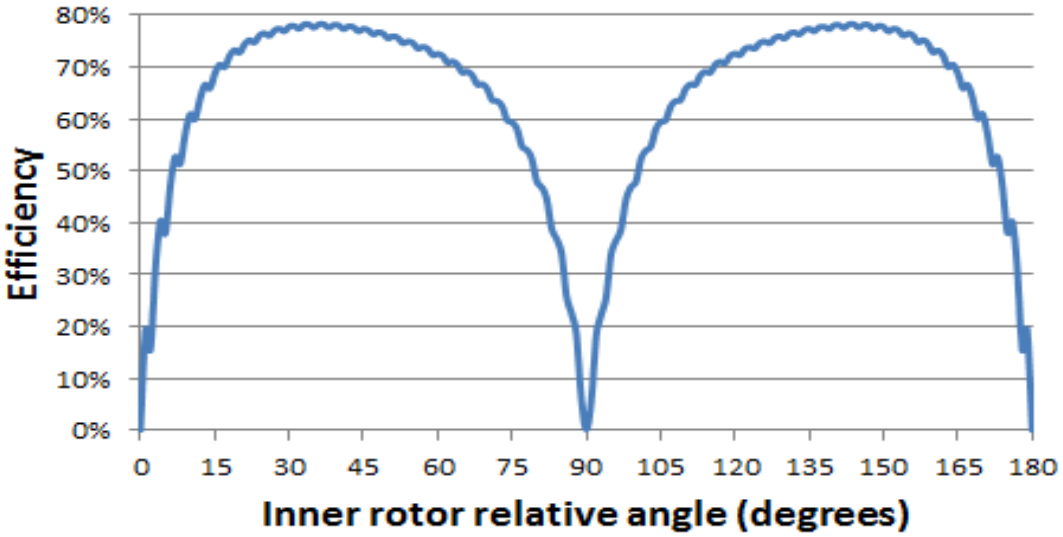

Source: The author

As seen in Fig. 51, the angles with the highest efficiency are those where the average torque output is the highest as they result in the highest power outputs. For both the angles with highest and lowest losses, the average torque output is close to zero, resulting in no power output and zero efficiency.

The magnetic losses are affected by the frequency of the magnetic flux variation. As the proposed topology should be able to accelerate the rotating mass from a very low speed up to full speed, the losses for different speeds are important for the determination of the overall efficiency. A parametric simulation varying the speed of both rotors, in the same way as in section 4.13, shows the resulting losses for each speed, shown in Fig. 52.

Figure 52 - Losses for different speeds

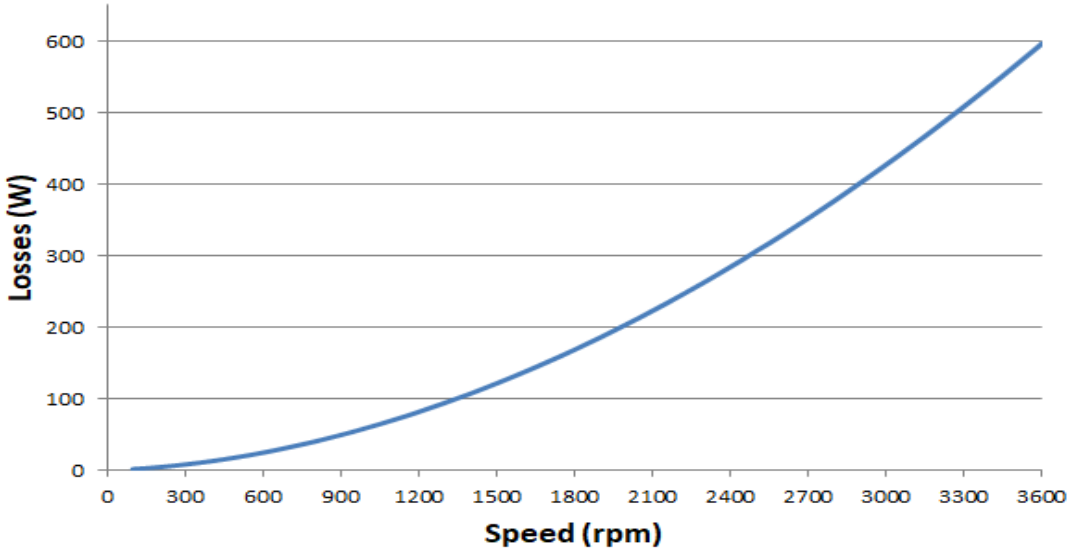

Source: The author

In Fig. 52, it can be seen that as the speed increases, so does the losses, as it would be expected since the magnetic flux is varying with a higher frequency as the rotors gain speed. Even with increasing losses, the power output also increases as the rotors become faster, and the overall efficiency for different speeds is shown in Fig. 53.

Figure 53 - Efficiency for different speeds

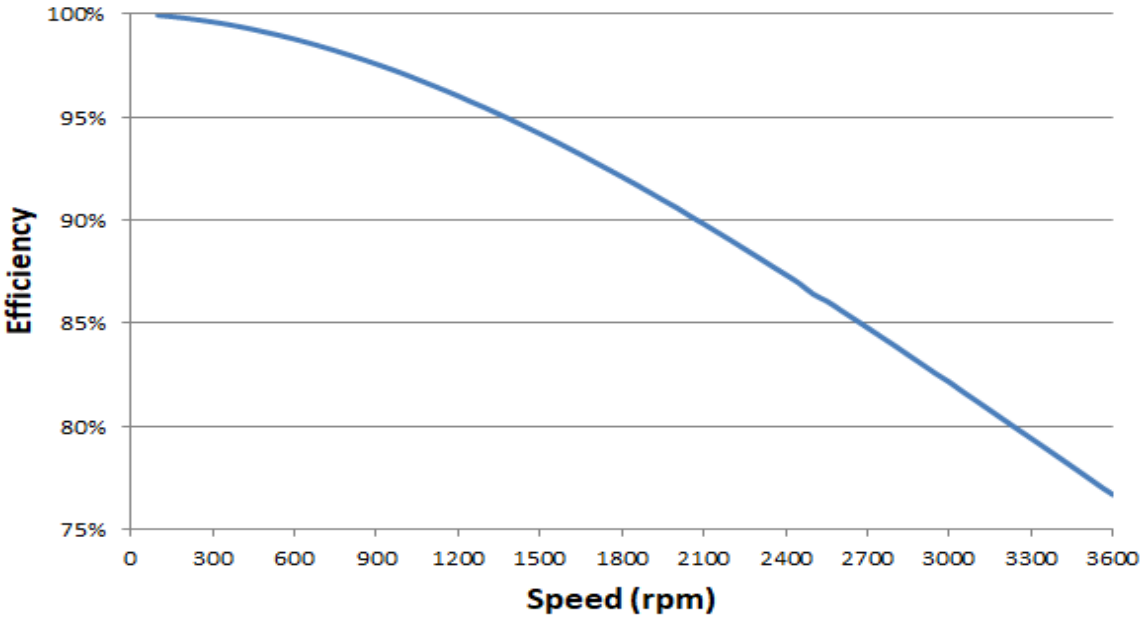

Source: The author

The average torque output is constant for the different speeds, as explained in section 4.13. As the losses increases with the speed of the rotors, the efficiency decreases as the speed increases, as seen in Fig. 53, because the losses increase at a faster ratio than the power output. With a final efficiency above 75% at full speed, the topology offers efficiency within the values described in the original paper [21].

5 MECHANICAL DESIGN

The magnetic design of the proposed topology determines the torque generation, its ripple and the speed and torque gains. Nevertheless, there are several mechanical considerations to be made, some of which can impose changes to the final design of the proposed topology and its application.

In this chapter the removal of each rotor to achieve the decoupling, the H_s along with R_{out} and the H_{mag} along with the back iron thickness will be addressed.

5.1 REMOVAL OF THE INTERNAL ROTOR

The use of a RMG in a FESS to provide speed gain and transfer energy through a containment wall requires the magnetic decoupling of the rotating mass, attached to the inner rotor, from the magnets in the outer rotor, attached to the primary machine, to achieve a no magnetic loss state from the RMG. Being the only part of the RMG attached to the rotating mass, moving the inner rotor away from the modulation ring would leave the inner rotor without any magnetic flux interacting with it. The force required to remove the inner rotor away from the modulation ring was simulated using FEA software. The results, shown in Fig. 54, are for an axial displacement of 60 mm, when the rotor would be 10 mm away from the edge of the modulation ring.

Figure 54 - Force required to remove the inner rotor

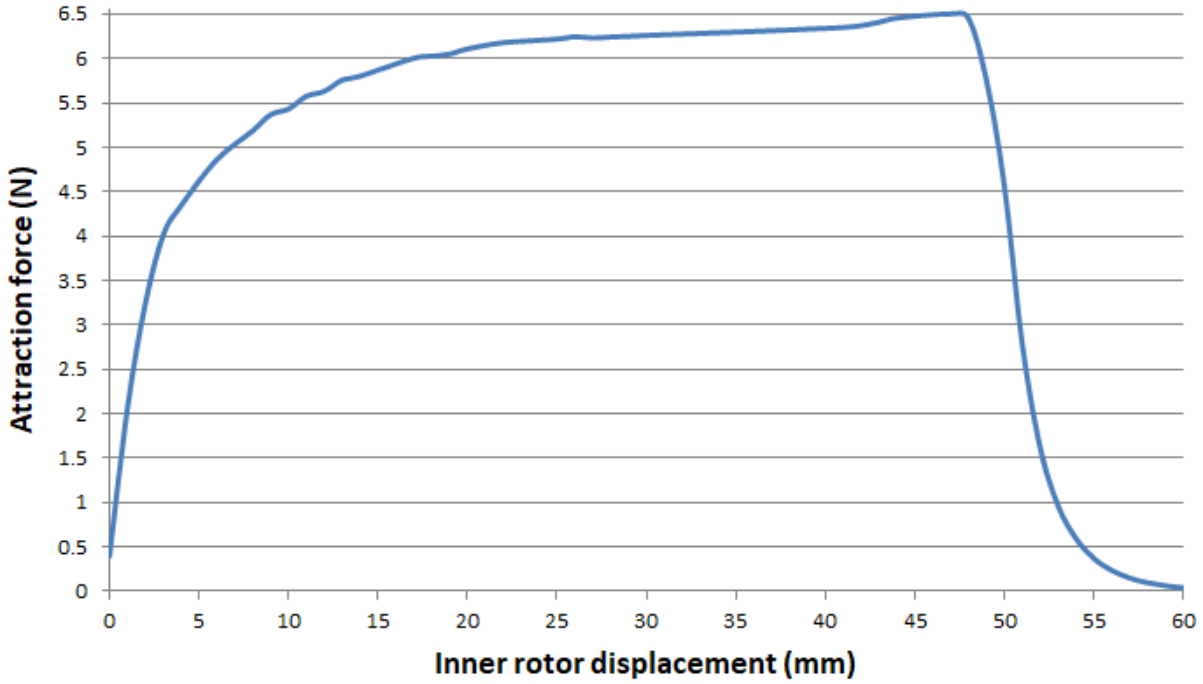

Source: The author

The force required to remove the inner rotor, according to Fig. 54, is less than 7 N at its peak. Even though this force, as will be shown in the next section, is much smaller than the force required to remove the outer rotor, the removal of the outer rotor is preferred. The removal of the inner rotor would require the rotating mass, which is being magnetically levitated, in a vacuum chamber and rotating at high speeds, to move or the shaft that connects the inner rotor and the rotating mass to retract. Both options can be achieved but the removal of the outer rotor is easier to be done.

5.2 REMOVAL OF THE EXTERNAL ROTOR

The magnets in the outer rotor are the only source of magnetic flux in the proposed RMG. Without the magnets of the outer rotor, the inner rotor would have no forces from outside the vacuum chamber acting upon it and, as a consequence, the rotating mass. As the outer rotor is attached to the primary machine, its removal can be done by moving the outer

rotor and the primary machine, moving the entire vacuum chamber away or making the shaft that connects the outer rotor to the primary machine to retract. Being usually larger, heavier and having other systems connected to it, moving the vacuum chamber can be difficult. Simulations were made to determine the force required to move the outer rotor away from the VC using FEA software. The result is shown in Fig. 55.

Figure 55 - Force required to remove the outer rotor

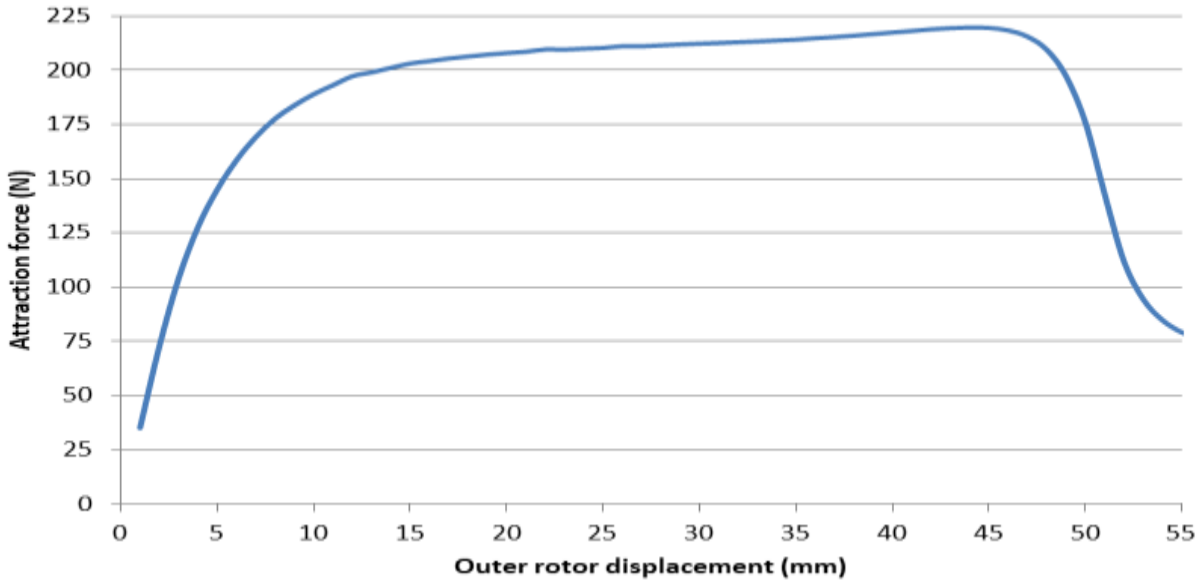

Source: The author

The force required to remove the outer rotor, shown in Fig. 55 as the result of the simulations, is higher than that of the removal of the inner rotor. An advantage of this approach is the drive system being outside the VC, which allows for a much easier use to move the outer rotor. This also helps with heat dissipation for not being in the vacuum. Not needing adjustments to the levitation and stability system to allow the movement of the rotating mass and/or the inner rotor are another benefit. These reasons help illustrate why a drive system to move the outer rotor is simpler to develop then a drive system to move the inner rotor.

5.3 INNER ROTOR RADIUS AND MODULATION RING THICKNESS

As shown in the magnetic design chapter, increasing the R_{out} increases the torque output. At the same time increases of the modulation ring past the optimal value reduces the torque output. Because the inner rotor is inside the VC, in order for it to get larger it requires a larger VC, even if a local increase of the VC where the modulation ring is inserted. The VC sustains the pressure of holding the vacuum and requires a strong wall to maintain its integrity. A larger VC with the same pressure will have to sustain a larger force due to its larger area. As the VCW defines the H_s, a larger VC will have larger H_s and a larger inner radius for a constant air gap. In order to determine the combined effect of increasing both variables, parametric simulations using FEA software were conducted. The values used were varied from 35 mm up to 80 mm with 0.1-mm steps for the R_{out}. For the H_s, the values are varied from 10 mm up to 40 mm with steps of 1 mm. Only the values of modulation ring varying from 10 mm up to 40 mm with 5-mm steps are shown for better visibility reasons. For the same reason, the results of Fig. 56 show the average torque density instead of average torque due to the large increases from R_{out}.

Figure 56 - Average torque output of inner rotor for various values of R_{out} and H_s

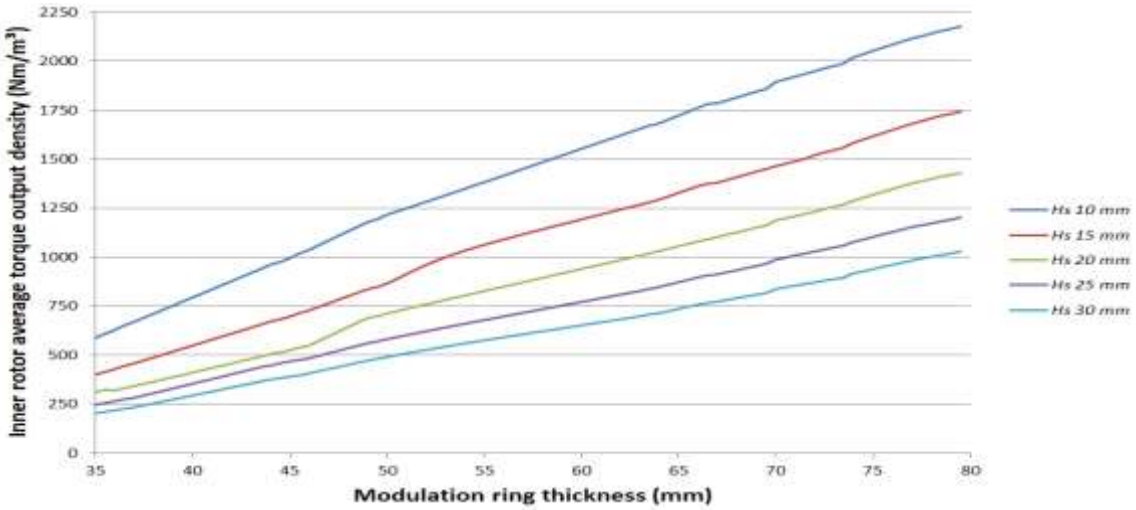

Source: The author

The results shown in Fig. 56 show good accordance with those of the previous chapter were increases of the R_{out} provide large increases of torque output and as the modulation ring increases, the torque output decreases. The result of the combined increase of H_s and R_{out} not only increases the torque output but also increases the torque density, even considering a bigger setup. These increase in torque density shows that as the proposed topology gets bigger, the higher the torque density. The problem with increasing the size of the RMG is the impact it has on the FESS, as a larger VC will be required. For that reason, the RMG torque output is determined by the size of the VC and its wall thickness.

5.4 MAGNETS AND BACK IRON THICKNESS

The outer rotor is made of magnets and the ferromagnetic structure that holds them. The point of operation of the magnets depends on the total reluctance seen on the inner part of the topology and the total reluctance seen on the outer part, the back iron. As shown in a previous section, the back iron thickness can be increased to improve the torque output until its magnetic reluctance no longer plays a major role in determining the magnets point of operation, when the back iron is saturated. A stronger magnet would require a thicker back iron as a bigger magnetic flux would have to be supported. The joint effect of H_{mag} and the back iron thickness is shown in Fig. 57, obtained by means of FEA parametric simulations.

Figure 57 - Inner rotor average torque output for various magnets and back iron thickness

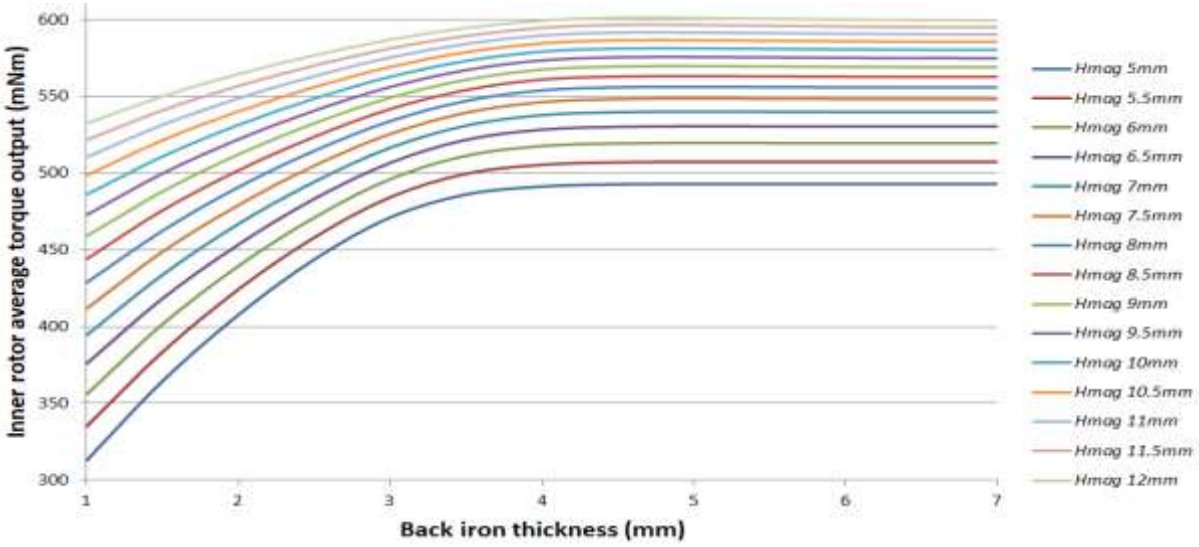

Source: The author

The inflection point, when the torque output no longer increases with thicker back iron thickness, as shown in Fig. 57 shifts from almost 3.5 mm of back iron thickness to about 4.5 mm as H_{mag} increases.

5.4.1 Outer rotor teeth

The magnets in the outer rotor see a much larger torque being applied to them when compared to the torque produced in the inner rotor because of the speed gain of the RMG. At the edges between the magnets most of the magnetic flux goes straight from one magnet to the next one, with this part of the magnetic flux not producing torque as explained in the previous chapter. An option to help improve the structure that holds the magnets, considering the flux leakage between magnets, is to use ferromagnetic teeth connected to the back iron in the outer rotor between the magnets.

Even though the teeth connected to the back iron provide additional mechanical strength to hold the magnets, as they get larger the magnets become smaller. In order to determine the trade-off between more mechanical strength from the teeth and loss of magnetic

flux from a reduction of the magnets, parametric simulations were conducted for teeth arcs varying from 0.1º up to 5º with steps of 0.1º for every simulation, where the results are shown in Fig. 58.

Figure 58 - Average torque output for different back iron teeth arcs

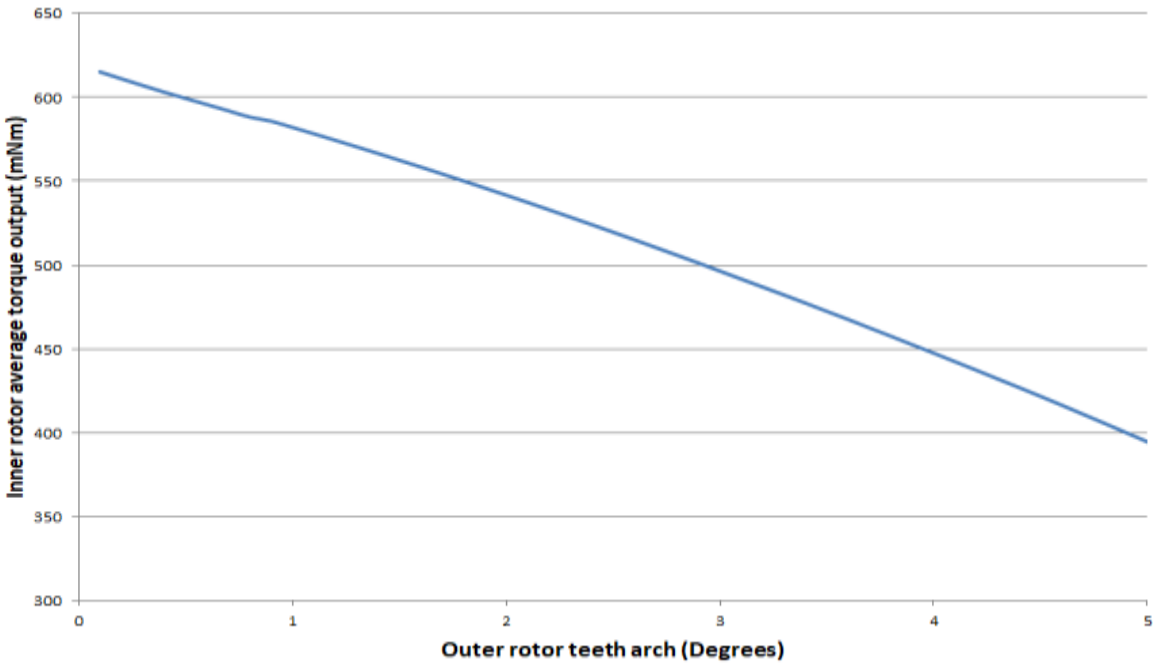

Source: The author

The results shown in Fig. 58 reveal that the torque output diminishes as the teeth used gets bigger, mainly due to the reduction of the magnets. The replacement of the parts of the magnets that is next to the other magnets by ferromagnetic material did reduce the torque output and as such, the trade-off between the additional mechanical strength provided by the teeth and the increased torque output must be considered.

The back iron teeth between the magnets is made of ferromagnetic material. For that reason, it can increase the flux the goes from one magnet to the next with crossing the air gaps. By reducing the length of the back iron teeth, this effect can be mitigated. In Fig. 59 the average torque output for several back iron teeth length and angles are shown.

Figure 59 - Average torque output for different back iron teeth arcs

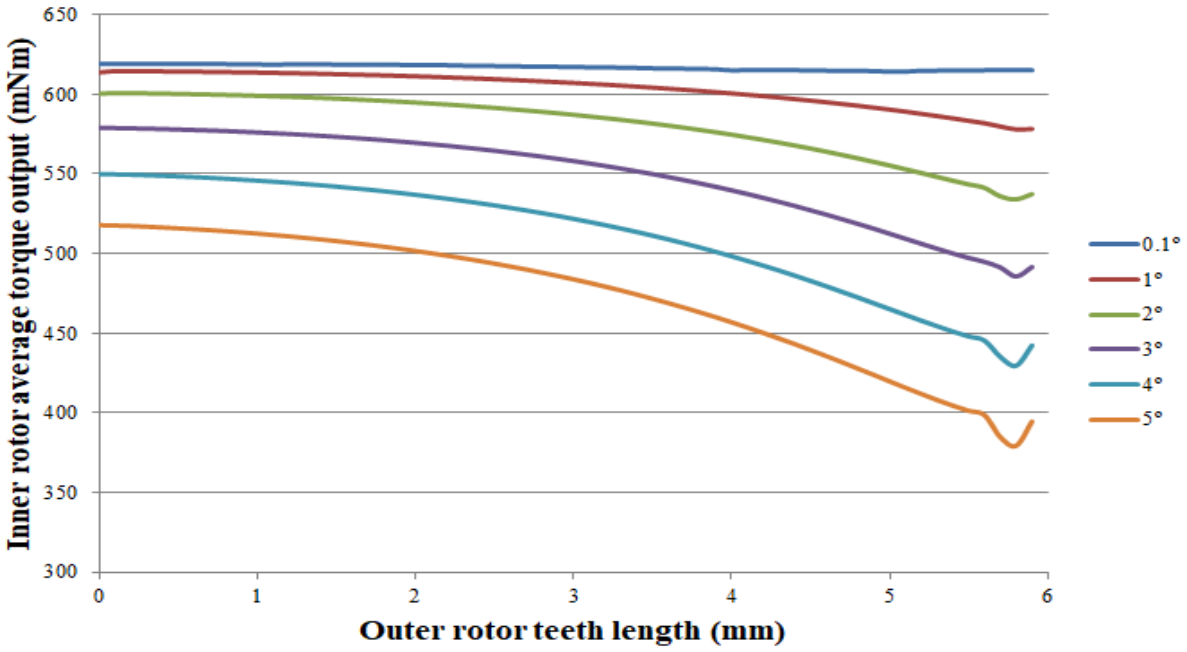

Source: The author

As seen in Fig. 59 the reduction of the back iron teeth length diminishes the average torque output drop as the angle of the back iron teeth angle increases.

5.4.2 Use of dove tail to hold the magnets

Aside from using ferromagnetic teeth between the magnets, another option to increase the mechanical strength of the structure that holds the magnets is to use an extension of the magnets called dovetail. This extension of the magnets is enveloped by the back iron, making a physical connection between the magnets and the back iron that help keep the magnets in place. Fig. 60 shows the used dovetail in green.

Figure 60 - Dovetail used

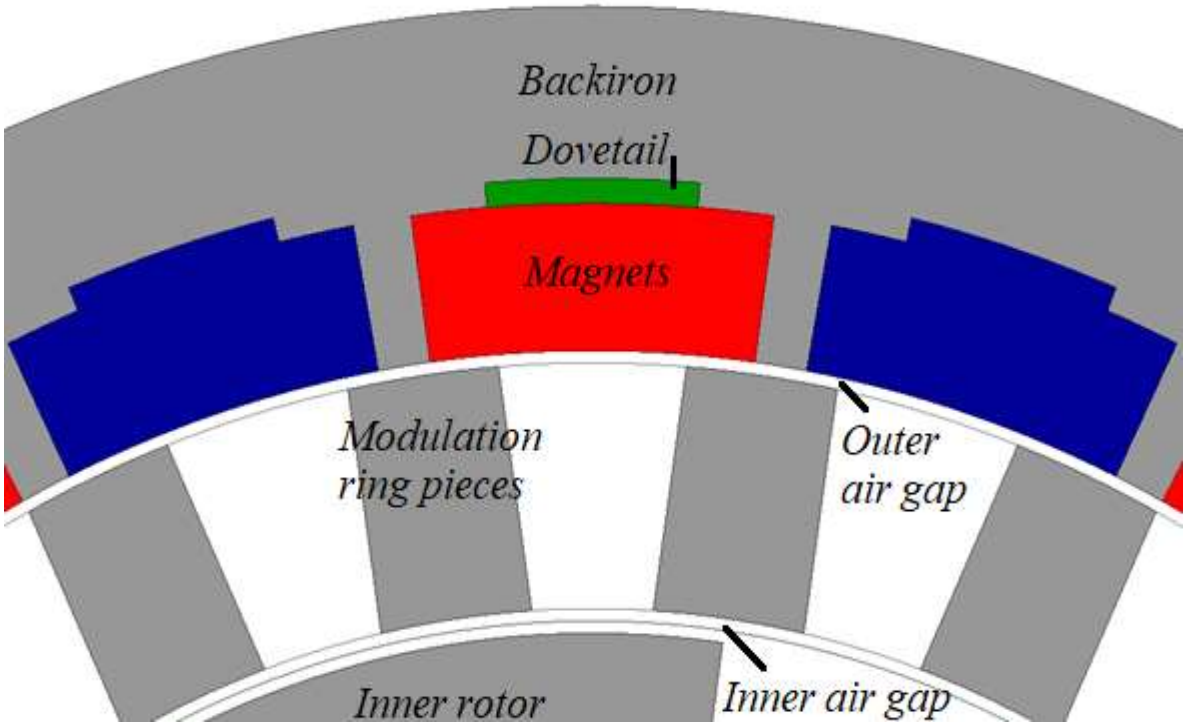

Source: The author

The used dovetail, shown in Fig. 60, has half the total arch of the magnet it is connected to. By using the dovetail, the magnets become thicker in the central part, and parametric simulations were conducted to verify the impact of their use on the torque output. In Fig. 61, the results for variations of dove tails thickness varying from 0.1 mm up to 2 mm with steps of 0.1 mm are shown.

Figure 61 - Torque output for various dovetail thickness

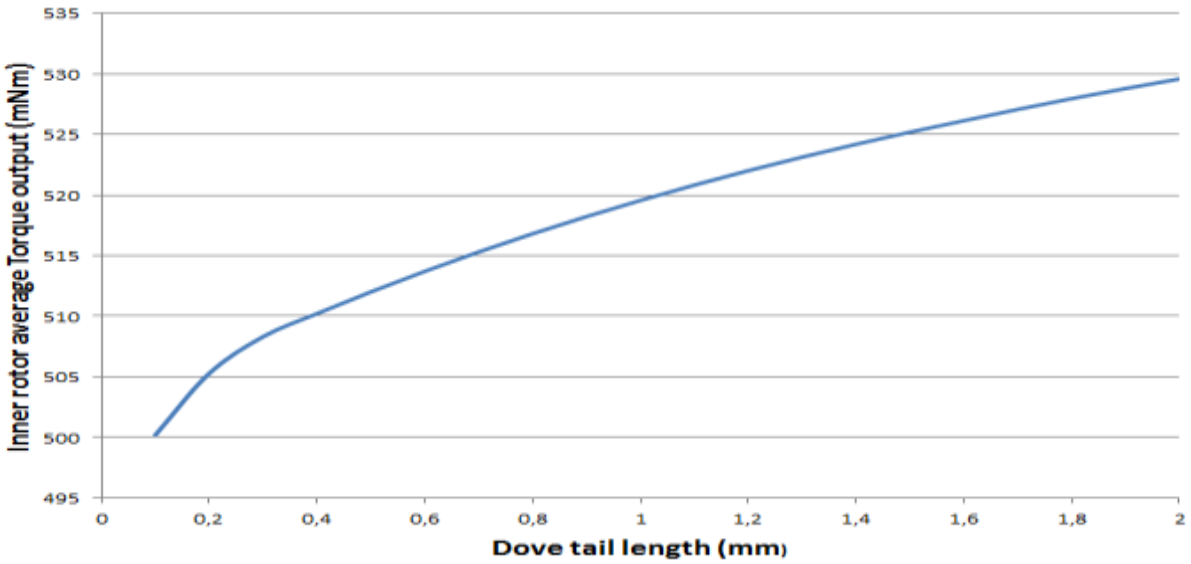

Source: The author

The results of Fig. 61 show an increase of the average torque output of the inner rotor, but considering that this was due to an increase of H_{mag} in the central part, the results were compared to an equivalent value of H_{mag} with a dovetail 1-mm thick, and the results are shown in Fig. 62.

Figure 62 - Torque output comparative for different dovetail and magnet thickness combinations

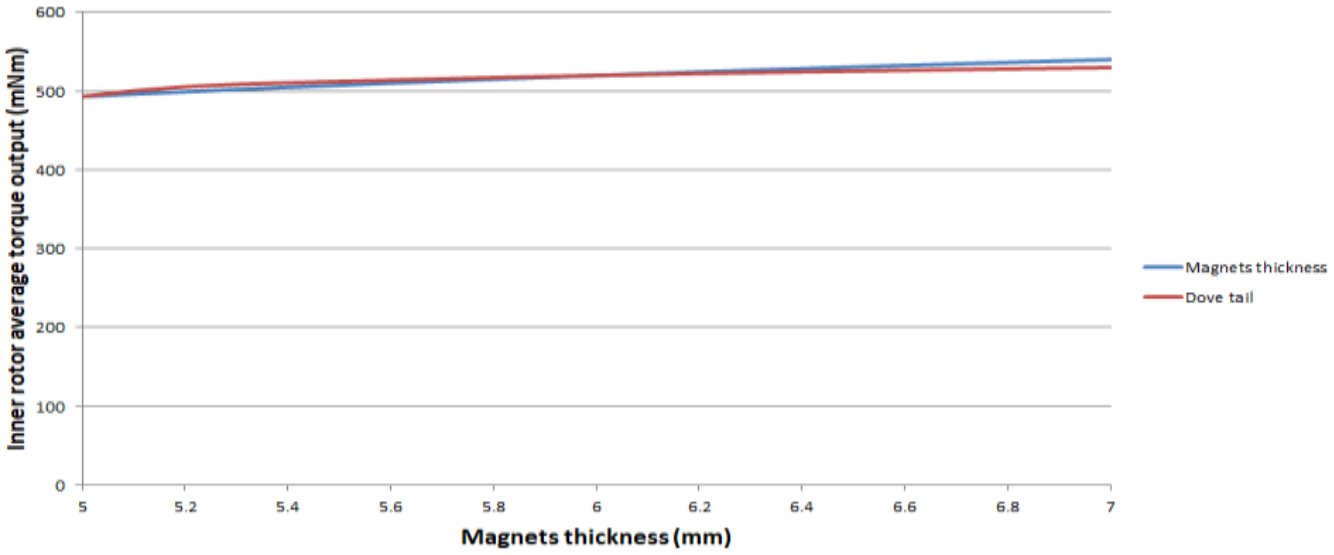

Source: The author

By comparing the results shown in Fig. 62, it is clear that the torque increase comes from the increased H_{mag} and that for the same total thickness the use of dovetail has little impact on the torque output for the values simulated, but it provides the benefit of increased mechanical strength to the structure holding the magnets.

5.5 MODULATION RING MECHANICAL STRUCTURE

The modulation ring pieces are placed between the inner and the outer rotor, with only the inner and outer air gaps separating it from the rotors. As explained, the air gaps are crucial for the performance of the proposed topology and increasing them results in diminishing torque outputs. Since the modulation ring is a part of the VCW, the space between the modulation ring pieces must be sealed to maintain the vacuum. The region between the modulation ring pieces, must, in order to generate the magnetic flux modulation, have a magnetic permeability as low as possible to allow the magnetic flux modulation to occur, and previously described. The mechanical forces applied over the VCW to maintain the vacuum demands the material sealing the space between and holding the modulation ring pieces to have a high mechanical resistance. The region between the modulation ring pieces should have very few magnetic flux lines to for the modulation process to occur, but, as the permeability of the vacuum is higher than zero, some flux lines will pass through it as leakage flux. This leakage flux alternates with a frequency proportional to the speed of the outer rotor. For that reason, the electrical resistance of the material should be as high as possible to prevent eddy currents to be formed and produce losses. Combining all these considerations the material to fill the space between the modulation ring pieces should have a low magnetic permeability, a high mechanical strength, a high electrical resistance and should be able to be machined.

The material used in this study was aluminium. It has a very low magnetic permeability, enough mechanical resistance, can be machined and is cheap. It was chosen due to technical limitations, given that it has a low electrical resistance. This makes eddy currents produce extra losses. The eddy currents are proportional to the square of the magnetic flux density and to the square of the frequency. Even with low magnetic densities in it, the high frequencies cause the eddy currents to be an issue. A common solution to the eddy currents problem, the lamination of the material would be very hard to accomplish since it is part of the VCW. For that reason, for the final application, a better material should be selected. A polymer with high mechanical resistance, high electrical resistance and low permeability would be an interesting choice, but the costs and the possibility to be machined would have to be considered.

6 PROTOTYPE AND EXPERIMENTAL RESULTS

A prototype was assembled to compare experimental results with values obtained from FEM simulations. The values used in the making of the prototype are the ones shown in Chapter 4, Table I. The next sections will present each part of the assembled prototype, its considerations, and the experiments made.

6.1 PROTOTYPE PARTS

The assembled prototype is shown in Fig. 63.

Figure 63 - Assembled prototype

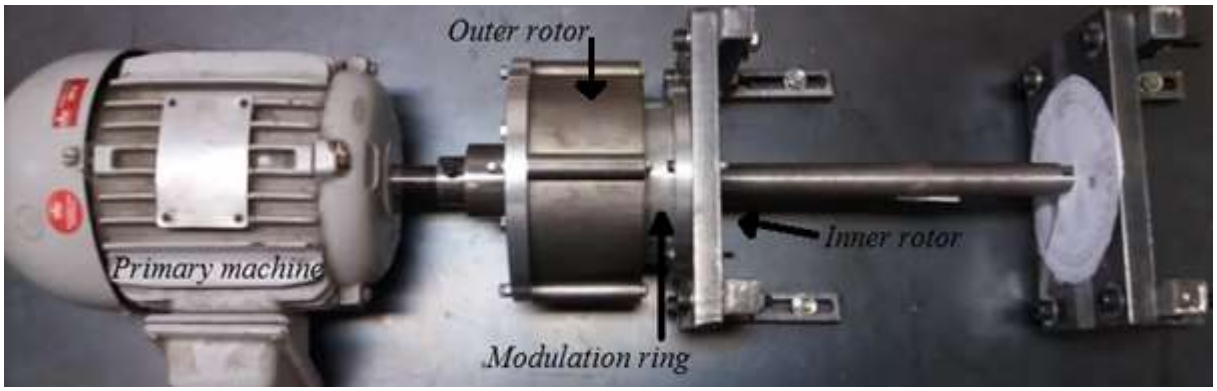

Source: The author

The prototype shown in Fig. 63 is fixed in a 6.3-mm thick steel sheet. The prototype was assembled in two main parts, one with the outer rotor connected to the primary machine and one with the modulation ring and the inner rotor, both connected and attached to the steel sheet by two steel supports with high-speed bearings.

6.1.1 Outer rotor and primary machine

The primary machine used is a 4-pole induction machine whose rotor has a diameter of 19mm and its centre is 70mm above the metal sheet that holds it. A flange connects the primary machine rotor to an aluminium disc, with a diameter of 121mm and 25-mm thick.

This aluminium disc has grooves to align and fix the outer rotor. Four M5 skewed bars, distributed along the circumference of the outer rotor, hold the outer rotor attached to the aluminium disc. The outer rotor has 70 mm of axial length, where the first 20 mm does not contain magnets grooves to fit on the grooves of the aluminium disc. The following 50 mm is where the magnets are placed, with grooves to form the outer rotor teeth and the dovetail, explained in chapter 5. The described assembly is shown in Fig. 64.

Figure 64 - Primary machine and outer rotor

Source: The author

The aluminium disc was machined in a lathe and the outer rotor was first machined in an EDM machine and later completed with a lathe.

6.1.2 Modulation ring and inner rotor

The inner rotor, with 50 mm of axial length, is connected to a shaft made of solid 1020 steel. The shaft that connects the inner rotor is held at each end by two HZZV 6003 bearings from SNR™. The bearings are inserted into two steel plates, 20-mm thick. The steel plates are held by two L shaped steel frames each, which are attached to the metal sheet that holds the primary machine and the outer rotor. The modulation ring, made of aluminium and 2200 0.5-mm thick electrical steel sheets, is attached to the front steel plate, centred with the inner rotor. The described part of the prototype is shown in Fig. 65.

Figure 65 - Modulation ring and inner rotor

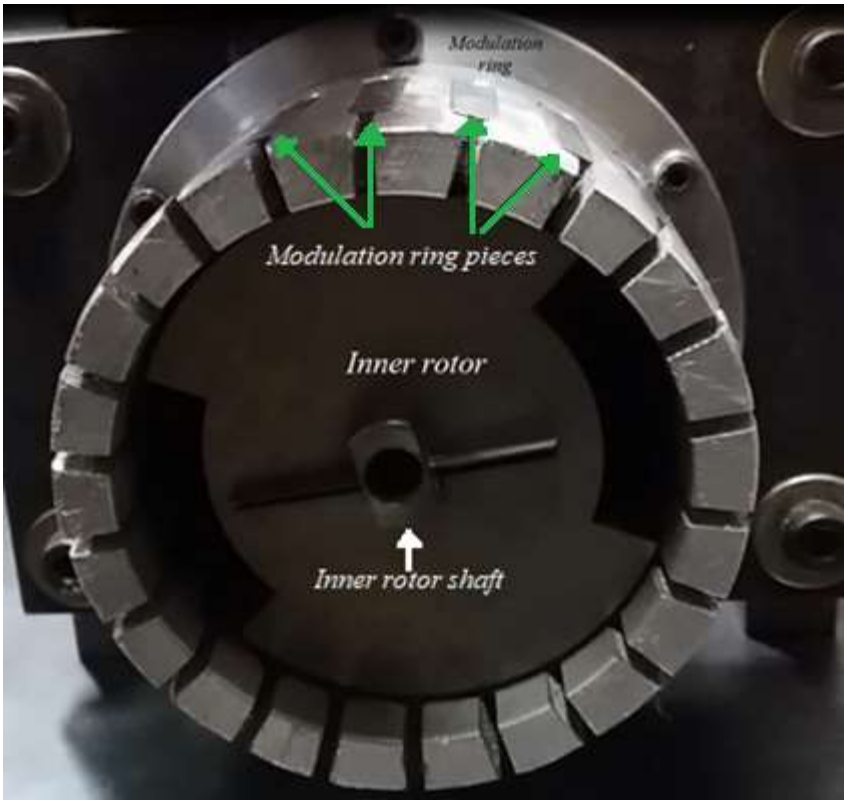

Source: The author

The modulation ring was machined using a lathe and a milling cutter to make the grooves and the inner and outer diameters. The electrical steel sheets were made by an EDM machine and placed in the grooves. The electrical sheets are 1 mm wider than the grooves so

they are placed with a small inclination. An M5 screw presses each electrical sheet stack against the aluminium structure to hold them in place, causing them to make small grooves in the aluminium, which helps the aluminium to hold the individual electrical steel sheets.

6.2 EXPERIMENTAL TESTS AND RESULTS

The gear ratio and the maximum torque of the prototype were determined in order to compare with the FEM simulations.

6.2.1 Gear ratio

The gear ratio determines the resulting speed of the inner rotor for a given outer rotor speed and magnetic flux modulation. As the prototype was designed to have a gear ratio of 10, one turn of the outer rotor should result in 10 turns of the inner rotor ideally. To verify the gear ratio of the prototype the outer rotor was spun for a quarter and half a turn, eight times each, and the resulting angle of the inner rotor was measured using an AK58M encoder. Fig. 66 shows the resulting angle variation of the inner rotor for a quarter of a turn of the outer rotor. Table IV shows the experimental results and the corresponding ideal value.

Figure 66 - Inner rotor angle variation for a quarter of a turn of the outer rotor

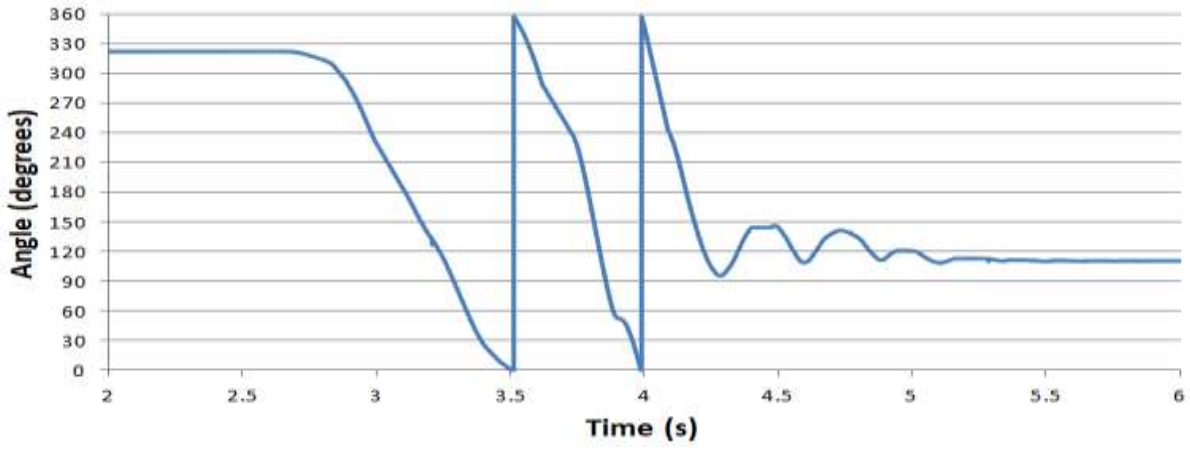

Source: The author

In Fig. 66, the starting angle of the inner rotor was 321º and the final angle was 110º. This means that the inner rotor spun 2 turns plus 211º for this experiment. The value for an ideal gear ratio would be 2 turns and 180º. The difference of 3% from the ideal value can be associated to the precision of the rotating angle of the outer rotor.

Table 4 Gear ratio results

Outer rotor angle	Inner rotor resulting angle	Average difference	Variation
90º	931º	3.4%	+/- 0.3%
180º	1825º	1.3%	+/- 0.1%

By spinning the outer rotor a quarter of a turn and half a turn the results in Table 4 show that the gear ratio is maintained, even with several turns of the inner rotor.

The setup used is shown in Fig. 67.

Figure 67 - Experimental setup to measure the gear ratio

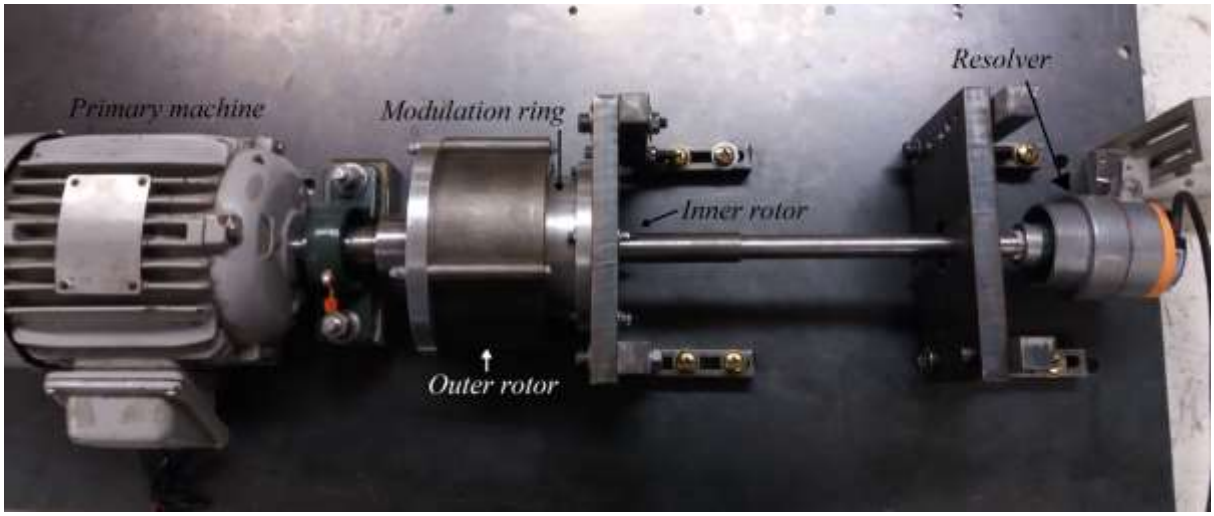

Source: The author

The gear ratio not only gives the resulting angle variation of the inner rotor as a function of the angle variation of the outer rotor, but it also sets the speed relation between the inner rotor and the outer rotor. In order to drive the outer rotor without risking a collision of the outer rotor and the modulation ring, the prototype was set in a lathe, with the outer rotor

being fixed to the spindle and the modulation ring and inner rotor attached to the tool post. The setup is shown in Fig. 68.

Figure 68 - Experimental setup to measure the gear ratio and speeds

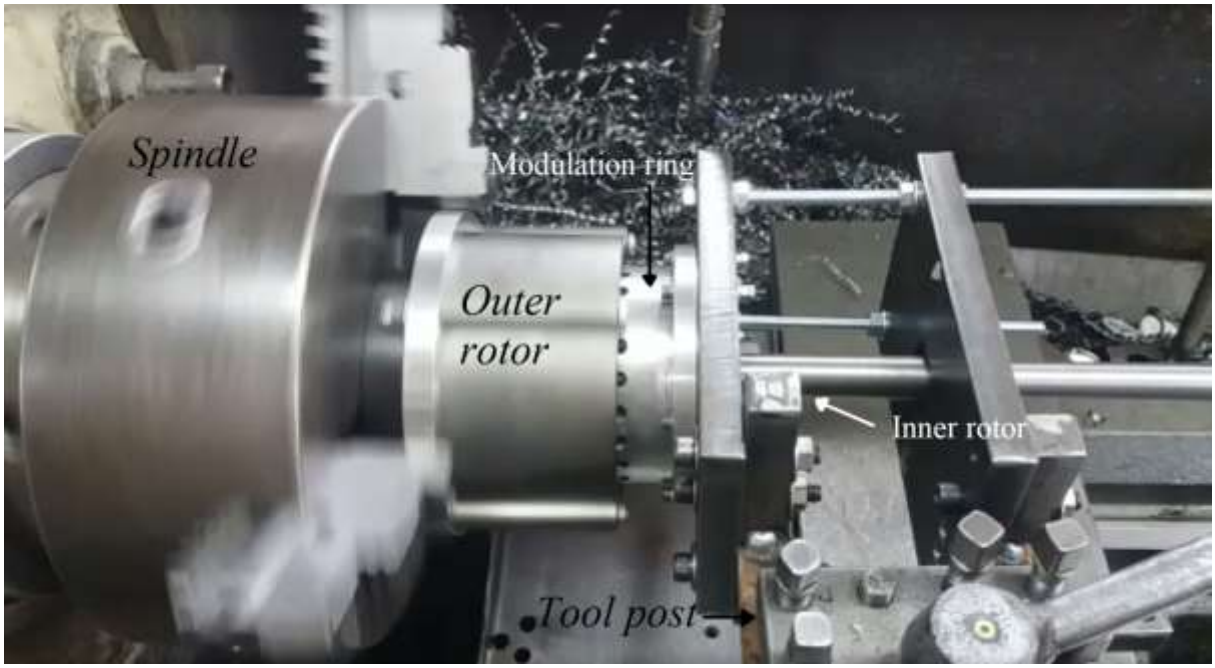

Source: The author

The measured speeds of the inner and outer rotors are given in Table 5, where the values were obtained using 2 MDT-2245B Minipa tachometers. The tachometer that measured the outer rotor speed had a wheel with 32.5 mm of diameter. The lathes spindle has 10 inches of diameter, so the value measured must be converted to match the actual speed of the outer rotor, with a factor of 1 rpm measured being equivalent to 0.127 rpm of the outer rotor.

Table 5 Inner and outer rotor speed results

Lathe speed	Inner rotor speed average speed	Variation
25 rpm	252 rpm	± 0.12 rpm
40 rpm	399 rpm	± 0.20 rpm
60 rpm	570 rpm	± 0.28 rpm
120 rpm	1190 rpm	± 0.59 rpm

Given that the lathe has a much higher torque on its spindle than the prototype can produce on its inner rotor, the spindle goes from zero to full speed in a very short time. As the lathe only has fixed speed values, for higher speed values the inner rotor cannot accelerate in time to overcome its inertia as the outer rotor speed increases too fast. As a result, for the first 2 speed measurements the inner rotor managed to start with the outer rotor and achieve full speed. For the third measurement, the inner rotor required an initial movement to synchronize with the outer rotor speed. For the fourth measurement, an electric motor had to be connected to provide the initial speed for the inner rotor. It would not start with the outer rotor for higher speeds as the torque required by the inertia to follow the corresponding speed of the outer rotor was larger than the maximum torque of the inner rotor. When the speed ramp was too steep, the inner rotor lost synchronism, started to slip poles, and stopped turning. When the speed of the outer rotor was set to the value of the third measurement the inner rotor started to vibrate with the torque alternating its direction as the inner rotor could not follow it. For higher values of outer rotor speed, such as the speed of the fourth measurement and higher, the inertia and mass of the inner rotor made the vibration from the alternating torque to diminish to a level where the inner rotor was as if there were no magnets in the outer rotor. In conclusion, if the speed of the outer rotor is much higher than that of the inner rotor, and the inner rotor has enough inertia, the inner rotor appears to be in a condition where the outer rotor was removed, with no torque being produced upon it.

6.2.2 Maximum inner rotor output torque

The torque output of the inner rotor when it is spun and the outer rotor is kept fixed was measured using a T20WN torque sensor from HBM™ connected between the inner rotor and a base. Fig. 69 shows the experimental setup.

Figure 69 - Experimental setup for torque measurement

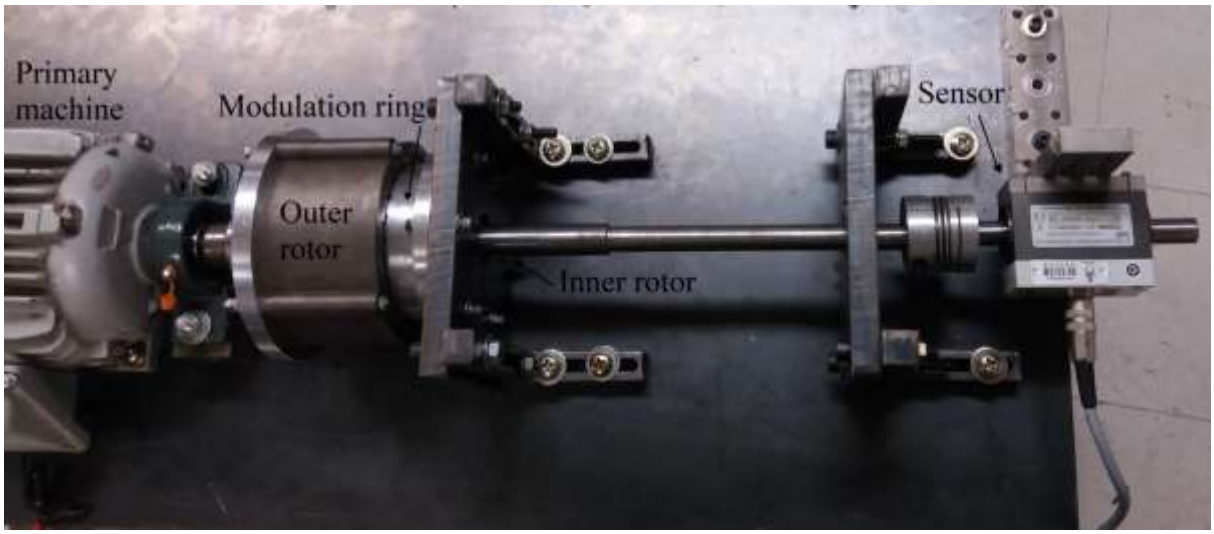

Source: The author

Fig. 70 shows the FEA simulations results for the rotation of the inner rotor while the outer rotor is fixed.

Figure 70 - Simulation results of maximum inner rotor static torque

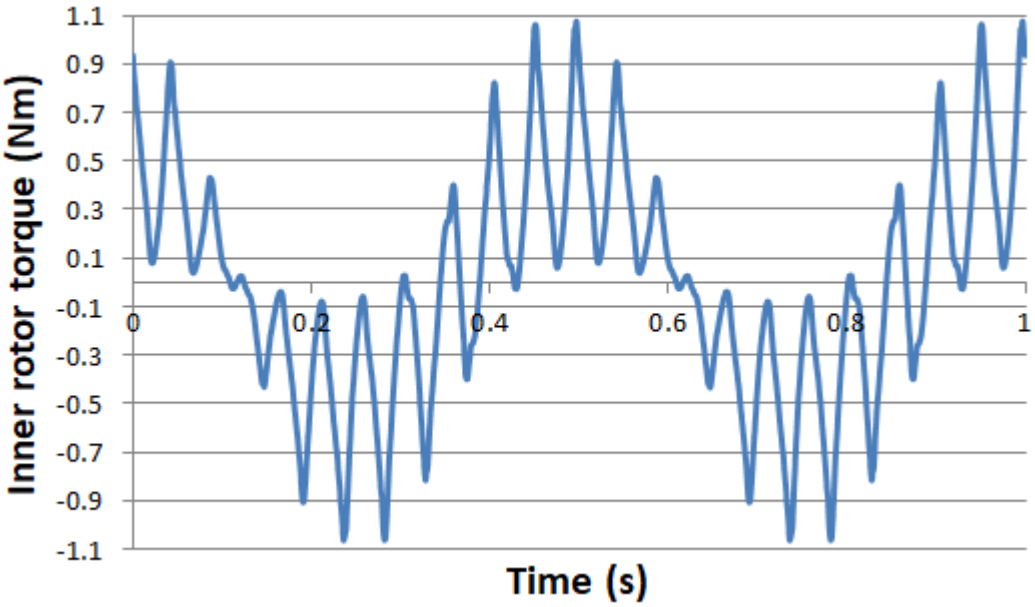

Source: The author

The simulation results show a periodic behaviour of the inner rotor torque, as expected, with about 10 peaks per turn. Fig. 71 shows the experimental results for a fixed outer rotor and a turning inner rotor.

Figure 71 - Experimental results of inner rotor torque

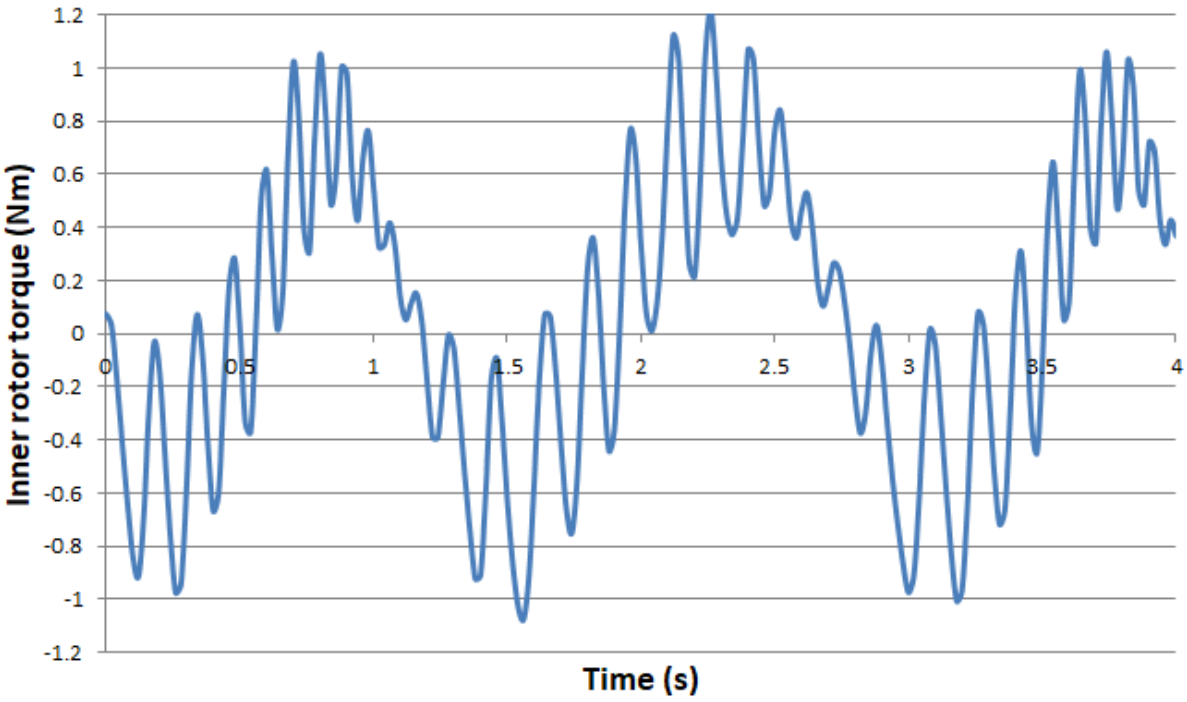

Source: The author

The experimental results in Fig. 71 show similarity with the simulation results of Fig. 70. Both show the 10 peaks per rotation and similar peak values. The main difference between both results is the transition from the positive torque peak to the negative torque peak. This difference can be explained by the fact that the simulation did not consider mechanical transients or inertia, only a constant speed.

The experimental results and the simulation results are shown in Fig. 72.

Figure 72 - Experimental and simulation results of inner rotor torque

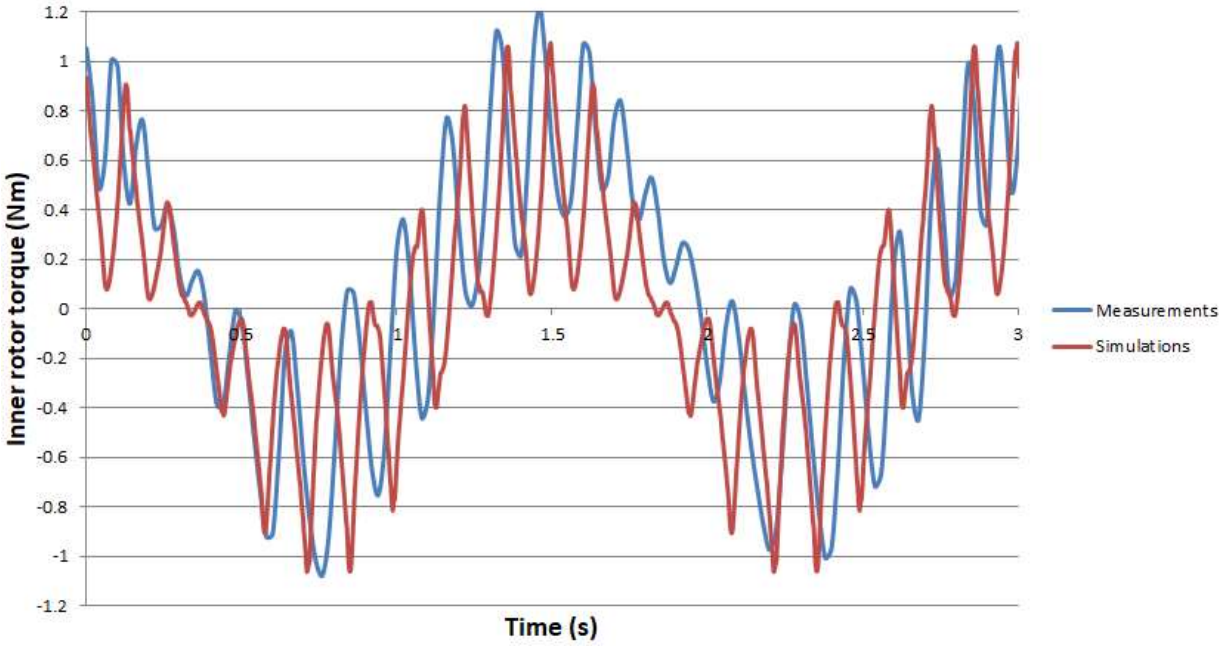

Source: The author

In Fig. 72, both the measured values and the values obtained with simulations are shown. A mismatch can be seen given by the difference of speed with which the inner rotor was spun. The peak values of torque for the simulations were 1.07 Nm and -1.06 Nm. The measured peak values were 1.22 Nm and -1.07 Nm. The difference between the measured and peak values was 13% for the positive peak values and 1.4% for the negative peak values. The negative peak values were closer than the positive peak values. The difference may be associated with the torque that comes from the inertia of the inner rotor and the friction of the bearings. The average value of the simulated results is 0.002 Nm, while the average value of the measured values is 0.12 Nm.

7 CONCLUSIONS AND RECOMMENDATIONS

The proposed topology offers several advantages compared to a traditional FESS: the possibility to use a conventional electric machine as the primary machine; the possibility to place the primary machine outside the vacuum chamber (VC); torque overload protection and the possibility to decouple the rotating mass from the primary machine to achieve a no-magnetic loss state when the device is not charging nor discharging.

Some issues with the proposed topology are: the difficulty to move the outer rotor to achieve the decoupling of the rotating mass, which requires a solid mechanical structure to be performed; the need to modify the vacuum chamber wall to incorporate the modulation ring; the torque density when compared to a conventional magnetic gearbox and limitation of the size of the vacuum chamber wall that contains the modulation ring.

Since MGs are capable of providing a speed gain from one rotor to another the high speeds usually employed in FESS can be achieved using a conventional two pole electrical machine. By determining the desired maximum speed, it is possible to set the speed gain to convert the maximum speed of the electrical machine, though some values of speed gain incur in increased torque ripple. The torque ripple can be mitigated by using the skewing effect as show in chapter 4.

As the MG can transfer energy through the VCW as the modulation ring inside it couples both rotors of the MG, the primary machine can be placed outside the vacuum chamber wall. This reduces the heat dissipation issues of the electrical machine, as it will no longer be in the vacuum and removes the need to allocate space inside the VC to accommodate the primary machine, which helps to compensate for the need to insert the modulation ring into the VCW.

The only connection of the rotating mass to the outside of the VC is through the MG. When an excessive torque is applied to the MG, it will lose synchronism until the torque applied to it is reduced. This prevents from an excessive torque to be applied to the rotating mass and it will not cause a break as it would with a mechanical gear.

In chapter 5 was explained how the decoupling of the rotating mass can be achieved by removing the outer rotor as it would leave no magnetic sources interacting with the modulation ring, and as a consequence, the inner rotor attached to the rotating mass. The main issue with this approach is the force required to remove the outer rotor and the time required to do so, resulting in a difficulty to decouple the rotating mass in very short periods.

Placing the primary machine outside the VC removes the need to allocate the primary machine inside the VC, which makes the VC design easier. However, the need to modify part of the VCW to incorporate the modulation ring incurs in design difficulties.

In order to increase the torque output, as shown in chapter 4, the increase of R_{out} provides the best results but this approach is limited by the size of the VC, which needs to be increased, at least in the region containing the MG.

The experimental results have shown a good accordance with the simulation results. The gear ratio matched the designed value both for speed and for angular variation. The torque results also matched the values obtained with the FEA simulations.

For future studies, the use of a different material between the modulation ring pieces is advised. The aluminium was used to test the prototype, but it incur in extra eddy currents losses. For a different material, a high mechanical strength, a high electrical resistance, a low magnetic permeability and cost should be evaluated to obtain better results.

Due to technical difficulties with maintaining the alignment of the outer rotor and the modulation ring, it was not possible to measure torque aside from the static torque. For future

works, the measurement of torque for different speeds and loads is advised as well as losses measurement to verify the simulation results.

The alternative topology proposed in chapter 3 can be improved by changing the way the levitation system is placed and can prove to be an interesting option as it has a maximum R_{out} for a given VC size.

In the same way as with CMG and RMG, should a reluctance axial magnetic gearbox, where the magnets of the rotor inside the VC are replaced with electrical steel, be proposed, it can prove to be a good option given the simplicity with which it could be installed inside the VC. Its removal to obtain a decoupling would also be easier, but the resulting torque output would have to be examined to compare with a topology with a RMG. A reluctance pseudo-drive, if proposed, can offset the drawbacks shown in the literature should the time to turn the device on and off be a critical factor. As the use of a RMG makes it difficult to decouple the rotating mass in the range of milliseconds, the capability of a reluctance pseudo-drive to achieve decoupling faster could offset its drawbacks.

REFERENCES

[1] RASMUSSEN, P. O.; ANDERSEN ,T. O.; JORGENSEN, F. T.; NIELSEN, O. Development of a high-performance magnetic gear. **IEEE Transactions on Industry Applications**, v. 41, n. 3, p. 764-770, May-June 2005. Available in: doi: 10.1109/TIA.2005.847319. Acessed in: 29 ago. 2020.

[2] MOLOKANOV, O.; DERGACHEV, P.; KIRUHIN, V.; KURBATOV, P. Analyses and experimental validation of coaxial magnetic planetary gear. *In*: INTERNATIONAL SYMPOSIUM ON ELECTRICAL APARATUS AND TECHNOLOGIES - SIELA EVENT, 18., 2014, Bourgas. **Proceedings[...]**. New York: IEEE, 2014. p. 1-4. Available in: doi: 10.1109/SIELA.2014.6871876. Acessed in: 29 ago. 2020.

[3] LI, K.; BIRD, J.; KADEL , J.; WILLIAMS, W. A flux-focusing cycloidal magnetic gearbox. **IEEE Transactions on Magnetics**, v. 51, n. 11, p. 1-4, Nov. 2015, Art n. 8109504. Available in: doi: 10.1109/TMAG.2015.2440218. Acessed in: 29 ago. 2020.

[4] LI, K.; WRIGHT, J.; MODARESAHMADI, S.; SOM, D.; WILLIAMS, W.; BIRD, J. Z. Designing the first stage of a series connected multistage coaxial magnetic gearbox for a wind turbine demonstrator. *In:* IEEE ENERGY CONVERSION CONGRESS AND EXPOSITION – ECCE, 9. 2017, Cincinati, Oh. **Proceedings[...]** New York: IEEE, 2017. p. 1247-1254. Available in: doi: 10.1109/ECCE.2017.8095932. Acessed in: 29 ago. 2020.

[5] ABDEL-KHALIK, A. S.; ELSEROUGI, A.; AHMED, S.; MASSOUD, A. A wind turbine architecture employing a new three port magnetic gear box. *In:* IEEE ENERGY CONVERSION CONGRESS AND EXPOSITION – ECCE, 4., 2012, Raleigh, NC. **Proceedings[...]** New York: IEEE, 2012. p. 1917-1924. Available in: doi: 10.1109/ECCE.2012.6342578. Acessed in: 29 ago. 2020.

[6] BAO, G. Q.; MAO, K. F. A wind energy conversion system with field modulated magnetic gear. *In:* ASIA-PACIFIC POWER AND ENERGY ENGINEERING CONFERENCE – APPEEC, 3., 2011, Wuhan **Proceedings[...]** New York: IEEE, 2011. p. 1-4. Available in: doi: 10.1109/APPEEC.2011.5748902. Acessed in: 29 ago. 2020.

[7] UPPALAPATI, K. K.; CALVIN, M. D.; WRIGHT, J. D.; PITCHARD, J.; WILLIAMS, W. B.; BIRD, J. Z. A magnetic gearbox with an active region torque density of 239 N·m/L. **IEEE Transactions on Industry Applications**, v. 54, n. 2, p. 1331-1338, March-April 2018. Available in: doi: 10.1109/TIA.2017.2779418. Acessed in: 29 ago. 2020.

[8] AKCAY, Y.; COX , T.; COSTABEBER, A. Improving magnetic gear overload torque with cage rotor bars. *In:* INTERNATIONAL CONFERENCE ON ELECTRICAL MACHINES AND SYSTEMS (ICEMS), 20., 2017, Sydney, NSW. **Proceedings[...]** New

York: IEEE, 2017. p. 1-5. Available in: doi: 10.1109/ICEMS.2017.8056295. Acessed in: 29 ago. 2020.

[9] AUBERTIN, M.; TOUNZI, A.; LE MENACH, Y. Study of an electromagnetic gearbox involving two permanent magnet synchronous machines using 3-D-FEM. **IEEE Transactions on Magnetics**, v. 44, n. 11, p. 4381-4384, Nov. 2008. Available in: doi: 10.1109/TMAG.2008.2001513. Acessed in: 29 ago. 2020.

[10] PRITCHARD, J.; PADMANATHAN, P.; BIRD, J. Z. Designing a continuously variable magnetic gear. *In:* IET INTERNATIONAL CONFERENCE ON POWER ELECTRONICS, MACHINES AND DRIVES (PEMD 2016), 8., 2016, Glasgow. **Proceedings[...]** New York: IEEE, 2016. p. 1-6. Available in: doi: 10.1049/cp.2016.0223. Acessed in: 29 ago. 2020.

[11] RASHIDI, H.; PISHDAD, D. Integrated multispeed magnetic gears: a novel approach to design of magnetic transmission systems. **IEEE Transactions on Magnetics**, v. 51, n. 4, p. 1-8, April 2015, Art no. 8700308. Available in: doi: 10.1109/TMAG.2014.2359639. Acessed in: 29 ago. 2020.

[12] MONTAGUE, R. G.; BINGHAM, C. M.; ATALLAH, K. Magnetic gear overload detection and remedial strategies for servo-drive systems. SPEEDAM 2010, Pisa, 2010, p. 523-528. Available in: doi: 10.1109/SPEEDAM.2010.5544957. Acessed in: 29 ago. 2020.

[13] FILIPPINI, M.; ALOTTO, P. Coaxial magnetic gear design and optimization. **IEEE Transactions on Industrial Electronics**, v. 64, n. 12, p. 9934-9942, Dec. 2017. Available in: doi: 10.1109/TIE.2017.2721918. Acessed in: 29 ago. 2020.

[14] NEVES, C. G. C.; FLORES FILHO, ALY F. Magnetic Gearing Electromagnetic Concepts. **Journal of Microwaves, Optoelectronics and Electromagnetic Applications**., v.16, p.108 - 119, 2017. Available in: doi: 10.1590/2179-10742017v16i1874. Acessed in: 29 ago. 2020.

[15] ZAYTOON, H.; ABDEL-KHALIK, A. S.; AHMED, S.; MASSOUD, A. Cogging torque reduction of axial magnetic gearbox using pole pairing technique. *In:* IEEE INTERNATIONAL CONFERENCE ON INDUSTRIAL TECHNOLOGY (ICIT), 16., 2015, Seville, **Proceedings[...]** New York: IEEE, 2015. p. 652-657. Available in: doi: 10.1109/ICIT.2015.7125172. Acessed in: 29 ago. 2020.

[16] FAYSAL, A. A.; HARIS, S. M.; SAAD, M. H. M. An axial magnetic gear design with changeable ratios. *In:* IEEE INTERNATIONAL CONFERENCE ON CONTROL SYSTEM, COMPUTING AND ENGINEERING (ICCSCE), 8., 2018, Penang, Malaysia, **Proceedings[...]** New York: IEEE, 2018. p. 195-200. Available in: doi: 10.1109/ICCSCE.2018.8684958. Acessed in: 29 ago. 2020.

[17] HUANG, C.; TSAI, M.; DORRELL, D. G.; LIN, B. Development of a magnetic planetary gearbox. **IEEE Transactions on Magnetics**, v. 44, n. 3, p. 403-412, March 2008. Available in: doi: 10.1109/TMAG.2007.914665. Acessed in: 29 ago. 2020.

[18] FRANK, N. W.; TOLIYAT, H. A. Gearing ratios of a magnetic gear for marine applications. *In:* IEEE ELECTRIC SHIP TECHNOLOGIES SYMPOSIUM, 3., 2009, Baltimore, MD, **Proceedings[...]** New York: IEEE, 2009. p. 477-481. Available in: doi: 10.1109/ESTS.2009.4906554. Acessed in: 29 ago. 2020.

[19] BANINAJAR, H.; BIRD, J. Z.; MODARESAHMADI, S.; WILLIAMS, W. Electromagnetic and mechanical design of a hermetically sealed magnetic gear for a marine hydrokinetic generator. *In:* IEEE ENERGY CONVERSION CONGRESS AND EXPOSITION (ECCE), 10., 2018, Portland, OR. **Proceedings[...]** New York: IEEE, 2018. p. 4987-4993, Available in: doi: 10.1109/ECCE.2018.8557386. Acessed in: 29 ago. 2020.

[20] ZAYTOON, H.; ABDEL-KHALIK, A. S.; AHMED, S.; MASSOUD, A. Torque ripple alleviation of a radial magnetic gearbox using step skewing approach. *In:* INTERNATIONAL CONFERENCE ON ELECTRICAL MACHINES (ICEM), 21., 2014, Berlin. **Proceedings[...]** New York: IEEE, 2014. p. 648-653. Available in: doi: 10.1109/ICELMACH.2014.6960249. Acessed in: 29 ago. 2020.

[21] AISO, K.; AKATSU, K. A novel reluctance magnetic gear for high speed motor. *In:* IEEE ENERGY COVERSION CONGRESS AND EXPOSITION (ECCE), 8., 2016, Milwaukee, WI. **Proceedings[...]** New York: IEEE, 2016. p. 1-7. Available in: doi: 10.1109/ECCE.2016.7854742. Acessed in: 29 ago. 2020.

[22] AISO, K.; AKATSU, K.; AOYAMA, Y. A novel reluctance magnetic gear for high-speed motor. **IEEE Transactions on Industry Applications**, v. 55, n. 3, p. 2690-2699, May-June 2019. Available in: doi: 10.1109/TIA.2019.2900205. Acessed in: 29 ago. 2020.

[23] BIRD, J.; LI, K.; WILLIAMS, W.; KADEL, J. A flux focusing cycloidal magnetic gearbox. *In:* IEEE INTERNATIONAL MAGETICS CONFERENCE (INTERMAG), 50., 2015, Beijing. **Proceedings[...]** New York: IEEE, 2015. p. 1-1. Available in: doi: 10.1109/INTMAG.2015.7157684. Acessed in: 29 ago. 2020.

[24] FITZGERALD, A. E.; KINGSLEY, C; UMANS, S. D. **Electric machinery**. Boston, Mass: McGraw-Hill, 2003.

[25] WIMER, B.; SANTORA, M.; BERVEN, C.; LAW, J. Dynamic modeling of an integrated flywheel energy storage system. *In:* IECON 2018 - ANNUAL CONFERENCE OF THE IEEE INDUSTRIAL ELECTRONICS SOCIETY, 44., 2018, Washington, DC. **Proceedings[...]** New York: IEEE, 2018. p. 483-489. Available in: doi: 10.1109/IECON.2018.8595147. Acessed in: 29 ago. 2020.

APPENDIX A

Prototype Parts: Mechanical Drawings.

APPENDIX A: PROTOTYPE PARTS MECHANICAL DRAWINGS

FRONT PLATE – 1020 STEEL - LATHE AND MILLING CUTTER

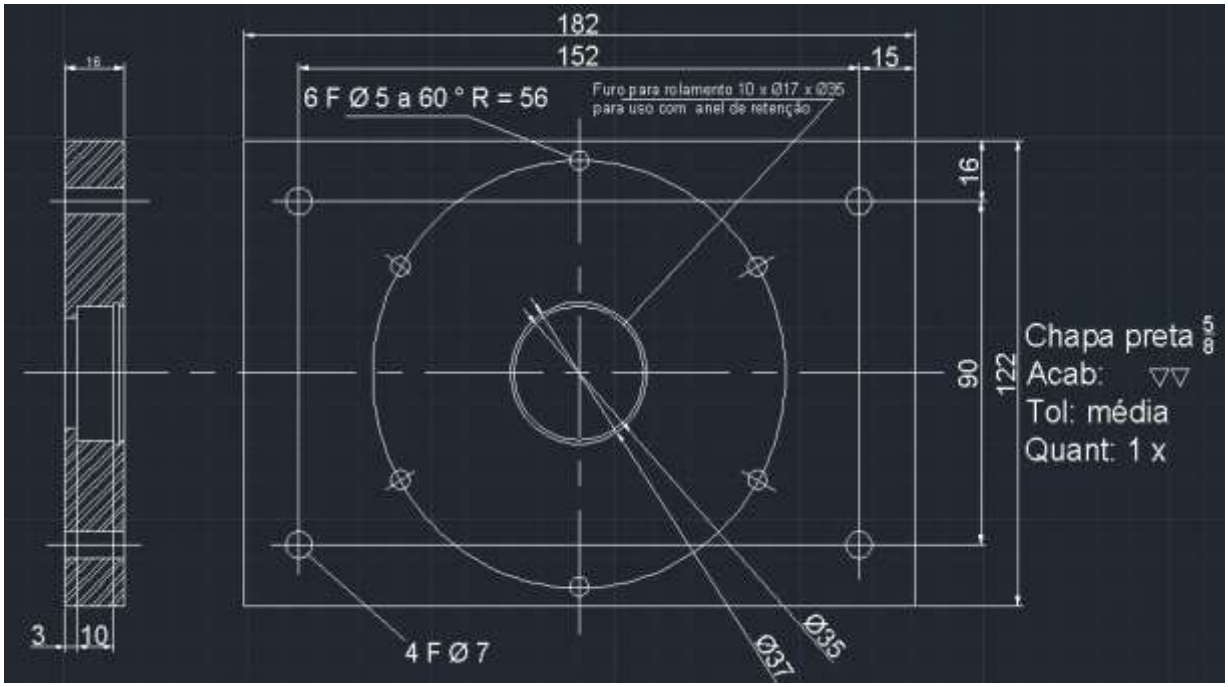

BACK PLATE – 1020 STEEL - LATHE AND MILLING CUTTER

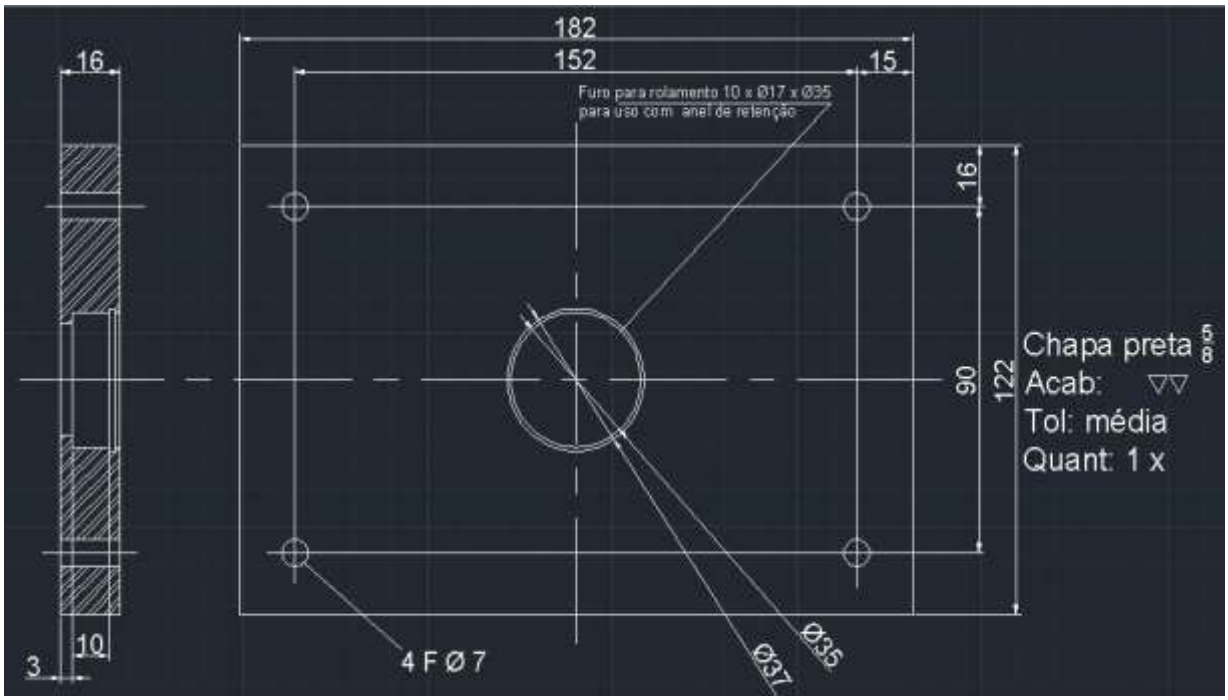

L FRAMES – 1020 STEEL - MILLING CUTTER

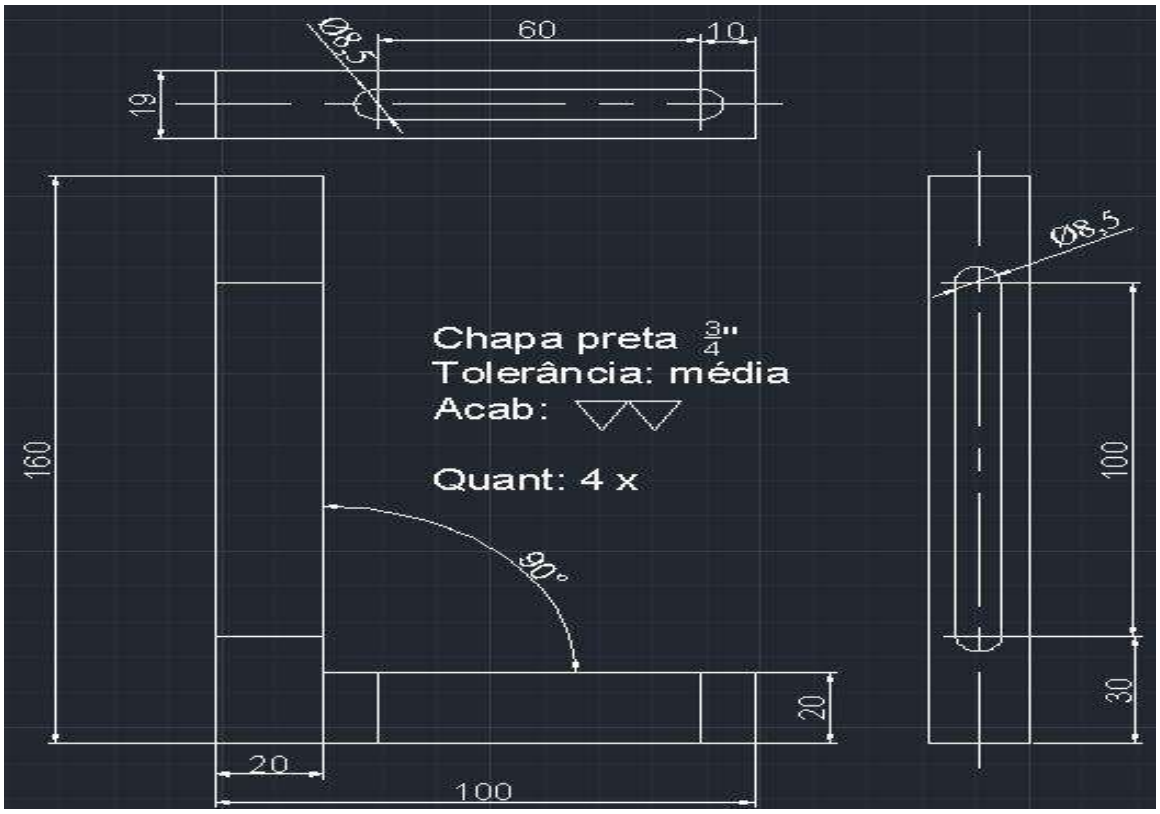

ALUMINIUM DISK – ALUMINIUM - LATHE AND MILLING CUTTER

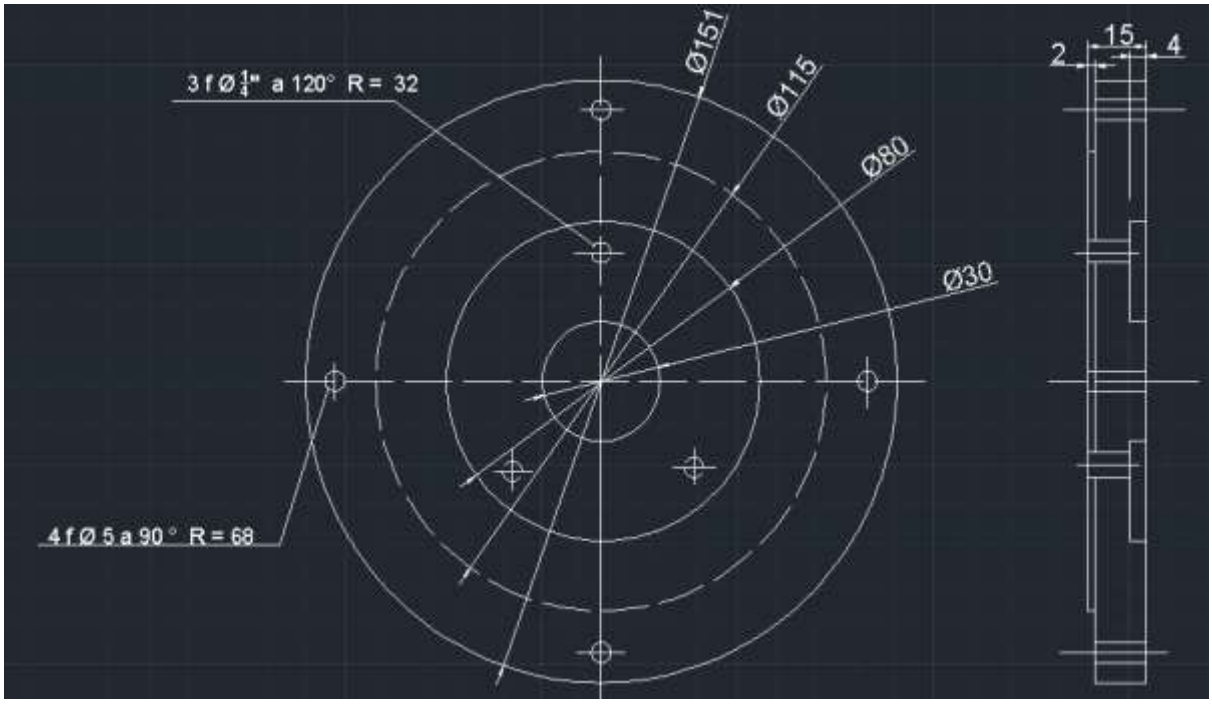

ALUMINUM MODULATION RING STRUCTURE – ALUMINUM - LATHE AND MILLING CUTTER

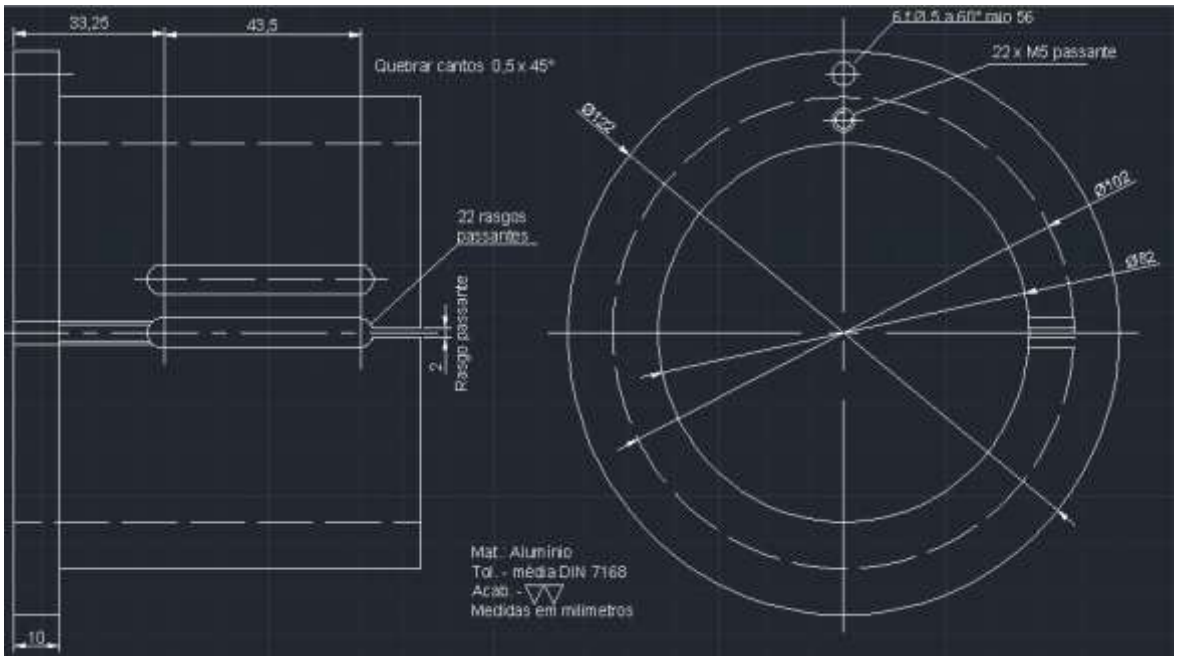

INNER ROTOR SHAFT – 1020 STEEL - LATHE

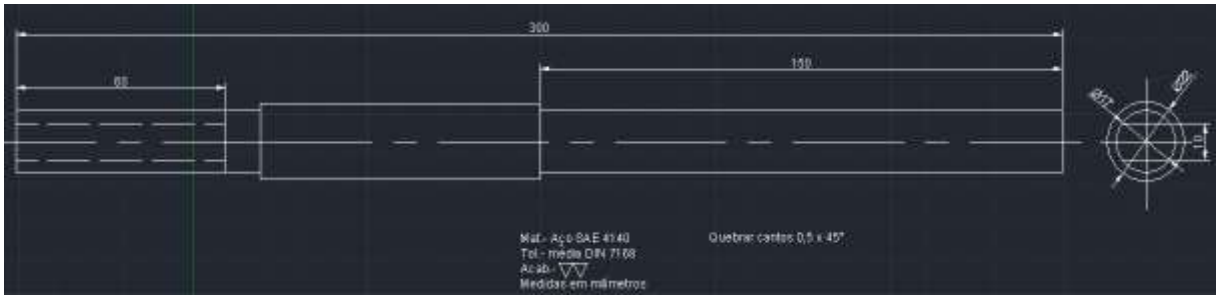

MODULATION RING PIECES – E230 0.5MM ELECTRICAL STEEL - EDM MACHINE

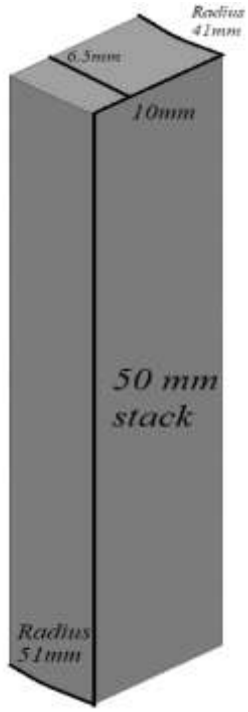

MAGNETS – NDFEB N35 - EDM MACHINE

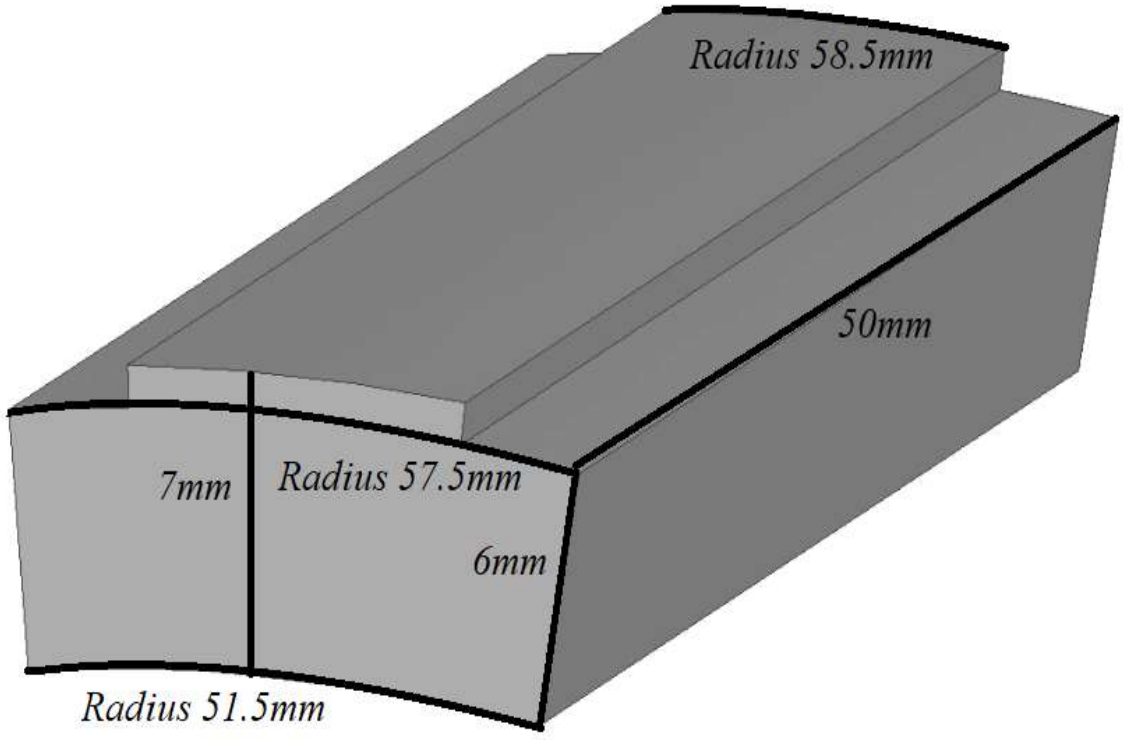

OUTER ROTOR – 1020 STEEL - EDM MACHINE AND LATHE

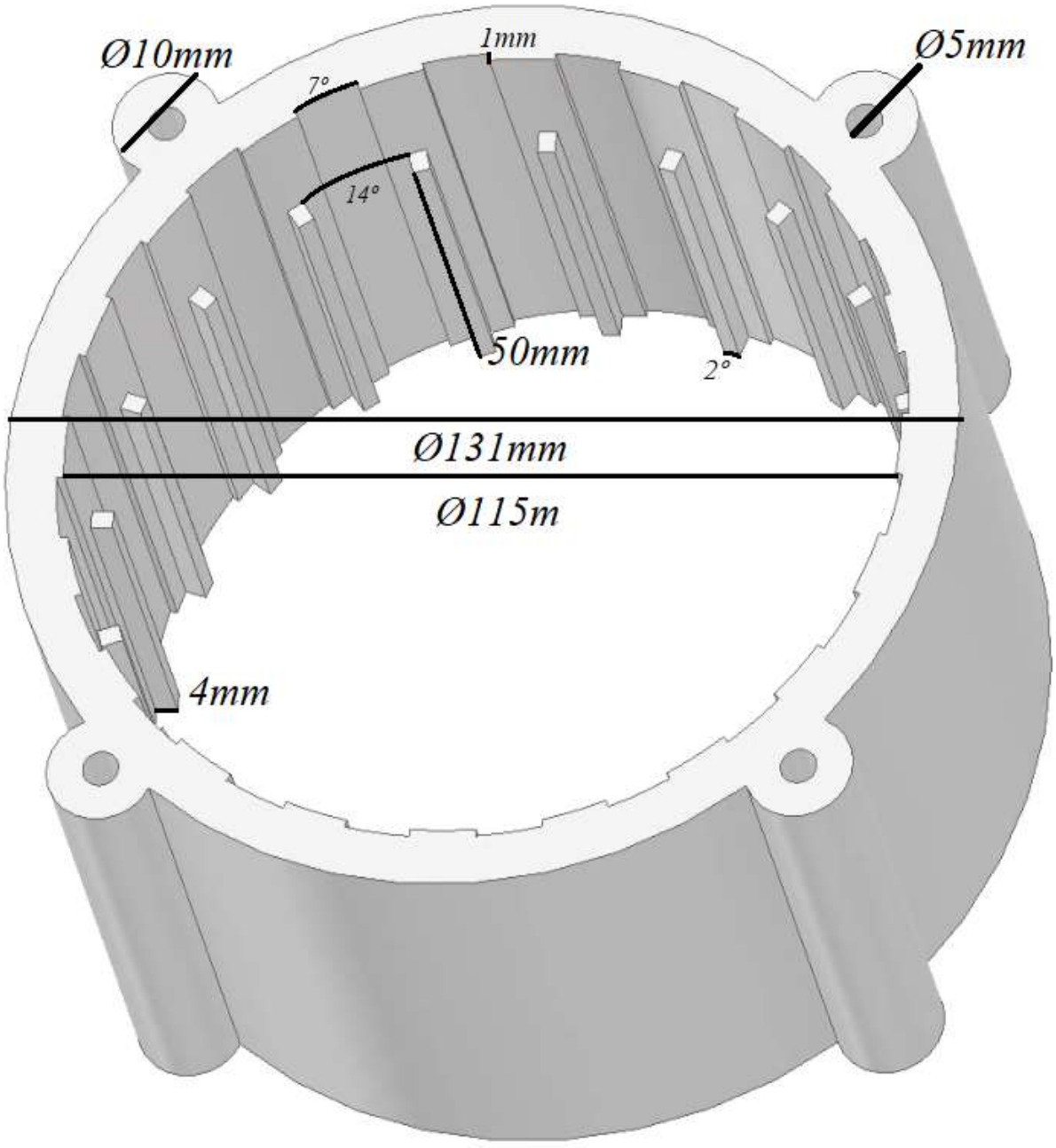

INNER ROTOR – E230 0.5MM ELECTRICAL STEEL - EDM MACHINE